Molecular Thermodynamics and Solvation Behaviour of Protic Ionic Liquid Systems

Joshua Elias Samuel James Reid

PhD

University of York

Chemistry

July 2017

Abstract

Protic ionic liquids (PILs) are a class of solvents prepared from the mixing of equimolar quantities of a Brønsted acid and base resulting in both neutral and ionic species in equilibrium with one another. Their evolving application as solvents for innovative processes requires further understanding of their properties and how they originate at the molecular level. Three topics remain widely debated concerning PILs: 1) the effects of low concentrations of water as an impurity, 2) the structure–property relations in PILs and 3) the connection between PILs and their precursor components in terms of both molecular interactions and bulk properties.

In this work, these three topics are studied using a variety of experimental techniques and fundamental theory for selected representative PIL systems. To clarify the effect of water at low concentrations, the statistical thermodynamic theory of solutions has been applied to quantify the interactions between species solely from thermodynamic data. Results showed both a strong composition dependence of the effect of water on the liquid structure in aprotic and protic ILs, but also that water did not significantly weaken ion–ion interactions at low concentrations. After clarifying the effects of water at low concentration on PIL behaviour, it has been shown that incorporating hydrogen bond donor functionality to the cation can increase the ionic nature of acetate PILs. This increase in ionic nature provides an excellent rationalization for the effect of cation structure on the thermodynamic and solvatochromic properties of three PILs. By studying the effect of varying composition of precursor acid and base, a deeper insight into the molecular origin of trends in bulk properties and solvation behaviour can be found. Furthermore, it has been shown that the solvation environment is highly composition dependent, offering insight into a new strategy in the application of PILs and their precursor materials as tuneable solvation media.

Table of Contents

List of Tables

Table 4.6 Cohesive energy densities (CED) of each PIL studied as determined from the directly measured standard molar enthalpy of vaporization and their molar volume, at 298 K.

Table 4.7 Solvatochromic parameters for the three PILs in this study.

Table 4.8 Molar volumes (V_m), enthalpies of vaporization, $\Delta_{vap}H^{\circ}_{m}$, cohesive energy densities (CED), viscosities (η) and Hildebrand parameter (δ) for the three PILs in this study.

Table 5.1 Mass of precursors used for the preparation of the binary mixtures of acetic acid and *N*,*N*–dimethylbutylamine. Water content was determined from Karl Fischer titration.

Table 5.2 Mass of precursors used for the preparation of the binary mixtures of acetic acid and *N*,*N*,*N'*,*N'*–tetramethylethan–1,2–diamine. Water content was determined from Karl Fischer titration.

Table 5.3 Mass of precursors used for the preparation of the binary mixtures of acetic acid and *N*,*N*–dimethylethanolamine. Water content was determined from Karl Fischer titration.

Table 5.4 Density (ρ) and molar volume (V_m) of the acetic acid–*N*,*N*–dimethylbutylamine binary system over the complete composition range. Additive quantities are denoted by (Id). All values are recorded at 293 K.

Table 5.5 Density (ρ) and molar volume (V_m) of the acetic acid–*N*,*N*,*N*,*N*–tetramethylethan–1,2–diamine binary system over the complete composition range. Additive quantities are denoted by (Id). All values are recorded at 293 K.

Table 5.6 Density (ρ) and molar volume (V_m) of the acetic acid–*N*,*N*–dimethylethanolamine binary system over the complete composition range. Additive quantities are denoted by (Id). All values are recorded at 293 K.

Table 6.1 Mass of precursors used for the preparation of the binary mixtures of acetic acid and *N*,*N*–dimethylbutylamine. Water content was determined from Karl Fischer titration.

Table 6.2 Mass of precursors used for the preparation of the binary mixtures of acetic acid and *N*,*N*,*N'*,*N'*–tetramethylethan–1,2–diamine. Water content was determined from Karl Fischer titration.

Table 6.3 Mass of precursors used for the preparation of the binary mixtures of acetic acid and *N*,*N*–dimethylethanolamine. Water content was determined from Karl Fischer titration.

Table 6.4 Properties of the solutes used in the miscibility profiling of acid–amine binary mixtures.

Table 6.5 The miscibility profiles of the *N*,*N*–dimethylbutylamine (DMBuA) – acetic acid (HOAc) binary system at 0.1 mole fraction intervals.

Table 6.6 The miscibility profiles of the *N*,*N*,*N'*,*N'*–tetramethylethan–1,2–diamine (TMEDA) – acetic acid (HOAc) binary system at 0.1 mole fraction intervals.

Table 6.7 The miscibility profiles of the *N*,*N*–dimethylethanolamine (DMEtA) – acetic acid (HOAc) binary system at 0.1 mole fraction intervals.

Table 6.8 Miscibility of Hexane, Cyclohexane and Toluene in the DMBuA–HOAc binary system at 0.1 mole fraction intervals.

Table 6.9 Miscibility of Hexane, Cyclohexane and Toluene in the TMEDA–HOAc binary system at 0.1 mole fraction intervals.

Table 6.10 Miscibility of Hexane, Cyclohexane and Toluene in the DMEtA–HOAc binary system at 0.1 mole fraction intervals.

Table 6.11 Miscibility of Dichloromethane, Diiodomethane and Bromotrichloromethane in the DMBuA–HOAc binary system at 0.1 mole fraction intervals.

Table 6.12 Miscibility of Dichloromethane, Diiodomethane and Bromotrichloromethane in the TMEDA–HOAc binary system at 0.1 mole fraction intervals.

Table 6.13 Miscibility of Dichloromethane, Diiodomethane and Bromotrichloromethane in the DMEtA–HOAc binary system at 0.1 mole fraction intervals.

Table 6.14 Miscibility of Diethyl ether, Ethyl acetate, Acetone, Acetonitrile, Dimethyl sulfoxide and 1,3–Bis(trifluoromethyl)benzene in the DMBuA–HOAc binary system at 0.1 mole fraction intervals.

Table 6.15 Miscibility of Diethyl ether, Ethyl acetate, Acetone, Acetonitrile, Dimethyl sulfoxide and 1,3–Bis(trifluoromethyl)benzene in the TMEDA–HOAc binary system at 0.1 mole fraction intervals.

Table 6.16 Miscibility of Diethyl ether, Ethyl acetate, Acetone, Acetonitrile, Dimethyl sulfoxide and 1,3–Bis(trifluoromethyl)benzene in the DMEtA–HOAc binary system at 0.1 mole fraction intervals.

Table 6.17 Miscibility of Ethanol, 1–Octanol and Water in the DMBuA–HOAc binary system at 0.1 mole fraction intervals.

Table 6.18 Miscibility of Ethanol, 1–Octanol and Water in the TMEDA–HOAc binary system at 0.1 mole fraction intervals.

Table 6.19 Miscibility of Ethanol, 1–Octanol and Water in the DMEtA–HOAc binary system at 0.1 mole fraction intervals.

List of Figures

Figure 4.5. ATR–IR spectra of the three PILs and of their corresponding precursors in the region of 1500–1800 cm^{-1}. The spectrum of [HDMEtA][OAc] shows a significantly greater absorbance for the acetate species (~1570 cm^{-1}) than for the neutral species (~1710 cm^{-1}) when compared with the spectra of either [HDMBuA][OAc] or [HTMEDA][OAc].

Figure 5.1. Structures of the precursor amines and acid used to prepare the non-equivalent mixtures in this chapter

Figure 5.2 Dependence of the excess molar volume (V_m^E) (top) and the relative excess molar volume ($V_m^E(rel.)$) (bottom) on the mole fraction of amine for each of the three acid–amine binary mixtures.

Figure 5.3 Far infrared (FIR) spectra of the acid–rich mixtures of each acid–amine binary mixture in the region of 50 – 300 cm^{-1} as a function of acetic acid mole fraction.

Figure 5.4 Far infrared (FIR) spectra of the amine–rich mixtures of each acid–amine binary mixture in the region of 50 – 300 cm^{-1} as a function of acetic acid mole fraction.

Figure 5.5 ATR–IR spectra of the acid–rich compositions of the three acid–amine mixtures in the region of 1500–1800 cm^{-1}. The peak for the acetate species occurs at ~1570 cm^{-1} and the peak corresponding to HOAc species is at ~1710 cm^{-1}.

Figure 5.6 Dependence of the ^{13}C chemical shift of the C_1 carbon on the mole fraction of the amine of acetic acid for the three binary mixtures.

Figure 5.7 Dependence of the ^{13}C chemical shift of the C_2 carbon on the mole fraction of the amine of acetic acid for the three binary mixtures.

Figure 5.8 ATR–IR spectra of the acid–rich compositions of the three acid–amine mixtures in the region of 1500–1800 cm^{-1}. The peak for the acetate species occurs at ~1570 cm^{-1} and the peak corresponding to acetic acid species is at ~1710 cm^{-1}.

Figure 5.9 Dependence of the absolute (top) and relative (bottom) change in ^{15}N chemical shift of the nitrogen centre signal for the three binary mixtures on the amine mole fraction.

Figure 5.10 Dependence of the ^{13}C chemical shift of the C_3 and C_4 carbon environments of each amine on the mole fraction of the amine for the three binary mixtures.

Acknowledgements

The journey I have taken to write this thesis has been made possible by the love and support of colleagues, friends and family.

First, I wish to extend the deepest of thanks to my supervisors throughout this PhD thesis, Dr. Seishi Shimizu and Dr. Adam Walker. Both were there to guide me through the tough times of my studies, gave me the freedom to pursue my research interests and supported my frequently hectic schedule. Seishi, whose combination of analytical reviewing of all aspects of my work, theoretical brain–bashing sessions and the Yorkshireman approach to saying what I have accomplished have made me grow tremendously as an academic and as a person. Adam, who introduced me to protic ionic liquids and the reality of industrial solvation chemistry, guided me through tough times with work and always encouraged me to think outside the box and challenge myself. These two maverick scientists started out as my supervisors, but now they are my friends.

I would like to thank Prof. Nicholas Gathergood and Dr. Hannah Prydderch, who hosted me during my research visit at Dublin City University and taught me much about the design, synthesis, toxicology and biodegradation assessment of ionic liquids. I also want to thank Prof. Manuel Minas de Piedade, Prof. Filomena Martins, Dr. Carlos Bernardes and Dr. Filipe Agapito for hosting me at the Universidade de Lisboa and teaching me extensively about calorimetry and high precision design of experiment. I would like to thank Dr. Tristan Youngs of the STFC Rutherford Appleton Lab (ISIS Pulsed Neutron & Muon Source), who guided myself through the acquisition and interpretation of neutron scattering data in work carried out in parallel to this thesis. I extend my gratitude to Prof. Ruggero Caminiti, Prof. Alessandro Nucara, Dr. Lorenzo Gontrani and Dr. Alessandro Mariani for hosting me at La Sapienza Università di Roma, and teaching me about the spectroscopic, scattering and simulation of protic ionic liquid systems.

There are many people from the University of York that I am grateful for their support. The administrators of the Chemistry Graduate office, to Catherine and Jane of the YSBL administration, to Louise, Simon, Tim and Juliet of the YSBL technician team, to Dr. John Slattery and Prof. Duncan Bruce for advisory discussions about my work, to Dr. Pedro Aguiar, Dr. Andrew Leech, Mr. Karl Heaton, Dr. Paul Elliot, Dr. Stephen Cowling and Dr. Lucia D'Andrea for technical support with departmental analytical instruments, to the members of the YSBL, Materials and Green Chemistry groups who made my time at York more enjoyable.

There are numerous colleagues from TWI ltd. that have helped me along the way; to Dr. Chris Tighe who encouraged me to pursuit the role at TWI in the beginning, the former Polymers section and current Coatings section members who welcomed me, the technicians, notably Mr. Jacob Greenwood and Mr. Alex Russel, who did most of the support work on larger projects I was involved with, all the students and colleagues at TWI who helped make my time at TWI so enjoyable and the administration staff, without whom TWI would have descended into chaos long ago.

To the Cambridge Baseball Club, who taught me so much about the beautiful game and welcomed me as family when I first arrived in Cambridge.

To the friends who have shared parts of this journey with me, to share the good times and the bad, I am thankful. In particular, To Mike, Pricey, Emily, Jackie, the housemates of 11 Devonshire road, Shaheer, Ben, Gerald, Mirjim, Helen, Rashmi and Sonia.

To my brothers Tobias and Joel, who put me up during my visits to York, who were always there for me through good times and bad and could bring a smile to my face when I most needed it. To my dad, who I learned a lot about myself from and always believed in me. To my mum, who inspired me to keep doing what I loved, offering her

strength for me when I had none left and who I could always depend on when I needed you. We have all gone through so much, both together and alone. I love you all, and I am so grateful to have you as my family.

To Galatée, who helped me more than anyone these last four years to become the man I am today, who saw in me what I couldn't, listened when I needed someone to talk to and supported me without hesitation, sharing the greatest highs and the deepest lows of my journey. I thank you with all the love of my heart. Though we may now walk on separate paths, I will cherish the time we were in stride with each other. Shine on, you crazy diamond.

In loving memory of my late uncle Brian. Though we may not have shared much of life together, that time has left an impact on me. I will cherish the memories we have made together, forever entwined with my love of Utah. May your soul find peace on its eternal journey.

In loving memory of my late cats Frisky and Bitty. I grew up with your unconditional love since you were both barely born. Your lives brought happiness to myself and any who knew you. There will never be a cat as regal and beautiful as Frisky, nor a cat as loyal and friendly as Bitty. May your souls find peace on their eternal journey.

Declaration

I declare that this thesis is a presentation of original work and I am the sole author. This work has not previously been presented for an award at this, or any other, University. All sources are acknowledged as References.

Contribution of original results from colleagues in collaboration with this thesis are:

Dr. Filipe Agapito, Universidade de Lisboa, who performed *ab initio* calculations to obtain thermochemical quantities necessary for chapter four. Details of the calculations are provided in the Appendix of this thesis.

The following publications have arisen from this PhD thesis:

J. E. S. J. Reid, A. J. Walker and S. Shimizu, *Residual water in ionic liquids: clustered or dissociated? Phys. Chem. Chem. Phys.*, 2015, **17**, 14710–14718

J. E. S. J. Reid, N. Sullivan, L. Swift, G. A. Hembury, S. Shimizu and A. J. Walker, *Assessing the mutagenicity of protic ionic liquids using the mini Ames test, Sustain. Chem. Process.*, 2015, **3**, 17(10).

J. E. S. J. Reid, R. J. Gammons, J. M. Slattery, A. J. Walker and S. Shimizu, *Interactions in Water−Ionic Liquid Mixtures: Comparing Protic and Aprotic Systems, J. Phys. Chem. B*, 2017, **121**, 599–609.

J. E. S. J. Reid, F. Agapito, C. E. S. Bernardes, F. Martins, A. J. Walker, S. Shimizu and M. E. Minas da Piedade, *Structure–Property Relationships in Protic Ionic Liquids: A Thermochemical Study, Phys. Chem. Chem. Phys.*, 2017, **19**, 19928-19936.

J. E. S. J. Reid, F. Agapito, C. E. S. Bernardes, F. Martins, M. E. Minas da Piedade, S. Shimizu and A. J. Walker, *Structure-Property Relationships in Protic Ionic Liquids: A Study of Solvent-Solvent and Solvent-Solute Interactions, Phys. Chem. Chem. Phys.*, 2017, **19**, 28133-28138.

J. E. S. J. Reid, H. Prydderch, M. Spulak, S. Shimizu, A. J. Walker and N. Gathergood, *Green profiling of Aprotic versus Protic Ionic Liquids: Synthesis and Microbial toxicity of analogous structures, Sustain. Chem. Pharmacol.*, 2017, Accepted

.

Chapter 1: Introduction

1.1 On Solvents and their Importance in The World

Solvents are a class of liquid chemicals defined by their capability to combine with a different chemical, called a solute, to produce either an emulsion, a suspension or a homogeneous solution.[1–5] By using solvents, it has been possible to observe, appreciate and study numerous biological, chemical and physical processes. Conditions such as temperature, pressure, and the choice of solvent can significantly influence these processes. By modifying these conditions, it has been possible to unlock the fundamental science that underpins many of these processes occurring in solution. Put simply, understanding the solvation effect can allow for significant control over a particular process by modifying the solvent environment. [1–5] With control of a process that occurs in solution comes the capability to harness it for a desired outcome. This has contributed significantly to the manufacture of chemical products on industrial scales.[3]

Solvents are also vital for a variety of applications in our day–to–day life, such as in cleaning products,[6] cosmetics and toiletries,[7,8] medication and health products,[9] paints and adhesives [10] and for the fluids used extensively in machinery and automobiles.[11,12] Even making a cup of coffee is a result of using water as a solvent to extract caffeine and other natural products from the roasted seeds of the *Coffea aribica* plant species.[13] In particular, water is the most abundant and important solvent on Earth – life as we know it depends on the role water plays as a solvent for biological processes and our planet has been moulded into the shape we see today by water and its ability to dissolve and transport matter.[14,15] Both the material and natural world we live in has been influenced significantly by solvents.

1.2 The Future of Solvents

It is estimated that the volume of solvents used in industrial chemical applications will reach approximately 21.5 million tons (~19.5 million tonnes) by 2018.[16] But what happens after these solvents are used? Typically, solvents (including water) are written off as waste, and account for the majority of waste generated in the chemical industry.[17] This is a result of the large excess volumes of solvent required to perform many of the reactions carried out at industrial scale product synthesis. While there are many ways by which the amount of solvent lost can be reduced, either by alternative reactor designs such as using flow chemistry or by effective recovery of the solvent through distillation, significant solvent waste is still generated. As many of the solvents used at industrial scale are still derived from the finite resource crude oil, there is great concern over the sustainable use of solvents in this manner.[18]

The concerns are intensified when one considers the potential impact that improper disposal of solvents can cause on the environment. Characterizing the potential environmental impact of chemicals in terms of the hazard they pose, their likely exposure to the environment and the resulting risk of solvents is a challenging exercise.[19,20] However, the amount of evidence suggesting that many solvents that have been used for decades at industrial scale are either acutely toxic, carcinogenic, non–biodegradable, highly combustible or some combination of them all.[18,21,22] Many traditionally used solvents are also highly volatile, and can have lasting impacts on our atmosphere as a result of unintended release of solvents. As a result of the growing evidence showing that some current chemical processes are highly hazardous, there has been growing pressure to develop new processes and products that use materials that are more benign. This pressure has culminated in legislative measures such as the Registration, Evaluation, Authorisation and Restriction of Chemicals (REACH) regulation, which seeks to limit the extensive use

of hazardous chemicals in the pursuit of better protection of the environment in the European Union.[23]

The development of chemical processes which rely on replacement solvents that are less hazardous, waste minimizing and, potentially, more efficient, forms a cornerstone of sustainable chemistry.[22,24,25] The successfulness of these replacement solvents is not defined alone by their favourable sustainability credentials, but also how effective they are at performing the chemistry required of them. There are a number of resources made available now to aid researchers in the selection of solvents that could be an appropriate replacement for a hazardous, unsustainable solvent.[26–30] Additionally, a number of lesser known types of solvents have emerged in recent years which present themselves as alternative solvents with more sustainable credentials. Two popular groups of these solvents include supercritical–phase solvents, most notably carbon dioxide,[31,32] and ionic liquids.[33,34]

1.3 Ionic Liquids

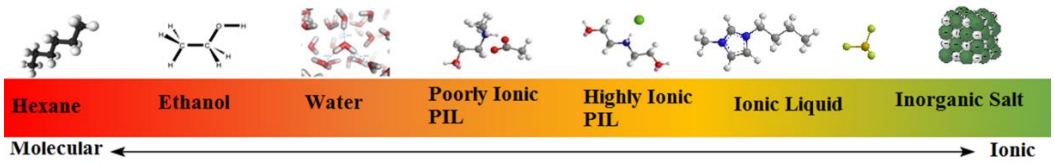

Figure 1.1 Scheme showing a qualitative continuum of chemical ionicity incorporating molecular solvents, ionic liquids and inorganic salts.

Ionic liquids (ILs) broadly encompass a class of liquid materials composed of ions. Depending on the conditions of the material, this could include compounds such as sodium chloride, which melts at around 800 °C to form a molten salt. However, it is the ILs that are composed of at least one organic (i.e. contains carbon) ion with melting temperatures below 100 °C that have typically been employed as solvents.[33,34] They initially drew much attention as solvents due to the high thermal stability and low volatility of many ILs, the

latter making them attractive in reducing volatile organic compound (VOC) emissions commonly attributed to solvents.[35] With the wide variety of structures of both anion and cation that can be used to make an ionic liquid, the concept of tuning the properties of ILs through modification of the structure of either ion helped to drive IL research.[34,36]

While many ILs have been showcased as solvents for applications,[33,34,36,37] there are many challenges faced with their application at commercial scale. The typical cost of an IL is several times greater than that of the solvents they are trying to replace, making many of them economically unfavourable as bulk solvents. ILs in general are also highly sensitive to impurities,[38] particularly atmospheric water, due to the hygroscopic nature of many ILs.[39] While distillation of ILs is possible, the high temperatures and low pressures required pose high energy barriers to distillation of many ILs.[40,41] This makes ILs a poor replacement for solvents where volatility is required for a process. Perhaps the most alarming shortcoming of ILs is that many IL structures have been found to be either acutely toxic or non–biodegradable.[42–45]

Does this mean that ILs are impractical solvents at industrial scales? The above statements are true for many ILs, typically those with a quaternary ammonium or phosphonium cation commonly referred to as aprotic ionic liquids (AILs). [42–45] Two other classes of solvents under the umbrella definition of ionic liquid are emerging as potentially more practical solvents with ionic characteristics. One being deep eutectic solvents (DES), an organic salt mixed with a hydrogen bonding compound to produce a liquid with lower melting point than either precursor.[46–48] The second being protic ionic liquids (PILs), defined as the product of the proton transfer from a Brønsted acid (HA) to a suitable base (B) to produce ionic species of the form ([HB][A]).[36,49–52] Both DES and PILs are prepared from straightforward mixing of precursors, generating no waste and requiring no additional work up. [36,46–52] This makes them both potentially more cost effective than AILs, while still having the potential to tune properties thanks to the wide variety of possible structures.[49]

1.4 Protic ionic liquids

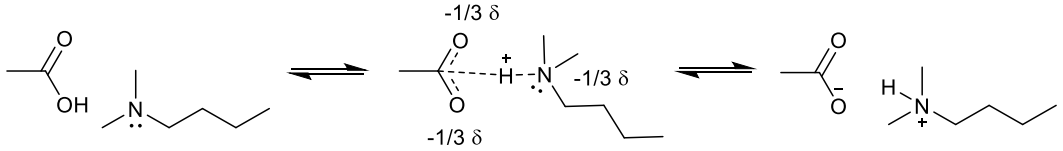

Figure 1.2 Scheme showing the proton transfer interaction between a Brønsted acid and base to produce a protic ionic liquid.

It has been widely acknowledged that the first paper that reported the preparation of an ionic liquid was from Paul Walden in 1914 for the PIL ethylammonium nitrate,[53] although salts formed from acid–base mixtures had been researched prior to his paper,[54] ethylammonium nitrate has a melting point of 12 °C, making it a room temperature ionic liquid (RTIL). It comes as some surprise that only in the 21st century has there been continued research interest in PILs. Nonetheless, there has been a healthy growth of original research on PILs, as evident from the multitude of review articles focusing on fundamentals and application of PILs.[36,50–52] It has even been shown that a PIL can occur in nature as well, with many more suggested to exist elsewhere.[55]

In addition to extensive research into their potential use in electrochemical applications as anhydrous fuel cells [56–60] and as pharmaceutically active compounds,[61–64] there has been extensive research showcasing the use of PILs as solvents for a range of important applications.[49] Perhaps the most notable is the the BASIL process, already used at industrial scale with great success.[37,65] In addition, topics such as natural product extraction,[66–68] biomass processing,[68–76] biocatalysis,[77–79] hydrometallurgy,[80–84] lubrication,[85–87] CO_2 capture[88,89] and fuel processing[90,91] have all seen PILs used with varying success.

In spite of these applications, the transition from laboratory to commercial scale raises questions about the use of PILs as solvents. As discussed in section 1.2, there is

increasing pressure to implement the use of less hazardous and more sustainable chemicals at industrial scales at all stages of its use. While PILs have ideal preparation procedures, this alone is insufficient to consider PILs as sustainable solvents. A critical assessment of many potential "green" credentials of a PIL as a solvent is required in order to make a rational judgement of their appropriateness as solvents at industrial scale.

1.5 Are protic ionic liquids green solvents?

When considering whether a chemical is considered to be low–hazardous or sustainable a.k.a. green, the 12 principles of green chemistry, outlined by Anastas and Warner, has been an excellent guideline to follow, if only as an introductory measure.[92] Indeed, principle no. 5 on their list promotes the use of innocuous auxiliary chemicals, including solvents, if they cannot be avoided completely. [92] Herein, how well PILs adhere to some of the more relevant principles is discussed.

Regarding atom economy (No. 2), the direct synthesis of PILs from the precursor components can readily be performed solvent–free and yields no by–products, and could therefore be considered 100% atom economic and also a low hazardous synthetic procedure (No. 3).[92] However, the precursor materials themselves must be prepared first, and the stages required to prepare the Brønsted acid and base are almost always less than 100% atom economic. This is true for most solvents, including AILs, but that there is no *additional* loss in atom economy when preparing a PIL from its precursor components is the point to remember.

Whether PILs can be considered to have low toxicity (No. 4) [92] remains an open topic for discussion due to the limited results available. To date, a select number of ammonium (primary, secondary and tertiary) carboxylate PILs has been screened for their microbial and ecological toxicity with varying results.[93–98] In a direct comparison with some common AILs, PILs have been shown to have much lower toxicity towards terrestrial

plant species.[99] Yet there had been no clear results to explore how systematic variation of the ionic nature of the IL influences its toxicity. In work carried out in parallel to this thesis, the author has explored how variation of anion, cation and ionic nature of a series of ammonium carboxylate ILs affects their bacterial and fungal toxicity.[100] In this work, it was found that the ionic nature of an IL appears to have minor contribution to the toxicity of an IL, whereas the lipophilicity of the cation proved to be the dominant influence of toxicity in the studied ILs. [100]

It is also worth noting that the mutagenicity of PILs had not been considered until very recently.[101] This is despite the suggested mutagenic activity of some common precursor amines used to make PILs. While mutagenic activity is not inherently a measure of toxicity, it is a further measure of the potential hazards a chemical can have upon exposure to the environment and humanity.[102–105] The author published the first results of the mini Ames test on a variety of PILs with varying anion and cation structure, providing the initial results to suggest PILs have low mutagenic activity.[101] However, it was stressed that the results do not definitively prove that PILs are non–mutagenic, and that further assessment is required before PILs could definitely be classified as non–mutagenic. [101,105]

The capability to prepare PILs from renewable feedstocks is imperative to their long–term feasibility as solvents (No. 7).[92] While fossil fuel–derived chemicals are the economically more viable option at the time of writing,[106] this will not always be the case as these reserves begin to diminish. The topic of chemical transformation of biomass to platform molecules has grown sensationally in recent times,[107–110] particularly molecules that could potentially be used as liquid fuel.[111–114]

Both amines and carboxylic acids, arguably the most commonly used PIL precursor materials, have been shown to be derivable from biomass sources.[109,115] A vast majority of the amines available commercially are derived from ammonia produced using

the Haber–Bosch process.[116] The functionalization of ammonia can be done with organic molecules from biomass feedstocks such as carbohydrates and soybean oil.[117,118]

Perhaps the most recognized bioderived carboxylic acid is acetic acid,[119,120] as the component of vinegar which gives it its sharp taste. Utilising submerged oxidative fermentation with bacteria from the genus *Acetobacter*, aqueous solutions of up to 12 % w/w acetic acid could be achieved within 24 hours.[121] There are also a number of other carboxylic acids that have been shown to be derivable from biomass resources using fermentation techniques, opening up a variety of potential biomass–derived PIL anions.[119,122] Finally, amino acids offer a convenient source of both amine–functionalized and carboxylic acid–functionalized building blocks; there are a number of ILs, both protic and aprotic, prepared with amino acid derived ions present in the literature.[123–130]

The low biodegradability of many AILs highlighted the need for caution when considering their possibility as green solvents (No. 10).[43,45,92] For PILs, the screening of biodegradability has often been carried out in parallel with toxicity screening.[95,97–99,131] This is because of the growing evidence showing a connection between toxicity and biodegradability of ILs, particularly microbial toxicity.[45,130,132–134] Many of the PILs screened have shown to be readily biodegradable based on standard procedures, such as CO_2 evolved or O_2 consumed. However, there are some PILs that have shown to not be readily biodegradable, yet the reasons why they do not fully decompose is not well understood.[97,98] Further study of the biodegradation products a.k.a. metabolites is necessary to understand the likely biodegradation mechanism and how structure of ILs influence this mechanism. [45,130,132–134] Ultimately, greater understanding of how ILs undergo biodegradation will allow for better design of ILs which are readily biodegradable and are of low toxicity.[100]

With these results, it is fair to say that PILs have the potential to be considered appropriate as sustainable materials. However, they also have the potential to be

unsustainable, particularly if they are completely inappropriate for their given role. A candidate green solvent must primarily be a good solvent for the task it has been chosen for, which requires a fundamental understanding of these materials. There has been significant research on the physical chemistry of PILs which has developed the understanding of these systems,[51,52] however there are some obvious gaps in the literature which are discussed below.

1.6 Residual Water in Ionic Liquids

A major challenge in the application of ILs in general has been the effect of water, and the same holds true for PILs also.[38,135] While many methods have been employed over the years to minimize impurity content during the synthesis of ILs, significant levels of atmospheric water can be absorbed into hygroscopic ILs during their application.[39,136] Even though a majority of the absorbed water can be removed through appropriate drying protocols, an increasingly substantial body of evidence strongly suggests that even trace concentrations of water can have a significant effect on the properties of ILs, posing challenges in their industrial application.[38,137–140] The ubiquitous nature of water in ILs leads to a realisation that studies on "pure" ILs may often actually be studies of IL–water mixtures in themselves.

It should be emphasized that the study of water–IL mixtures is of practical importance. This is because of the following reasons: (1) finer tuning of IL physical and solvation properties could be possible through mixing with other solvents, especially with water; [141–143] (2) residual water is often present in IL samples from their synthesis and the hygroscopic nature of many ILs will inevitably introduce small amounts of water when they are utilized unless they are prepared, stored and handled under anhydrous conditions,[38,136,144] so that permitting residual water in ILs seems to be more sustainable due to the energy required for the removal of water; (3) The costs associated with using an

IL–water mixture for a given process in place of the pure IL would be significantly reduced, due to the typical high costs of ILs with respect to water; (4) the addition of molecular solvents, such as water, to ILs can have anti–solvating effects, leading to the precipitation of a dissolved species;[66,145,146] (5) in the context of reason (4), water is regarded as the "greenest" solvent.[21,22,26,147]

Based on the available literature on the study of water–in–ionic liquid systems, there remain a number of unresolved questions on the interactions present in these systems.[148,149]

1.6.1 **Question 1** Does water exist as discrete molecules or clusters at low concentration in ILs?

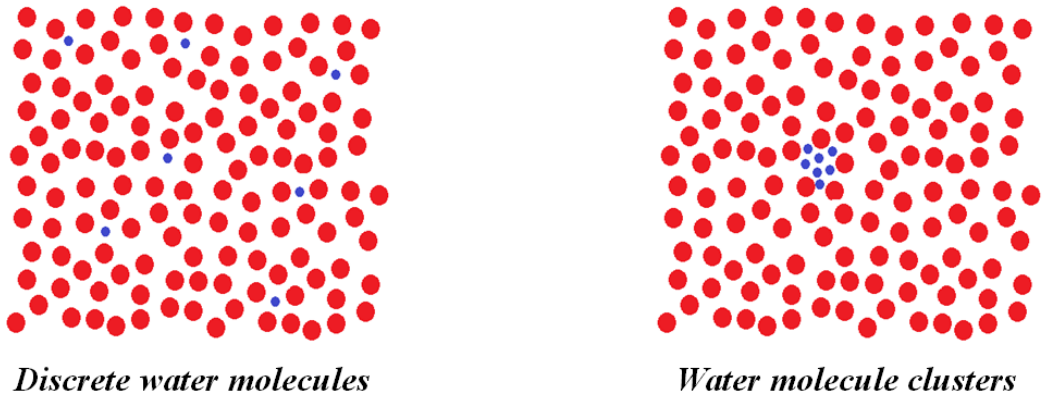

Figure 1.3 Schemes showing the two hypothesized states of water at low concentrations in Ionic Liquids.

The structure of water at low concentrations in ionic liquids has been debated extensively.[148,149] One popular hypothesis is that water molecules prefer association with the ionic liquid rather than each other at low water concentrations. This was first proposed by Cammarata *et al.*, who measured attenuated total reflectance (ATR)–infrared spectra of a range of ionic liquids with various anions and cations in the presence of low concentrations of water. This has led to the proposed hydrogen–bonding structure between two anions (anion…H–O–H…anion).[150] This same structure was later supported by the vibrational spectra of ionic liquids [BMIm][BF_4] and [BMIm][PF_6] with residual water,

that were best explained by anion–water–anion structures as calculated from density fluctuation theory calculations.[151,152] A combination of ^{1}H NMR and the local composition model also supported this hypothesis.[153,154]

Another hypothesis was that water molecules preferentially self–associate when at low concentrations in ionic liquids.[148,149] From the FT–IR spectra of [EMIm][BF_4], [BMIm][BF_4] and [BMIm][PF_6] with low concentrations of water, Lopez–Pastor showed that a small fraction of water exists as a dimer at low concentrations in the tetrafluoroborate anion ionic liquids and as a monomeric species in the hexafluorophosphate ionic liquid.[155] This conclusion was confirmed by the far–infrared spectrum of the same series of ionic liquids with residual water for hydrophilic ILs, whereas the water dimer was not observed in more hydrophobic ILs.[156] The idea that water molecules self–associate was developed further and made more explicit in the modelling of water uptake by ILs, in which the tetrameric form of water has been assumed to exist at low water concentration in ILs based on dialkylimidazolium cations.[157] Diffusion and conductivity measurements have also supported the view of nano–structuring of water within the solvent.[158]

1.6.2 Question 2 Does the presence of water weaken ion–ion interactions in ILs?

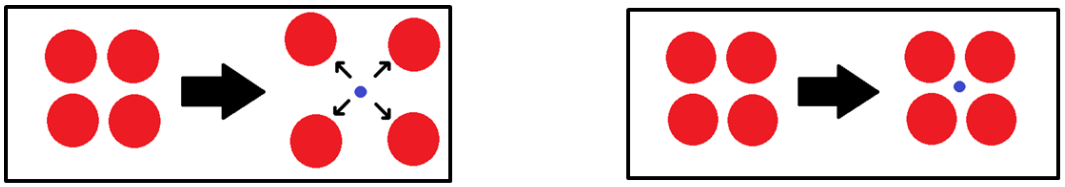

Figure 1.4 Schemes showing the proposed effects of water on the strength of average ion–ion interactions in Ionic Liquids.

It has also been suggested that cation–cation interactions (within dialkylimidazolium–type aprotic ionic liquids) become weaker due to the presence of water–cation hydrogen bonds.[148,149] Early evidence for this was based on nuclear

Overhauser enhancements (NOEs) of mixtures of [BMIm][BF_4] and water.[159] Brehm *et al.* used extensive *ab initio* calculations to propose that water can disrupt ring stacking interactions between dialkylimidazolium cations.[160] Further *ab initio* experiments from Shei *et al.* showed the disruption of anion–cation interactions in the presence of water at low concentrations, in addition to facilitating (anion…H–O–H…anion) interactions.[161]

Considering PIL–water mixtures, contact ion pairs (CIPs) as opposed to solvent–separated ion pairs (SIPs) were demonstrated to be most prominent in triethylammonium methanesulfonate ([TEA][MS]) water binary mixtures even at very high water concentrations. [162] This is supported by the work of Greaves *et al.*, demonstrating that certain PILs retain their mesostructure features in the presence of water, whereas the precursor materials do not when mixed with water. [163] However a study of the effect of water on the shear thinning of the PIL diethanolammonium acetate ([DEtAH][OAc]) suggested that less than molar equivalent quantities of water disrupt interactions between ions.[164] Indeed, many studies of the viscosity of PIL–water systems hypothesized that the presence of water disrupts ion–ion interactions through hydrogen bonding interactions.[165,166] Taking all of the above into consideration, there is no consensus as to whether water strengthens or weakens the IL–IL interaction.

1.6.3 Question 3 Does water interact more strongly with protic ILs than with aprotic ILs?

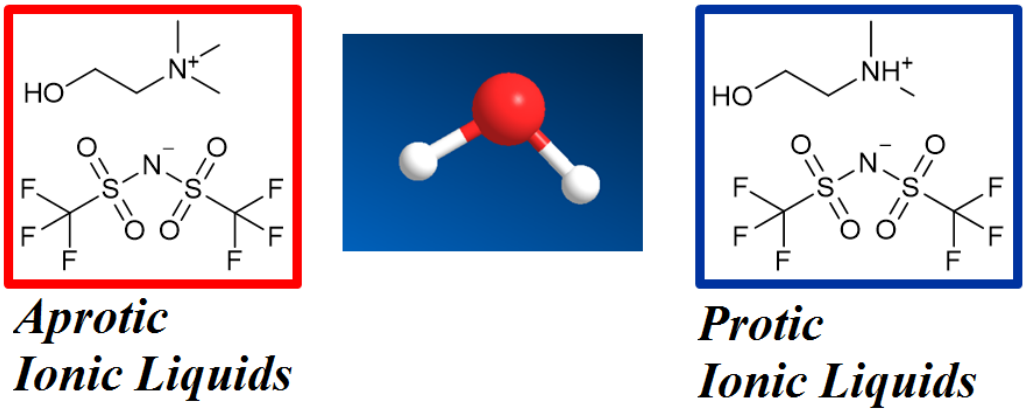

Figure 1.5 Diagram of analogous aprotic and protic ionic liquids.

That protic cations interact more strongly with water than their aprotic counterparts has been demonstrated by a comparison of the transport properties of analogous imidazolium aprotic and protic ILs, the cause of which was attributed to the tertiary N–H site of protic cations being able to hydrogen bond strongly with water, whereas the quaternary nitrogen on the aprotic cations could not. [167] This was complemented by a study of the effects of water on the vibrational spectra of two PILs; 1–ethylimidazolium trifluoromethanesulfonate ([EIm][OTf]) and 1–ethylimidazolium bis(trifluoromethanesulfonyl)imide ([EIm][NTf_2]), where similar water–cation vibration modes were observed in both systems.[168] The study also showed water–anion vibrational modes in the [EIm][OTf] system but not in the [EIm][NTf_2] system. These results suggest that water interacts differently between the two PILs and more favorably with [EIm][OTf] than with [EIm][NTf_2], contradicting the assumption that interactions between anion and water are related to the pK_a of the conjugate acid.[167,168] This view was best rationalized by the different polarization between the two PILs, not simply the acidity of the precursor

acid; water in methylammonium nitrate ([MA][NO_3]) becomes depolarized to a greater extent than in dialkylimidazolium ILs due to strong, directional hydrogen bonds. [169]

While the above investigations of analogous AIL and PIL mixtures with water appear to suggest stronger interactions between water and PILs, this does not represent a complete picture of IL–water interactions. The interactions between water and ILs have been inferred from the excess molar volume (V_m^E) and partial molar volume of species (V_i) of these binary systems from extensive density data.[170–175] The resultant deviations of molar volume from additivity suggest that both protic and aprotic ILs demonstrate weakening [176–179] and strengthening of interactions between ions and water.[165,180,181] The fact that both classes of ILs can demonstrate both strengthening and weakening of interactions with water implies that ionicity alone cannot explain the strength of interaction.

1.6.4 Question 4 Does the structure of PIL–water systems reflect homogeneous mixing or the formation of heterogeneous structures?

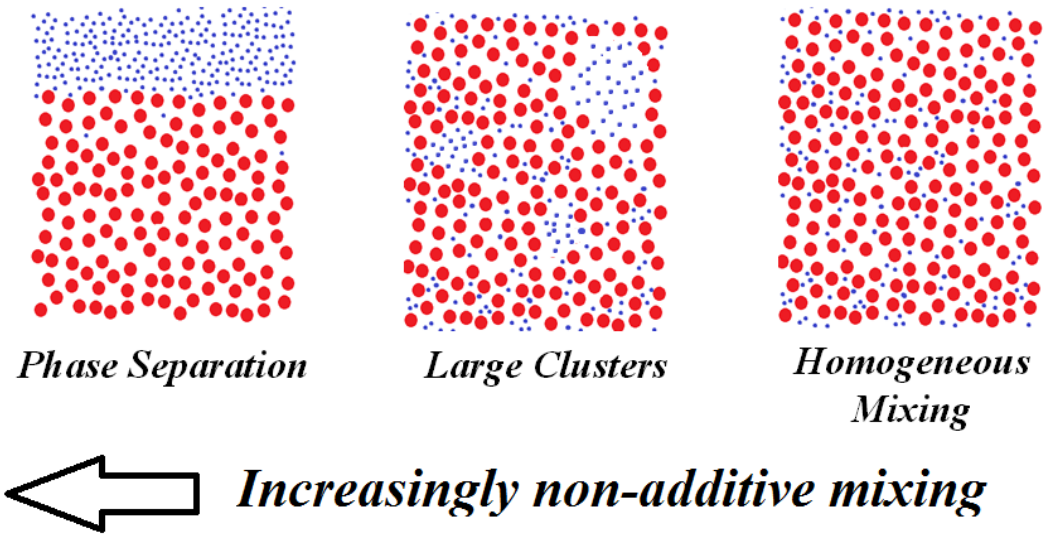

Figure 1.6 Scheme showing hypothetical mixing behaviour of ionic liquid and water systems.

Homogeneous distributions of water within mixtures have been reported by molecular dynamics simulations of the PIL ethylammonium nitrate ([EA][NO_3]).[182] This view is contradictory to a combined neutron diffraction and computational study of

[EA][NO_3] and water mixtures, which suggest that the local structure of each component resembles that of the pure materials in the polar domains.[183] The study did suggest that a modification of the PIL nanostructure is observed due to swelling of polar regions, increasing the interfacial curvature around the non–polar regions (the cation alkyl chain). The formation of heterogeneous structures in polar solvents is also supported by the Far–IR study of PILs in polar solvents.[184] This difference in the observed mixing behavior of water and protic ILs has been emphasized further by ethylammonium formate ([EA][Fr]) mixtures with water. The static dielectric constant, ε_0, of the [EA][Fr]–water system showed consistent ε_0 values up to 60% mole fraction of water.[185] However, measurements of polarity of [EA][Fr]–water systems with the probe molecule 12'–apo–b–carotenoic–12'–acid showed additivity of the observed polarity.[186] The fact that these different spectroscopic techniques seem to offer contradictory conclusions for identical PIL–water systems shows that there is still a poor understanding of the mixing behavior of these systems. Indeed, a lack of the theoretical basis behind some of the experimental techniques often leads to a misinterpretation of the results that feeds controversy.

1.6.5 IL–water systems: addressing the controversy

The questions posed here remain unanswered despite the extensive research taken place. Understanding the mixing behaviour of water at low concentration in PILs is essential for their application as solvents. This requires a strategy for answering all of these questions for a given water–PIL system with a robust theoretical basis. While spectroscopic and computational techniques are indispensable for understanding short–range interactions, they cannot fully appreciate long range interactions that may take place. Unfortunately, the interpretation of thermodynamic data, which can account for long range interactions, has not been found to relate to molecular interactions beyond mere speculation.

1.7 Characterization of Protic Ionic Liquids

For there to be progress on the application of PILs, there must also be progress on the fundamental understanding of the structure and interactions of PILs. By connecting how variation of a PILs structure influences the interactions between species, how said variations in structure influence the bulk properties of PILs relevant to their industrial application can be rationalized. In addition, clarifying how structural variation of PILs influences the interactions in PILs will prove to be indispensable in rationalising the solvation capabilities of PILs.

Establishing such a theoretical basis for PILs requires accurate characterization of these materials. In this context, three areas on the physical chemistry of PILs that underpin their use as solvents; (1) thermodynamics and bulk properties, (2) intermolecular interactions such as hydrogen bonding and (3) ionicity and proton transfer.

1.7.1 Thermodynamics and Bulk Properties of Protic Ionic Liquids

There is a lack in appreciation as to how the molecular interactions in PILs that emerge from the mixing of precursor acids and bases correlate with their bulk properties. Properties such as density and viscosity are valuable for the chemical engineering challenges involved with scaling up processes.[187,188] While prediction of some of these properties is feasible,[189,190] a rational understanding of their origin is not clear beyond fitting to an equation of state.[179,191,192] A more beneficial strategy is the characterization of the phase change behaviour of PILs. For example, it has been proposed that the glass transition temperature (T_g) can give insight into the non–additive mixing behaviour of PILs in general. [36,51,193–196] The effect of molecular structure on T_g and T_m (often not appearing due to the glassy nature of some PILs[197]) can give rise to structure–property trends that connect the molecular structure, liquid structure and bulk thermodynamic properties.[196,198–200]

Another important phase transition is from liquid to gas, highly relevant for PILs in general due to their capability of being distilled in an analogous fashion to conventional

organic solvents.[69–71] Yet there is limited insight given from analysis of the boiling point temperature (T_b), which imparts neither quantitative or mechanistic insight into this phase transition. The vaporization mechanism of PILs under the reduced pressure distillation conditions used in practice is still debated, a key open question being whether they vaporize as contact ion pairs, as discrete precursor molecules, or as mixtures with varying proportions of both types of species.[41,201–208] Standard molar enthalpies of vaporization, $\Delta_{\mathrm{vap}}H_m^{\circ}$, provide important information to address this question, as previously illustrated by a study on 1–methylimidazolium acetate, [MImH][OAc].[204] In this case, a good agreement was found between the $\Delta_{\mathrm{vap}}H_m^{\circ}$ value directly measured by vaporization calorimetry and the enthalpy of the reaction calculated from the enthalpies of formation, $\Delta_{\mathrm{f}}H_m^{\circ}$, of [PIL](l), Am(g), and Ac(g), determined from calorimetric experiments, *ab–initio* calculations, and literature data.[204] This gave a good indication that the vaporization of [MImH][OAc] predominantly yields its neutral precursors, namely 1–methylimidazole and acetic acid, as had been previously demonstrated by Fourier transform ion cyclotron resonance mass spectrometry (FTICR–MS)[41] and Raman spectroscopy.[201] A similar approach was also used to show that for the highly ionic PIL 1,1,3,3–tetramethylguanidinium nitrate, a vaporization channel yielding its gaseous constituent

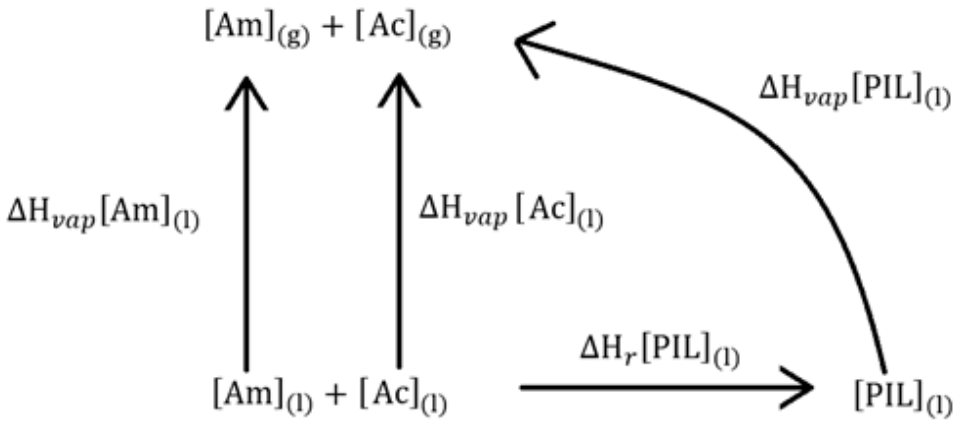

Figure 1.7 Thermodynamic cycle showing the processes involved in the direct vaporization of a PIL under reduced pressure to its precursor acid ([OAc]) and base ([Am]).

ions was implausible when compared to the pathway in which the neutral precursors were produced, eqn (1). This is consistent with the fact that ionic species were never found in PIL vapors produced by reduced pressure distillation.[41,201–203] It should nevertheless be stressed that the prime vaporization pathway of PILs may depend on the pressure–temperature conditions chosen for distillation. Indeed, there seems to be evidence that below 419 K the ethylammonium nitrate vapor essentially consists of ion pairs and above this temperature neutral precursors (ethylamine and nitric acid) progressively dominate.[208]

Besides their importance to understand the purification of protic ionic liquids by distillation, reliable $\Delta_{\mathrm{vap}}H_m^{\circ}$ and $\Delta_{\mathrm{f}}H_m^{\circ}$ data are also central in the investigation of molecular structure–energetics relationships in PILs. These relationships constitute, in turn, a very useful tool for the design of PILs with properties tailored for specific applications. For example, the enthalpy of vaporization of a PIL reflects its cohesive energy, which bears an obvious relation to structure and it is intimately connected to industrially relevant properties such as vapor pressure and solvation ability.

To date, only a small selection of PILs have been characterized energetically. The findings have nonetheless been significant, as demonstrated by the following two examples: (1) The PIL 1,5–diazabicyclo[4.3.0]non–5–enium acetate was comprehensively characterized from a thermochemical point of view, including the determination of $\Delta_{\mathrm{f}}H_m^{\circ}$ in the gas and condensed phases, and $\Delta_{\mathrm{vap}}H_m^{\circ}$. The obtained data subsequently provided fundamental information, , for cellulose processing such as energy requirements associated with PIL recovery.[209] (2) Differences in $\Delta_{\mathrm{vap}}H_m^{\circ}$ between protic and aprotic ionic liquids were found to correlate exceptionally well with the strength of intermolecular interactions as determined by far–infrared spectroscopy; furthermore, contributions to $\Delta_{\mathrm{vap}}H_m^{\circ}$ from

hydrogen bond and dispersion intermolecular interactions could both be inferred with the help of density functional theory.[210]

1.7.2 Intermolecular Interactions and Hydrogen Bonding

Perhaps the most commonly discussed aspect of PILs is their hydrogen bonding capabilities.[211] It is believed that the capability of PILs to form extensive hydrogen bonding networks gives them the solvation properties desirable for applications including protein stabilisation[212–215] and biomass processing.[216,217] As the ionic nature of PILs is also dependent on the proton transfer equilibrium in PILs, ionicity, hydrogen bonding and solvation capability are all related to one another. Characterizing the hydrogen bonding interactions in PILs therefore becomes an imperative task for understanding the molecular origin of the solvation capabilities of PILs.

One of the most versatile techniques to study hydrogen bonding in PILs is vibrational spectroscopy. The vibrational frequencies associated with the anion–cation interactions in a number of PILs has been shown to exist in the far infrared (FIR) region.[184,218–222] The FIR region can allow for the distinction in the types of short–range interactions in analogous protic and aprotic ILs due to the absence of peaks corresponding to the cation–anion hydrogen bond unique to PILs.[222,223] These findings were confirmed to be the anion–cation hydrogen bonding interactions by density functional theory (DFT) calculations. The calculated strength of these hydrogen bond interactions for various PILs correlated well with the observed shift in the vibration frequencies.[220] There has even been correlation of the frequencies of these hydrogen bonding interactions and the standard molar enthalpy of vaporization of PILs.[210]

The stretching vibrations of the N–H bond in some PILs have been observed in the FT–IR region between 3000 – 3500 cm^{-1}, however the overlap of C–H stretching vibrations make this difficult for all PILs.[224,225] Femtosecond FT–IR had been employed to observe

the Rotational motions of ethylammonium nitrate, showing large, angular jumps. These rotational motions further reinforcing the highly direction–dependent nature of the hydrogen bonding interactions in PILs.[226] Terahertz Spectroscopy of ethylammonium nitrate has also been undertaken to characterize the dynamics of the hydrogen bonding between ions as a damped harmonic oscillator.[227,228] Further studies of the hydrogen bonding in ethylammonium nitrate and propylammonium nitrate suggested further evidence of heterogeneous liquid structure forming as a result of hydrogen bonding interactions between anion and cation.[229,230]

These techniques, particularly FIR spectroscopy, have given valuable insight into the intermolecular hydrogen bonding interactions present in PILs. Yet to date, there have been only a small number of PILs studied using these techniques. The effect of additional functional groups (i.e hydroxyl, amino) on the types of intermolecular interactions have not been studied experimentally. Additionally, there have been no studies on carboxylate anions, which have been utilized for a number of potential applications (see section 1.4).

1.7.3 Ionicity and Proton Transfer

The extent of proton transfer in PILs has sparked significant controversy as to whether they should be considered as ILs at all.[231] Yet the understanding as to what governs the extent of proton transfer has not developed significantly.[51] The correlation between the conductivity and the fluidity (inverse of viscosity) have been widely used to understand the ion mobility or ionicity of PILs through the Walden relation.[51,58,194] Walden relations characterize the system in qualitative terms of ion mobility, where “good” ionicity ILs have trends comparable to a reference electrolyte solution and “poor” ionicity ILs have much lower ionicity than as expected from fluidity (figure 1.8). This relation is convenient when discussing the transport properties of the bulk system, but does not aid in understanding the proton transfer equilibrium. For example, a PIL which can have high extent of proton

transfer may result in being a “poor” ionic liquid due to the strong hydrogen bond interactions between anion and cation reducing ion mobility.[51]

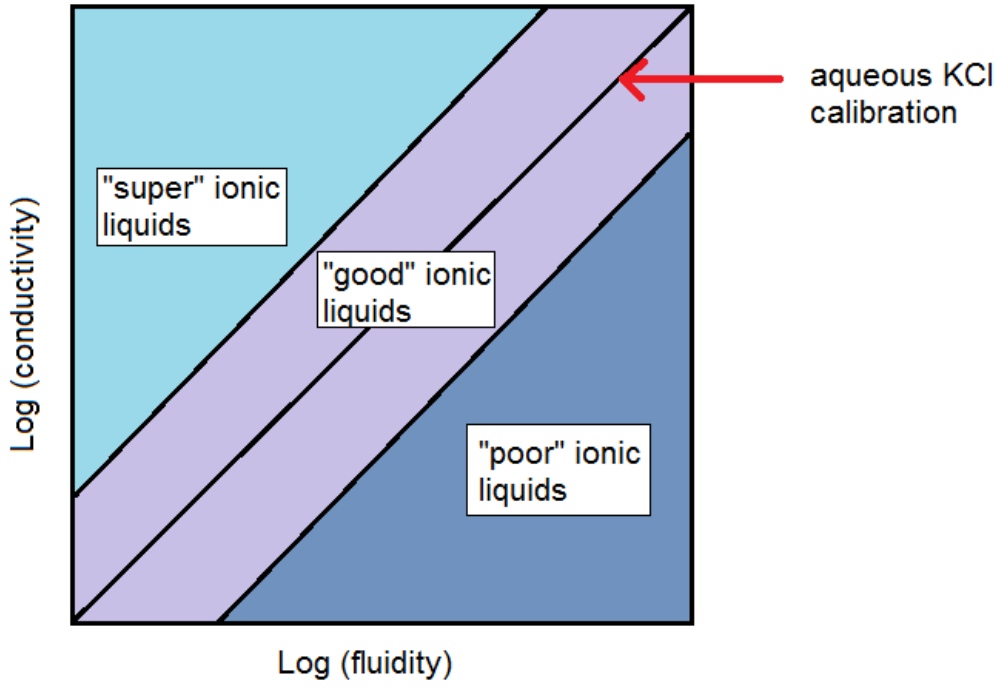

Figure 1.8 A qualitative representation of the Walden plot used to profile the ionicity of materials (here specified in the context of ionic liquids).

Another common way that the extent of proton transfer has been estimated is from the difference in aqueous proton dissociation constants of the precursor acid and conjugate acid (ΔpK_a).[193,194] For PILs, many have debated what an appropriate ΔpK_a would be to ensure proton transfer is effectively (i.e. > 99%) complete. However, it has already been shown that interpreting ΔpK_a as a cross–comparative measure of proton transfer for PILs can lead to erroneous results.[232] From earlier studies of proton transfer in diluted systems (i.e. a proton donor and acceptor at low concentration within a diluent solvent or gas.), it was widely appreciated that ΔpK_a values indicating a certain extent of proton transfer had taken place changes significantly from system to system.[233–236] In these studies, the extent of proton transfer is typically inferred from the presence of spectroscopic signal characteriztic of the ionic species. [233–243] Perhaps a more constructive approach to

determining the proton transfer interaction in PILs can be done through spectroscopy as oppose to empirical relations.

Broadly speaking, the two most commonly used spectroscopic techniques to study the proton transfer reaction in acid–base systems are NMR and infrared spectroscopy. [233–243] Yet there are only a small number using these techniques in the context of PILs. Correlations between the gas phase proton affinity of the precursor acid and the ^{1}H chemical shift of the labile proton of a series of PILs with the triethylammonium cation showed to be a better indicator of the extent of proton transfer than the difference in aqueous pKa of precursors (ΔpKa).[244] Studies of the ^{15}N chemical shift changing from pure amine to PIL indicated a gradual downfield shift of the single peak, suggested to indicate systematic proton transfer occurring.[245]

For carboxylate PILs, the FT–IR region can give insight into the ionic nature of a PIL through the relative intensities of vibrational bands unique to the acetate species and the carboxylic acid species. The asymmetric stretching frequency of the carboxylate functional groups occurs between 1550–1600 cm^{-1}, whereas the carbonyl stretching frequency of a carboxylic acid group has a distinctly sharp peak for liquid samples around 1710 cm^{-1}.[233,246] Recent work has shown that this spectral feature correlates with other properties of PILs such as conductivity where ΔpKa does not correlate well,[247,248] and clarified that some systems do not undergo proton transfer, despite being composed of a proton donor and acceptor, such as acetic acid and pyridine.[249]

Other techniques to study the nature of the protons in PILs include the hydrogen redox potential of H_2–saturated PILs, where the potential gap between the redox reactions correlated well with the proton affinities of both anion and cation.[56,57,250,251] Recent work using quantum chemical approaches such as density functional theory and valence band theory have been used to explore the proton transfer reaction for single ion pairs.[252–254]

While useful from a theory standpoint, the translation of such small scale simulations to the interactions in bulk liquids remains challenging.

By applying the variety of experimental techniques described above, connections between the bulk physical properties and the interactions at the molecular level can be evaluated. Similarly, connecting how the variance of molecular structure influences these interactions at both a bulk property scale and on the basis of short range interactions will yield a more in–depth understanding of structure–property interactions. To date however, there is limited data available which attempts to combine structure–property relationships at both bulk property scale and at a molecular level for tertiary ammonium carboxylate PILs.

1.8 Solvation Environment in Protic Ionic Liquids

Understanding how a variation in either anion or cation structure can influence the solvent properties of a PIL is crucial for the design a PIL for a given task. Yet the fundamental understanding of the solvation properties of PILs in general is still limited. While understanding the interactions of neat PILs will support our understanding of their solvation behaviour, only by studying (PIL + solute) systems can the solvation behaviour of PILs be developed.[255] The true benefit of characterizing the interactions in PILs, as described in section 1.7, is when this physicochemical insight can be used to rationalize the apparent solvent properties of PILs.

Perhaps the most widely used technique to characterize the solvent properties of PILs have been to use solvatochromic probes to calculate solvent–solute interaction parameters.[50] While a range of probe molecules have been used to characterize the non–specific polarity of PILs,[186,256] perhaps most popular are the pyridinium *N*–phenolate betaine dyes popularized by Reichardt.[257–259] Yet a single parameter is an insufficient description of solvent–solute interactions, particularly when hydrogen bonding interactions

play a crucial role, as is the case with PILs. Multiple contributions to solvation can be characterized independently from one another as outlined by Kamlet and Taft.[260] Specific solvent–solute interactions i.e. hydrogen bond donor acidity (α) and hydrogen bond acceptor basicity (β), as well as non–specific solvent–solute interactions such as dipolarity/polarizability (π^*), can be parameterized using multiple solvatochromic probes. These parameters have been characterized for a small number of PILs,[256,259,261] as well as a number of PIL–solvent binary mixtures.[262–265] However, there has been no previous work attempting to rationalize the calculated solvent–solute interaction parameters with the short–range interactions. A molecular understanding of what governs the solvent–solute interactions in PILs will greatly support the design of new protic ionic liquids with particular solvation properties.

While solvent–solute interactions are important, solvation is also dependant on solvent–solvent interactions.[4,260,266] In the correlations outlined by Kamlet and Taft to determine linear solvation energy relations (LSER), they accounted for solvent–solvent interaction strength through the Hildebrand solubility parameter.[260,266] These values can be determined from the cohesive energy density of a solvent, calculated from the standard molar enthalpy of vaporization and molar volume.[267] While quantifying the standard molar enthalpy of vaporization for PILs has been undertaken (see section 1.7.1), the cohesive energy density has not been determined for a PIL, and as such solvent–solvent interactions have not been considered previously for PILs.

Parameterising the solvent–solute or solvent–solvent interactions in PILs is insufficient to understand their properties as solvents. Rationalising these interactions at a molecular level will give the necessary insight required to understand how variation of PIL structure can influence its solvation environment. This connection between molecular structure and solvation property will improve understanding of how the solvation capability changes between precursor and PIL.

1.9 Protic Ionic Liquids; Just Equimolar Acid and Base Mixtures?

While PILs may yet find their place as new sustainable solvents (section 1.4), the study of acid–amine binary mixtures has been carried out for many decades.[268,269] The phenomena of a stable equimolar compound of ionic nature (albeit, usually a solid) was considered to be but one part of the continuum of these binary liquid systems. [268,269] This is exactly how a PIL has been defined, with the additional criteria of being a liquid. Systems typically focused around the combination of carboxylic acids with ammonia or primary, secondary or tertiary amines using relationships typical of binary liquid systems. They generated significant interest due to the combination of complementary hydrogen bonding components i.e. a hydrogen bond donor (acid) and acceptor (base).

Some of the earliest studies of acid–amine binary mixtures focused on the effect of composition on particular phase changes. By inspecting the change in melting point of acid–amine binary mixtures, the formation of stable, non–equivalent association complexes, both amine–rich and acid–rich, had been found to be stable.[268,270] Similar results could be deduced from the study of the boiling point–vapor composition with respect to composition.[269] The same study also showed that some acid–amine binary mixtures, such as the equimolar combination of acetic acid and triethylamine, are immiscible. This insight has been discussed by some more recent authors in the context of synthesising PILs, leading to speculation as to proper procedures to preparing these compounds.[271–273]

Studying excess molar properties, i.e. deviations from additive mixing behaviour (analogous to Raoult's law of mixing for ideal gases), can give qualitative insight into how interactions between species change upon mixing. Properties such as excess Gibbs free energy and excess molar volume have been explored for a number of acid–amine binary mixtures, often showing negative deviations from additive mixing.[274–278] This is also

supported by the limited data showing quantitatively the highly exothermic enthalpy change upon mixing of some carboxylic acids and amines.[274,278] While not an excess property, bulk viscosity of acid–amine binary mixtures has shown extensively how the net molecular cohesion changes significantly with respect to composition.[279] Extreme positive deviations indicated significant increase in the molecular cohesion in these types of systems, with maxima often occurring at acid rich compositions.[277,278,280,281]

Spectroscopic studies of non–equivalent acid–amine binary mixtures have also shown how molecular interactions and electrostatic effects change with composition. Infrared spectroscopy has shown that the proton transfer equilibrium changes with composition in some systems.[282,283] It has also been used in parallel with quantum chemical calculations to identify the formation of non–equimolar stable association compounds.[284,285] Similarly, NMR spectroscopy has been used mostly to investigate how the electron distribution and subsequent nature of the amine species change with composition.[245,275,286] Dielectric permittivity has been used to characterize both the bulk polarity and molecular re–orientation dynamics of multiple acid–amine binary mixtures.[277,278,281] To summarize broadly, spectroscopic techniques often support what has been suggested with thermodynamic techniques; in many acid–amine binary mixtures, there is evidence of non–equivalent acid–amine association compounds forming, typically featuring an excess of acid.

From the literature on non–equivalent mixtures, there is extensive evidence that 1:1 acid–amine or anion–cation compounds are not the only stable species that are likely to exist in a carboxylic acid–amine binary mixture. To date, there have been some papers that have attempted to make connections between the properties of the equimolar mixture (PIL) in the context of the complete acid–amine binary mixtures.[57,194,245,250] However none of these studies focus on the various interactions between species and how this relates to the solvation properties of these types of systems.

1.10 The Scope of the Thesis

The oft–mooted application of Protic Ionic Liquids as "designed solvents" requires a detailed understanding of both their solvation and physicochemical properties and how these properties may rationally be varied through changes in functionality and composition. Based upon the above survey of the current gaps in understanding of PIL systems, the following systems will be studied;

1. Binary systems of water and ILs (both aprotic and protic) at low water concentrations.
2. The equimolar binary mixture of a Brønsted acid and base, a "pure" protic ionic liquid.
3. Non–equivalent mixtures of a Brønsted acid and base.

For each of these systems, how the molecular interactions change as a result of mixing compared to the starting materials will be clarified. As each system requires different approaches to the characterization of interactions therein, various experimental and theoretical techniques to study these systems have been utilized.

To characterize the interactions in ionic liquid water mixtures, specifically at low water concentrations, the statistical mechanical theory of solutions initially outlined by Kirkwood and Buff,[287] which has been extended to be applicable to molecular and macromolecular solution mixtures,[288–291] has been applied. The Kirkwood–Buff (KB) theory of solutions has a proven track record for characterizing the mechanism of solvation in many systems, ranging from biochemical processes to pharmaceutical formulations.[287–299] Using KB theory, the intermolecular interactions are summarized as Kirkwood Buff parameters, G_{ab} which are directly related to the pairwise correlation function between the two species, $g_{ab}(r)$, using the following relation;

$$G_{ij} = \int \left[g_{ij}(r) - 1 \right] 4\pi r^2 \, dr \qquad 1.1$$

The KB theory has already been used to describe the solvation capabilities of some aprotic ILs based on molecular dynamics results,[300–302] while the small angle neutron scattering profile of the binary mixture of 1–butyl–3–methylimidazolium tetrafluoroborate at low concentrations in water was interpreted using KB interaction parameters.[303] For the first time, the interactions in IL–water binary mixtures at low water concentrations have been clarified using statistical thermodynamic theory, addressing the controversies outlined in section 1.6. These interactions are initially determined for well–studied IL–water binary mixtures and relate our results with previous experimental evidence (Chapter 2).[148] Using the same derivation of KB theory, the KB parameters for three IL–water systems to explore the difference between aprotic and protic IL–water binary mixtures (Chapter 3).[149]

In considering the neat PIL system in the context of equimolar mixing of a Brønsted acid and base, the effect of varying the functional groups on the precursor base to influence the properties of the PIL has been studied. Attention was focused on three key tertiary ammonium acetate PILs, based on their suggested favourable green credentials (see section 1.5). Four characteristics are explored; (1) the position of the proton transfer equilibrium as inferred from infrared spectroscopy, (2) the standard molar enthalpy of vaporization ($\Delta_{\mathrm{vap}}H_m^{\circ}$) and the mechanism of vaporization under reduced pressure, (3) solvent–solute and solvent–solvent interactions based on the Kamlet–Taft parameters and (4) bulk viscosity (Chapter 4). The cross–comparison of the effect of functional group modification for each of these characteristics will give a coherent starting point in understanding how molecular structure influences the molecular interactions in PILs, and how this in turn influences their thermodynamic and solvation properties.

To further expand on the relation between PILs and their precursor, the mixing behavior of the three acid–amine mixtures has been characterized to clarify the effect of varying amine structure on the mixing behavior towards a better understanding of the structure–property relationships in PILs. Combining spectroscopy, bulk property

characterization and solvation profiling, four aspects of the acid–amine mixtures are clarified; (1) the intramolecular bonding in both acid and base species and the state of the proton transfer equilibrium, (2) the intermolecular hydrogen bonding interactions between species, (3) density and excess molar volume, and (4) the solvation properties of the acid–amine binary mixtures. A connection of the short–range interactions with bulk physical properties will give a rational basis for the mixing behavior of the acid–amine binary mixtures (chapter 5). The final aspect attempts to rationalize extensive empirical data on the solvation properties of the acid–amine mixtures. By relating back to the physical chemistry of these systems, an explanation as to how variation of both amine functionality and composition can influence the solvation properties of these mixtures can be proposed (chapter 6).

Chapter 2: Statistical Thermodynamics of Ionic Liquid–Water Binary Mixtures at Low Water Concentrations

2.1 Introduction

How do residual water molecules in ionic liquids (ILs) interact with themselves, as well as with the ions? This question is crucial in understanding why the physical properties of ILs – and chemical reactions performed in them – are strongly affected by the residual water content.[148] As discussed in Chapter 1, there are two poorly answered questions regarding the structure and behaviour of the residual water: (i) Does water exist as discrete molecules or clusters at low concentration in ILs? (ii) Does the presence of water weaken ion–ion interactions in ILs?

Answering these questions has been hindered by the complexity and long range of the interactions in the water–IL mixture, as well as by the often profound differences in physical structure between various different ILs.[148,149] Herein, a strategy is presented to resolve these questions through a combination of a rigorous statistical thermodynamic theory (Kirkwood–Buff theory) with density and osmotic data from the literature.[148,149] The unique advantage of this approach is that the KB theory is rigorous, i.e, the theory does not involve any approximations.[287,304]

The goal of this chapter is to answer the questions stated above, thereby clarifying the role of residual water in ILs. By utilising the Kirkwood–Buff (KB) statistical thermodynamic theory of solutions, information on water–water, water–ion and ion–ion interaction in the mixture can be quantified in terms of KB parameters.[148,149] Based on the KB parameters, answers to the two questions stated above are given for three IL–water binary mixtures, featuring the ILs 1–butyl–3–methylimidazolium tetrafluoroborate, 1–ethyl–3–methylimidazolium tetrafluoroborate and 1–ethyl–3–methylimidazolium triflate.

2.2 Statistical thermodynamic theory of water–IL mixture

2.2.1 KB theory of binary mixture derived from inhomogeneous solution theory

Towards the resolution of conflicting hypotheses reviewed in sections 1.6 and 2.1, thermodynamic data can be used to reveal the structure of IL–water mixtures, based upon the well–established KB theory for binary mixtures.[288,289,291,303,305] A full derivation of this theory will be presented here, because (i) a strong non–ideality of water–IL mixture necessitates a careful analysis of experimental data and (ii) a novel, alternative derivation, which is simpler than the conventional route, is made possible through the use of inhomogeneous solution theory.[304]

Consider a mixture of water ($i = 1$) and IL ($i = 2$). Following the standard approach well–established for dissociative species, the IL is considered as the (averaged) ions for species 2 (because the composition is always equivalent, it is not possible to study the effects of changing either the cation, or anion, composition alone). [288,291,305] The grand potential J can be expressed in terms of grand partition function Ξ in the following manner:

$$J = -kT \ln \Xi(V, \mu_1, \mu_2) \tag{2.1}$$

where μ_i is the chemical potential of the species i, V is the volume of the system; the temperature T, which is kept constant throughout the discussion, is omitted.[304] Here, two systems are considered: with and without the water molecule fixed at the origin. [304] When the fixed water molecule is present, it acts as the source for an external field for the water molecules and ions. Such a solution is inhomogeneous. When the fixed water molecule is absent, the system consists only of water and ions, and is homogeneous. The chemical potential of the fixed water molecule μ_1^* can be expressed in terms of the grand partition functions of the homogeneous Ξ_0 and inhomogeneous systems Ξ_1 in the following manner:

$$\mu_1^* = J_1 - J_0 = -kT \ln \frac{\Xi_1(V_1, \mu_1, \mu_2)}{\Xi_0(V_0, \mu_1, \mu_2)} \tag{2.2}$$

where V_1 is the volume of the inhomogeneous system, V_0 is of the homogeneous system. [304] From Eq. (2.2), the following fundamental relationship is applied:

$$-d\mu_1^* = kT\sum_i\left[\frac{1}{\Xi_1}\frac{\partial\Xi_1}{\partial\mu_i} - \frac{1}{\Xi_0}\frac{\partial\Xi_0}{\partial\mu_i}\right]d\mu_i = \sum_i[\langle N_i\rangle_1 - \langle N_i\rangle_0]d\mu_i \quad (2.3)$$

where $\langle N_i\rangle_1$ is the number of molecules of the species i in the inhomogeneous system, whereas $\langle N_i\rangle_0$ is that of the homogeneous system. Note that effect of the fixed water molecule is localized; this is satisfied when $V_1 - V_0 = o(1)$. Consequently, in the following, $V_1 = V_0 \equiv V$. [304]

The next goal is to simplify Eq. (2.3) using another relationship between μ_1 and μ_2. This can be executed by considering the hydrostatic pressure P of the system, which can be obtained from the grand partition function as[304]

$$P = \frac{kT}{V}\ln\Xi(V,\mu_1,\mu_2) + o(1) \quad (2.4)$$

which is valid both for inhomogeneous and homogeneous systems (hence has been presented without the subscript 0 or 1). From Eq. (2.4), it easily follows that[304]

$$dP = \sum_i\frac{kT}{V}\frac{1}{\Xi}\frac{\partial\Xi}{\partial\mu_i}\,d\mu_i + o(1) = \sum_i\frac{\langle N_i\rangle}{V}d\mu_i + o(1) \quad (2.5)$$

which is the Gibbs–Duhem equation. Combining Eqs. (2.3) and (2.5) under constant pressure ($dP = 0$), the following is obtained:

$$-d\mu_1^* = \left\{[\langle N_1\rangle_1 - \langle N_1\rangle_0] - \frac{\frac{\langle N_1\rangle_0}{V}}{\frac{\langle N_2\rangle_0}{V}}[\langle N_2\rangle_1 - \langle N_2\rangle_0]\right\}d\mu_1 \quad (2.6)$$

Now the chemical potential of the fixed water μ_1^* can be related to μ_1 through the following well–known formula: [289,304]

$$d\mu_1^* = d\mu_1 - kTd\ln\frac{\langle N_1\rangle_0}{V} \quad (2.7)$$

Combining Eqs. (2.6) and (2.7) obtains the following:

$$\left(\frac{\partial\mu_1}{\partial\ln n_1}\right)_{T,P} = \frac{kT}{1+[\langle N_1\rangle_1-\langle N_1\rangle_0]-\frac{\frac{\langle N_1\rangle_0}{V}}{\frac{\langle N_2\rangle_0}{V}}[\langle N_2\rangle_1-\langle N_2\rangle_0]} \quad (2.8)$$

Rewriting Eq. (2.8) using the conventional notation: the number density $n_i = \frac{\langle N_i \rangle_0}{V}$ and the KB integrals defined as[296,304]

$$G_{ij} = V \frac{\langle N_j \rangle_i - \langle N_j \rangle_0}{\langle N_j \rangle_0} \tag{2.9}$$

Eq. (2.8) can then be simplified as:

$$\left(\frac{\partial \mu_1}{\partial \ln n_1}\right)_{T,P} = \frac{kT}{1+n_1(G_{11}-G_{12})} \tag{2.10}$$

Eq. (2.10) connects the thermodynamic data (l.h.s.) to the difference of KB integrals ($G_{11} - G_{12}$). The significance of the KB integral is that it is the measure of solution structure. This can be seen most clearly by rewriting Eq. (2.9) in terms of the radial distribution function between the species i and j, $g_{ij}(r)$ (where r is the distance between the centres of mass of i and j molecules), as[148,149,287–289,291–296,304–306]

$$G_{ij} = \int dr 4\pi r^2 \left[g_{ij}(r) - 1\right] \tag{2.11}$$

G_{ij} usually takes negative values, reflecting the contributions from small r where $g_{ij}(r) = 0$ due to steric repulsion, which contributes negatively to G_{ij}; however, if an attractive interaction exists between i and j, $g_{ij}(r)$ exhibits peak values much greater than 1, which contributes positively to G_{ij}. Thus G_{ij} reflects the excluded volume, as well as attraction between i and j.

Eq. (2.10) is well known in the KB theory of two–component solutions, which has been derived mainly via the inversion of two–component KB theory,[289,291] or via a pair of Gibbs–Duhem equations for a three–component system in the vicinity of the solute and in the bulk.[288,292–296,304,306] The present derivation is much simpler and more transparent, due to the explicit introduction of inhomogeneous solution theory.

In the following, a full theoretical background and procedure on how to determine G_{11}, G_{12} and G_{22} individually from experimental data is presented, even though the equations derived from the inversion of KB theory are well–known and have been widely used.[288,289,291–296,303–306] This is indispensable due to the strong non–ideality of our systems,

as well as the sizeable disparity in interactions, which necessitates a special care towards an accurate determination of the KB integrals, especially towards the low water concentration limit. The calculation procedure is therefore explained below in more detail than would be necessary for simpler mixtures.

2.2.2 Determination of ion–water and water–water KB integrals

Our first goal is to determine G_{11} and G_{12} from published data. To do so, let us first start from Eq. (2.6), and relate $G_{11} - G_{12}$ to the experimental data. Note that an equilibrium condition exists, $\mu_1 = \mu_1^{vap}$, where μ_1^{vap} is the chemical potential of the water vapor and consists of the following intramolecular and translational contributions: [288,289,291–296,303–306]

$$\mu_1^{gas} = \mu_1^{intra} + kT \ln n_1^{vap} \Lambda_1^3 \tag{2.12}$$

where Λ_1^3 is the momentum partition function and n_1^{vap} is the density of water vapor. Note that neither μ_1^{intra} nor Λ_1^3 depend on n_1, hence Eq. (2.10) can be simplified into the following form:

$$n_1(G_{11} - G_{12}) = \left(\frac{\partial \ln n_1}{\partial \ln n_1^{vap}}\right)_{T,P} - 1 \tag{2.13}$$

where n_1^{vap} can be obtained directly from the vapor pressure P^{vap} and the ideal gas equation of states.

In order to determine G_{11} and G_{12} from experimental data, an additional, independent equation is needed which involves these two parameters.[292–296,304,306] Such an equation can be obtained from the pressure derivative of Eq, (2.3), which yields:

$$(n_1 G_{11} + 1)V_1 + n_2 G_{12} V_2 - RT\kappa_T = 0 \tag{2.14}$$

where V_i is the partial molar volume of the species i, and κ_T is the isothermal compressibility of the solution mixture, which, again, is negligibly small. Using Eq. (2.13), Eq. (2.14) can be rewritten into the following parallel form:

$$G_{12} \equiv G_{21} = -V_1 \left(\frac{\partial \ln n_1}{\partial \ln n_1^{vap}}\right)_{T,P} + kT\kappa_T \tag{2.15}$$

where $n_1V_1 + n_2V_2 = 1$, whch can easily be derived from Eq. (2.5), was used in conjunction. Note that $G_{12} \to -V_1 + kT\kappa_T$ at $n_1 \to 0$, which can be derived easily by the help of Eq. (2.10). This clarifies the limiting behaviour $\left(\frac{\partial \ln n_1}{\partial \ln n_1^{vap}}\right)_{T,P} \to 1$ as $n_1 \to 0$. Combining Eqs. (2.13) and (2.14), the following expression for G_{11} is obtained:

$$G_{11} = \frac{1}{n_1}\left[n_2V_2\left(\frac{\partial \ln n_1}{\partial \ln n_1^{vap}}\right)_{T,P} - 1\right] \tag{2.16}$$

The KB integrals G_{11} and G_{12} can thus be determined from experimental data through Eqs. (2.15) and (2.16).

The form of Eq. (2.16) shows that special care is required in obtaining G_{11} at low water concentrations; as n_1 becomes smaller, n_2V_2 tends to 1, as well as $\left(\frac{\partial \ln n_1}{\partial \ln n_1^{vap}}\right)_{T,P}$ – hence the calculation of G_{11} requires a careful evaluation of $n_2V_2\left(\frac{\partial \ln n_1}{\partial \ln n_1^{vap}}\right)_{T,P}$ at low n_1.

2.2.3 Determination of ion–ion KB integral

The presence of water in ILs has been postulated to weaken ion–ion interactions (Section 1.6.2). To answer this question,[159–166] let us determine the ion–ion KB integral, G_{22} in the presence of residual water. Exchanging the indices 1 and 2 in Eq. (2.10), and combining it with the Gibbs–Duhem equation (Eq. (2.5) with $dP = 0$), the following equation is obtained:

$$\left(\frac{\partial \mu_1}{\partial n_2}\right)_{T,P} = -\frac{kT}{n_1[1+n_2(G_{22}-G_{21})]} \tag{2.17}$$

which is consistent with the result from KB inversion.[292] Combining Eq. (2.17) with Eq. (2.13), the following simple expression analogous to Eq. (2.13) is obtained:

$$n_1(G_{21} - G_{22}) = \left(\frac{\partial \ln n_2}{\partial \ln n_1^{vap}}\right)_{T,P} + \frac{n_1}{n_2} \tag{2.18}$$

Note here that

$$\left(\frac{\partial \ln n_2}{\partial \ln n_1^{vap}}\right)_{T,P} = \left(\frac{\partial \ln n_1}{\partial \ln n_1^{vap}}\right)_{T,P}\left(\frac{\partial \ln n_2}{\partial \ln n_1}\right)_{T,P} = \frac{n_1}{n_2}\left(\frac{\partial n_2}{\partial n_1}\right)_{T,P}\left(\frac{\partial \ln n_1}{\partial \ln n_1^{vap}}\right)_{T,P} \tag{2.19}$$

Combining Eqs. (18) and (19) with Eq. (12), the following expression for G_{22} emerges:

$$G_{22} = -V_1\left(1 - \frac{1}{n_2 V_2}\right)\left(\frac{\partial \ln n_1}{\partial \ln n_1^{vap}}\right)_{T,P} - \frac{1}{n_2} + kT\kappa_T \quad (2.20)$$

where a thermodynamic relationship $\left(\frac{\partial n_2}{\partial n_1}\right)_{T,P} = -\frac{V_1}{V_2}$ has been used in conjunction.[289] At the limit of $n_1 \to 0$, $1 - \frac{1}{n_2 V_2} \to 0$ and $\left(\frac{\partial \ln n_1}{\partial \ln n_1^{vap}}\right)_{T,P} \to 1$, which leads to $G_{22} \to -\frac{1}{n_2} + kT\kappa_T \simeq -V_2$, as one expects from one–component systems.

To summarize, all the KB integrals necessary to describe molecular interactions in the IL–water mixture can be obtained by the combination of vapor pressure and density data.

2.3 Results and Discussion

2.3.1 Source of experimental data

The objective is to clarify the how residual water molecules interact in ILs. This was achieved through the evaluation of three hypotheses proposed thus far on the role of residual water. The evaluation will be carried out in the framework of the KB theory (Section 2.2), through the calculation of the water–water (G_{11}), water–ion (G_{12}) and ion–ion (G_{22}) KB integrals.[288,289,291–296,304–306] The calculation of KB integrals requires experimental data as input: vapor pressure[307,308] and density[309,310] of IL–water mixtures. There are three systems in the literature for which density and vapor pressure have been measured in the IL–rich region as a function of water concentration, which are 1–butyl–3–methylimidazolium tetrafluoroborate ([BMIm][BF_4]), 1–ethyl–3–methylimidazolium tetrafluoroborate ([EMIm][BF_4]) and 1–ethyl–3–methylimidazolium trifluoromethanesulfonate ([EMIm][OTf]) (Figure 2.1). Due to the very low volatility of pure ionic liquids, the assumption that the vapor pressure of an IL/water mixture is the partial vapor pressure of water is made.

The key to calculating water–water and water–ion KB integrals, G_{11} and G_{12}, is $\left(\frac{\partial \ln n_1}{\partial \ln n_1^{vap}}\right)_{T,P} = \left(\frac{\partial \ln n_1^{vap}}{\partial \ln n_1}\right)_{T,P}^{-1}$, as seen in Eqs. (2.14) and (2.15). Here the quantity is calculated by combining vapor pressure and density data, as shown in Figure 2.1. The regression equations necessary to calculate the derivative have been summarized in Tables 2.1 and 2.2.

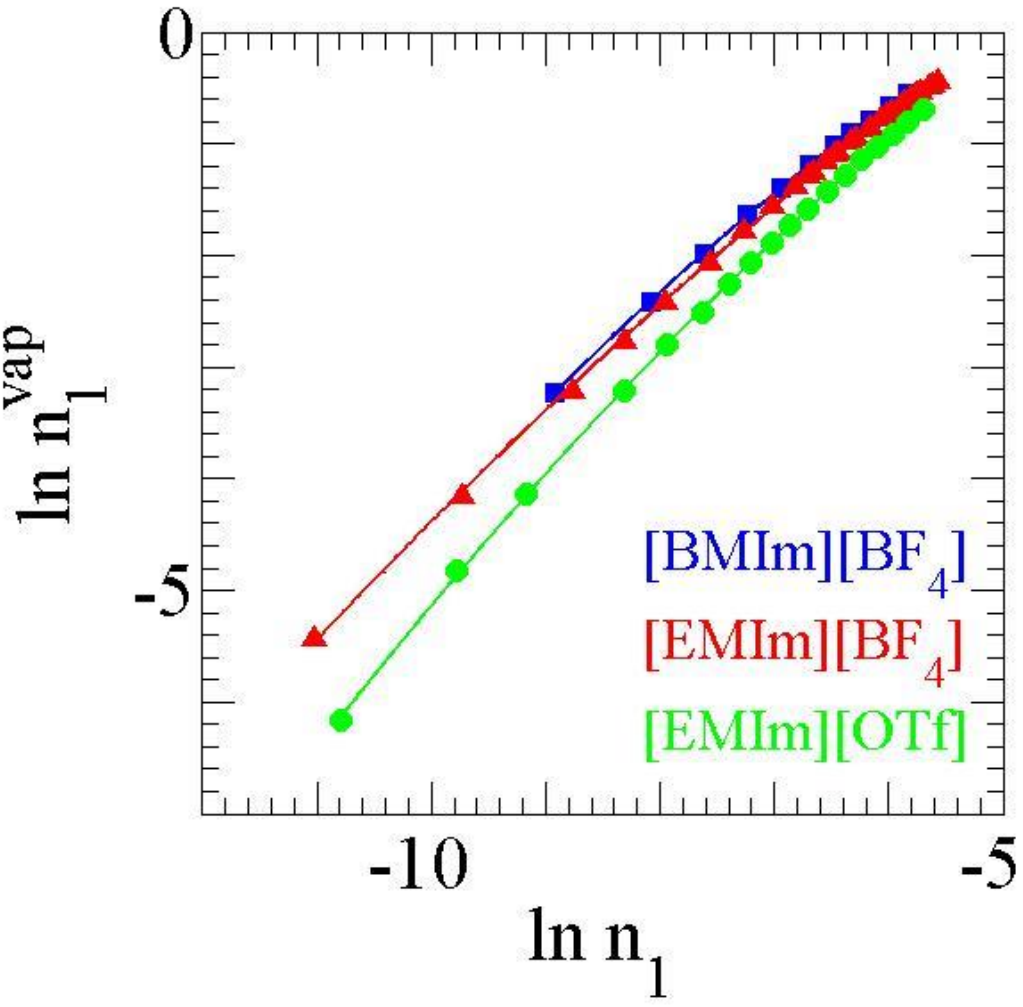

Figure 2.1 Dependence of the density of water vapor, $\ln n_1^{vap}$, on the molarity of water dissolved in IL, $\ln n_1$. $\ln n_1^{vap}$ was calculated using vapor pressure data from ref. 307 & 308, and $\ln n_1$ was calculated from density data from Refs. 309 and 310. The KB parameters were subsequently calculated using the gradient of the graph.

Table 2.1: Fitting parameters for the calculation of $\left(\frac{\partial \ln n_1^{vap}}{\partial \ln n_1}\right)_{T,P}$ necessary for Eqs (2.12), (2.15), (2.16) and (2.20). To this end, the experimental data (taken from Refs [307] and [308]) in Figure 1 is fitted against the equation $\ln n_1^{vap} = a + b \ln n_1 + c(\ln n_1)^2$.

IL/water system	a	b	c	R^2
[BMIm][BF_4]	1.9220	0.1287	–0.0503	0.9999
[EMIm][BF_4]	3.0209	0.4526	–0.0288	0.9995
[EMIm][OTf]	2.6929	0.3415	–0.0442	0.9999

Table 2.2: Parameters for the fitting function $\rho = \frac{ax_2+b}{x_2+c}$ where ρ is the density of mixture and x_2 is the mole fraction of IL, necessary for the calculation of partial molar volumes following a well–established procedure.[291,292,294,306] Density data taken from Refs [309] and [310].

IL/water system	a	b	c	R^2
[BMIm][BF_4]	1.223	0.1243	0.1244	0.9997
[EMIm][BF_4]	1.338	0.2097	0.2103	0.9999
[EMIm][OTf]	1.423	01058	0.1060	1.0000

2.3.2 Water–water and water–ion interaction

From $\left(\frac{\partial \ln n_1}{\partial \ln n_1^{vap}}\right)_{T,P}$ one can readily calculate the preferential water–water interaction relative to the water–ion interaction, namely $n_1(G_{11} - G_{12})$, based upon Eq. (13). The $n_1(G_{11} - G_{12})$, as can be seen from Figure 2.2, shows a preferential water–ion interaction (relative to water–water) at very low water concentrations. From here onwards, conventional mole fraction of water, $x_1 = \frac{n_1}{n_1 + \frac{n_2}{2}}$, which is commonly used in the literature, has been used in the Figures; note that $\frac{n_2}{2}$ is the concentration of the IL, expressed via the concentration of ions, n_2.[288,291,305] As the water concentration increases, all the systems exhibit preferential water–water interactions in comparison to water–ion.

In order to address the cause of the strong concentration–dependence of the preferential water–ion interaction as observed in Figure 2.2, especially the strong preferential water–ion interaction at low x_1, it was necessary to calculate G_{11} and G_{12} individually, through Eqs. (15) and (16). G_{12}, calculated using Eq. (15) and shown in Figure 2.3, is negative in value (as one expects from Eq. (15)) and depends weakly on n_1; hence the strong x_1 dependence of the preferential water–ion interaction should come from the x_1 dependence of G_{11}.

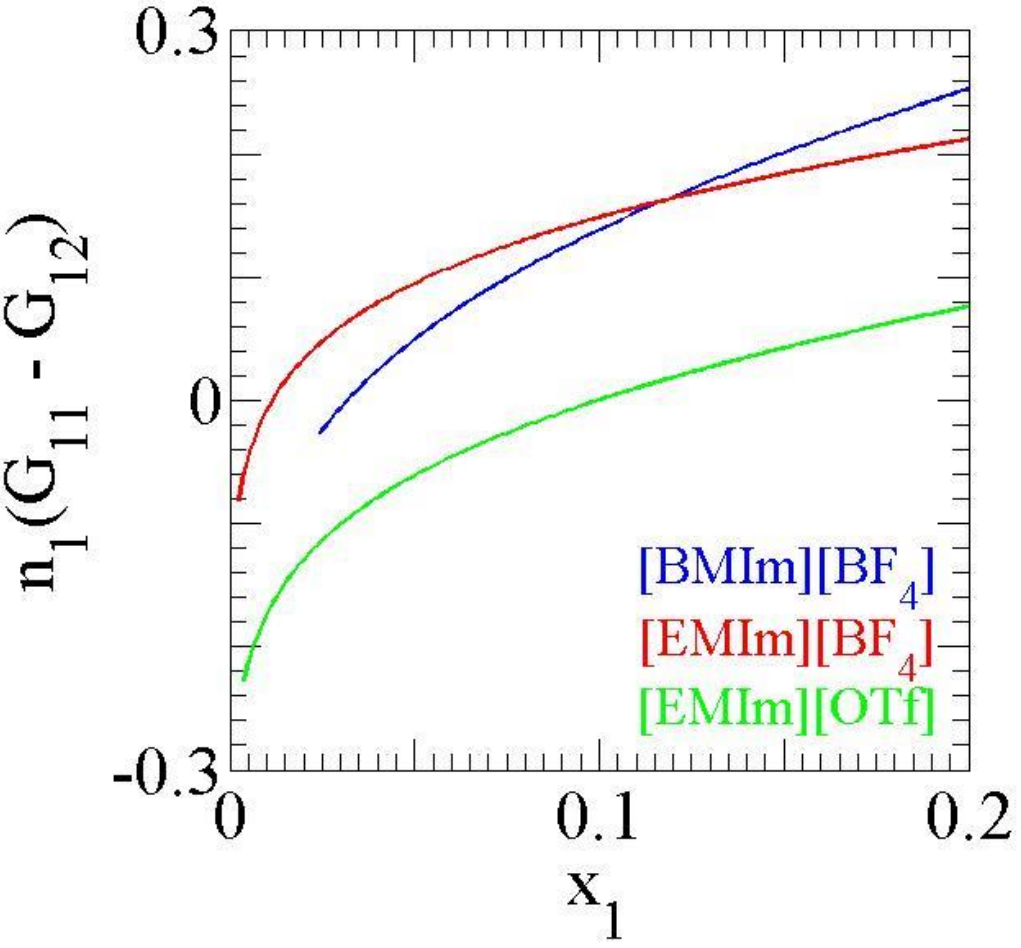

Figure 2.2 Dependence of the preferential solvation of water $n_1(G_{11} - G_{12})$ ($cm^3\ mol^{-1}$) on the mole fraction of water (x_1) as calculated by equation (2.13).

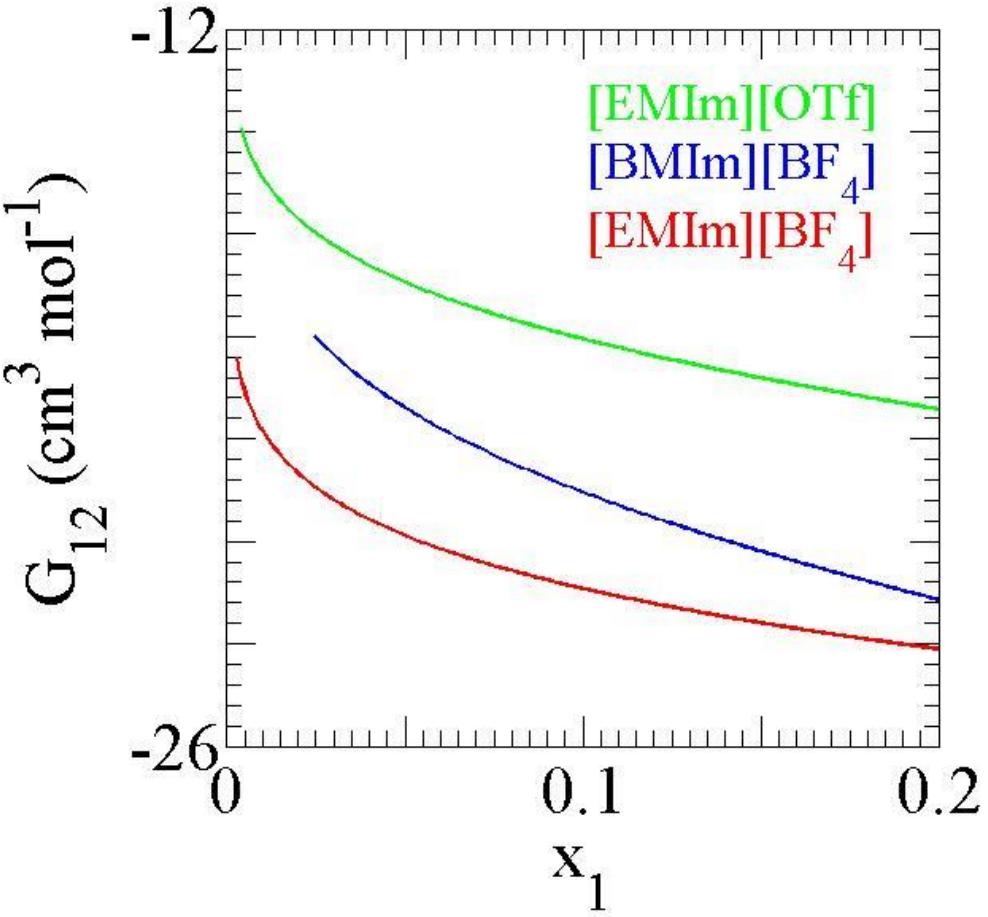

Figure 2.3 The water–ion Kirkwood Buff Integral G_{12} (cm^3 mol^{-1}) at low water mole fraction (x_1) for the three systems studied as calculated by equation (2.15).

That G_{11} is indeed strongly dependent upon x_1 is shown by Figure 2.4, which has been calculated through Eq. (2.16). This addresses the question posed in section 1.6.1; whether the water is dispersed throughout the ILs (hypothesis 1),[150–154] or is clustered around some specific sites (hypothesis 2).[155–158] G_{11} is large and negative at low n_1 (Figure 2.4), reflecting the $\frac{1}{n_1}$ factor in Eq. (2.15), suggesting that the water molecules tend to be excluded from one another. This is in contrast to hypothesis 2, according to which residual water molecules tend to self–associate or to form clusters;[155–158] the effect of self–association is negligible overall compared to self–dissociation.

The KB integral $G_{11}$is the overall measure of the water–water interaction; as is clear from Eq. (2.11), it is the spatial integral of $g_{11}(r) - 1$ – hence the conclusion from KB theory of strong *net* dissociation of water molecules is not necessarily inconsistent with the observation based upon the FT–IR and far–infrared spectra that water molecules dissociate weakly at low concentrations in hydrophilic ILs.[155,156] That the fraction of water that form dimers is a minority is indeed consistent with the results in this chapter, because such a contribution to G_{11}, namely the contribution from $g_{11}(r)$ peak at water–water contact distance, is overwhelmed by the majority of water molecules that do not form dimers, thereby making $g_{11}(r)$ smaller than 1 at distances larger than water–water contact.

The results shown support hypothesis 1, according to which water molecules are dispersed throughout the medium through favourable interactions. The calculation cannot exclude the existence of a small fraction of dimeric water, yet is consistent with the observation that only a small fraction of water molecules dimerize in ILs. Note that, due to the lack of experimental data, the limiting value of G_{11} could not be determined from this method; nevertheless, the analysis here has clarified that, in the three IL–water systems evaluated, water molecules tend to be far apart from each other, rather than clustered together.

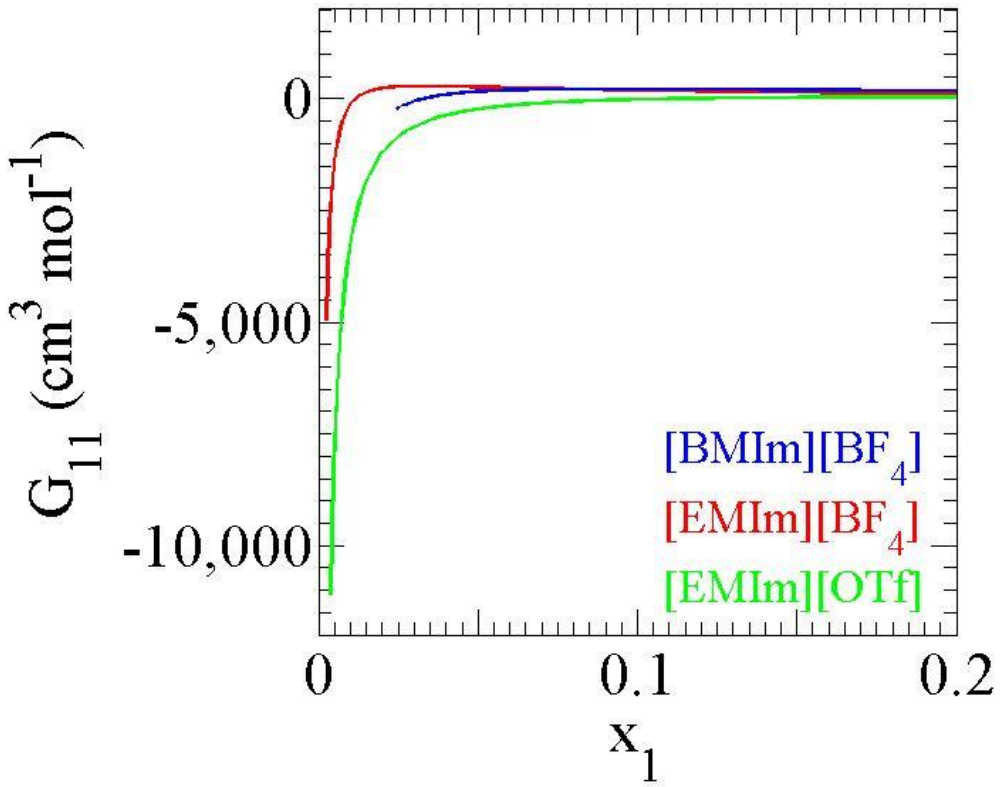

Figure 2.4 The water–water Kirkwood Buff Integral G_{11} (cm^3 mol^{-1}) at low water mole fraction (x_1) for the three systems studied as calculated by equation (2.16).

2.3.3. Ion–ion interaction

In order to address question 2 outlined in section 1.6.2, it was necessary to assess the extent to which residual water molecules weaken the ion–ion interaction (hypothesis 3). [159–161] If residual water does indeed exert such an effect, the KB integral between ion and ion would be affected by the presence of the residual water. To examine whether this occurs, G_{22} was calculated using Eq. (18), as shown in Figure 2.5. The negative sign of G_{22} at low water concentration is rationalized by its pure IL limit, $G_{22} \to -V_2$, as discussed in the previous section. Indeed V_2 at this limit can be calculated from the density data[309,310] to be –94.3, –77.4 and –93.1 $cm^3\ mol^{-1}$ for [BMIm][BF_4], [EMIm][BF_4] and [EMIm][OTf], respectively, which is consistent with Figure 2.5. Note that the positive sign of V_2 comes from the excluded volume of the ions, which rationalizes the negative G_{22}.

If residual water molecules were to weaken the ion–ion interaction, a decrease (i.e., change towards less positive) in the ion–ion radial distribution function should be observed, making G_{22} more negative as the water concentration increases. As seen in Figure 2.5, the results do indeed support this expectation: a slight weakening of ion–ion interaction does take place in the presence of water. This effect seems to be very weak however, barely seeming to affect the thermodynamics of mixture (Eq. (2.17)), in which the chemical potential of water is hardly affected by G_{22}. This is also illustrated by the dependence of the preferential solvation of the ions, $G_{21} - G_{22}$, as seen in Figure 2.6. It should be emphasized that G_{22} represents the overall measure of ion–ion interactions; while on the whole the interactions do not change, there may be competing effects as a result of residual water molecules.

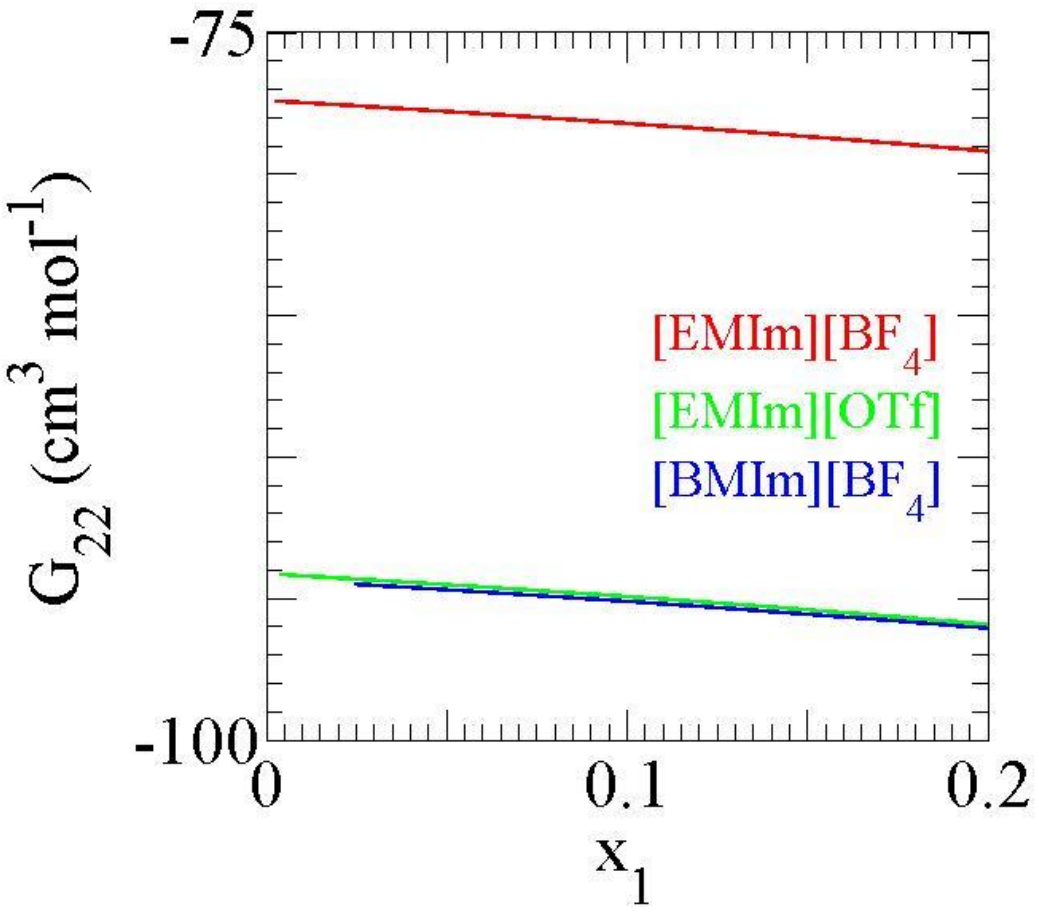

Figure 2.5 The ion–ion Kirkwood Buff Integral G_{22} (cm^3 mol^{-1}) at low water mole fraction (x_1) for the three systems studied as calculated by equation (2.20).

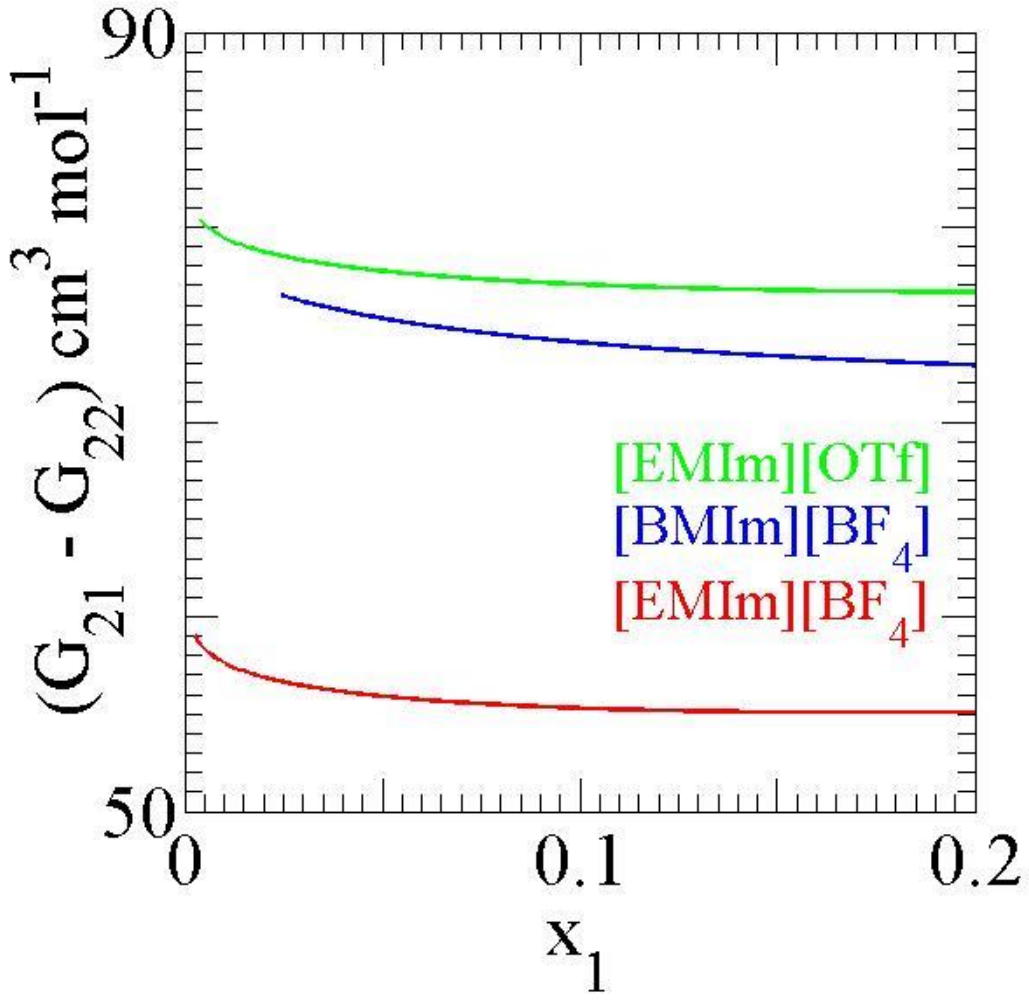

Figure 2.6 Dependence of the preferential solvation of the ions, ($G_{21} - G_{22}$) (cm^3 mol^{-1}) on the molarity of water, x_1 as calculated by equation (2.18).

2.4. Comparison between different ILs

Finally, the extent of preferential water–ion interaction over water–water interaction $(n_1(G_{11} - G_{21}))$ and preferential water–ion interaction over ion–ion interaction $(G_{21} - G_{22})$ was evaluated between the three different ILs. At low water concentrations, $n_1(G_{11} - G_{21})$ and $G_{21} - G_{22}$ show the following order, as seen in Figures 2.2 and 2.6, respectively: [EMIm][OTf] > [BMIm][BF_4] > [EMIm][BF_4]. This is the same as the order of the lattice free energies of the pure ILs, as seen in Table 3,[311] suggesting that the preferential ion–water interaction at low water concentrations is determined chiefly by the ease of breaking ion–ion interactions.

As the water concentration increases, the magnitude of $G_{11} - G_{21}$changes its order to the following: [EMIm][OTf] > [EMIm][BF_4] > [BMIm][BF_4]. This now reflects the order of the static dielectric constant of each pure IL,[312] suggesting that with increasing water concentration, the IL's ability to solvate water bears greater resemblance to the "polarity" of the pure IL as described by the static dielectric constant.[313,314] Rationalising this observation at a molecular scale requires further studies involving computer simulation.[315,316] The magnitude of $G_{21} - G_{22}$ changes very little, showing that increasing the water content of these ILs doesn't change the preference of the ion–water interactions over the ion–ion interactions.

Table 2.3: Literature values of the lattice free energy ($\Delta_{latt}G°$) and the static dielectric constant at 298.15K (ε) of each IL used in this study. Lattice free energies are from ref. 48 and static dielectric constants are from ref. 49.

IL/water system	$\Delta_{latt}G°$ / kJ mol^{-1}	ε
[BMIm][BF_4]	373	11.7 ± 0.6
[EMIm][BF_4]	395	12.8 ± 0.6
[EMIm][OTf]	363	15.2 ± 0.3

To summarize, the relative strengths of water–ion interactions at low water concentrations correlate well with the difficulty of breaking ion–ion interactions. At higher water concentrations, the solvation properties of the three ILs correlate with the static dielectric constants of the pure ILs. What is observed in all three systems is a preference of water–ion interactions over ion–ion interactions, which describes well the hydrophilic nature of these solvents. At this time, there is no complete hygroscopic data to draw quantitative comparison with our results.

2.5 Conclusions

Residual water in ILs profoundly affects their structure, properties and behaviour as solvents, hence a better understanding of the role of residual water at the molecular level is indispensable when assessing the potential of ILs to be applied in anything other than fully anhydrous environments. Conflicting hypotheses have been proposed on molecular interactions in ILs in the presence of residual water. The Kirkwood–Buff (KB) theory of solutions[287–289,291–296,303–306] has facilitated the clarification of water–water, water–IL and IL–IL interactions in three ILs of varying hydrophilicity mixed with a small quantity of water. These interactions have been calculated based only on published density and activity data of the mixtures.

The KB calculations show that at low water concentration, the structure of water is highly concentration dependant, as evident by the change in G_{11} (Figure 2.4). At the lowest calculated concentrations of water for all three systems, water molecules are preferentially solvated by the IL (i.e. do not form aggregates or nanoclusters).[157,158] if they form dimers, only a fraction of the water molecules participate,[155,156] hence the effect of dimerization is negligible (hypothesis 2). As water concentration increases, a change in the preferential solvation of water is observed; Water molecules tend to be far apart from each other, rather than aggregated, which supports previous suggestions (hypothesis 1).[150–154] In

contrast to hypothesis 3,[159–161] the effect on thermodynamics of the water–induced weakening of ion–ion interactions seems to be very weak, at least in the three ILs studied.

The primary conclusion to result from our KB analysis was therefore that the water molecules bind strongly to ions individually, instead of as an aggregate or cluster. Residual water molecules are overall kept well apart from each other. The KB theory does not permit the more detailed breakdown of water–anion *vis–à–vis* water–cation interactions; computer simulation is indispensable, albeit in a force field dependent manner, to disseminate the two interactions. [315,316]

The observed trends in the magnitude of preferential water–water relative to water–ion interactions, $n_1(G_{11} - G_{21})$, can be rationalized by the lattice free energies and the static dielectric constants of the pure ILs, which suggests the importance of both ion–ion binding and solvent polarity in understanding the behaviour of residual water in ILs. The preferential solvation of ions, $G_{21} - G_{22}$, indicates that all three ILs studied are hydrophilic, however there is insufficient hygroscopic data to draw conclusions at this time.

Chapter 3: Comparing the Interactions in Ionic Liquid–Water Mixtures in Protic and Aprotic Systems.

3.1 Introduction

The sensitivity of ionic liquids (ILs) to water affects their physical and chemical properties, even at relatively low concentrations, yet the structural thermodynamics of protic IL (PIL)–water systems at low water concentrations remains unclear. In the context of PIL–water mixtures, the following important questions have been posed in the literature (as discussed in section 1.6), and have not been answered clearly;

1) Does water interact more strongly with protic ILs than with aprotic ILs?[165,167–181]
2) Does the presence of water weaken ion–ion interactions in PILs?[162–164,166,317]
3) Does the structure of PIL–water systems reflect homogeneous mixture or the formation of heterogeneous structures?[182–186]

In continuation from Chapter 2, three additional systems have been selected to study how the ionic nature of an IL influences its interactions with water. Using the rigorous Kirkwood–Buff (KB) theory of solutions, the interactions between species in IL–water systems summarized as KB parameters are determined solely from thermodynamic data. The three additional systems in question feature both PILs (*N*,*N*–dimethylethanolammonium bis(trifluoromethanesulfonyl)imide ([HDMEtA][NTf_2]) and *N*,*N*–dimethylethanolammonium propionate ([HDMEtA][Pr])) and an aprotic IL (AIL) (cholinium bis(trifluoromethanesulfonyl)imide ([Ch][NTf_2]). For comparison, the same three systems discussed in Chapter 2 are retained for discussion in this chapter. While not representative of the wide variety of PIL and AIL structures, the variation in both anion and cation structure allow for study on how the ionic nature (protic vs. aprotic, high ionicity PIL vs. low ionicity PIL) influences the interactions in IL–water binary mixtures at low water compositions.

3.2 The Kirkwood–Buff theory of binary mixtures

3.2.1 General Strategy for Understanding Interactions in Ionic Liquid–Water Binary Mixtures

Based upon the rigorous statistical thermodynamic KB theory for binary mixtures, thermodynamic data can be used to reveal the structure of IL–water mixtures. [148,287,289,291,304,305] A more detailed discussion on the derivation of the KB parameters as used in this work has been shown in Chapter 2. [148,149,287–289,291–299,304–306,318]

The KB integrals in a two component system can be determined through the well–known formulae: [148,149,287–289,291–299,304–306,318]

$$G_{21} = -\frac{nV_1V_2}{D} + kT\kappa_T \tag{3.1}$$

$$G_{11} = \frac{n_2V_2^2n}{n_1D} - \frac{1}{n_1} + kT\kappa_T \tag{3.2}$$

$$G_{22} = -\frac{1}{n_2} + \frac{n_1V_1^2n}{n_2D} \tag{3.3}$$

where n_i and V_i respectively express the concentration and the partial molar volume of species i, and κ_T is the isothermal compressibility (typically of negligible contribution to KBI values); $n = n_1 + n_2$ has also been used. Here, D is the key quantity for KB integral determination: [148,149,287–289,291–299,304–306,318]

$$D = \frac{x_1}{kT}\left(\frac{\partial\mu_1}{\partial x_1}\right)_{T,P} = \left(\frac{\partial \ln a_1}{\partial \ln x_1}\right)_{T,P} \tag{3.4}$$

where μ_i , x_i and a_i respectively express the chemical potential, the mole fraction and the activity of the species i.

The above formulae to calculate the KB integrals are equivalent yet slightly different to the formulae used in Chapter 2 to calculate the same quantities. This was necessary, as the quantity *D* is required for the discussion of overall mixing behavior in IL–water systems (section 3.2.2). That these two sets of formulae are equivalent can be shown in a straightforward manner: by using the following relation:

$$\left(\frac{\partial n_1}{\partial x_1}\right) = n^2 V_2 \tag{3.5}$$

And in combination with Eqn. (3.4), the following expression for *D* is obtained:

$$D = \frac{V_2 n n_1}{kT}\left(\frac{\partial \mu_1}{\partial n_1}\right)_{T,P} \tag{3.6}$$

Equation 3.6 is equivalent to the following:

$$\frac{kT}{n_1}\left(\frac{\partial n_1}{\partial \mu_1}\right)_{T,P} = \left(\frac{\partial \ln a_1}{\partial \ln n_1}\right)_{T,P}^{-1} = \left(\frac{\partial \ln n_1^{vap}}{\partial \ln n_1}\right)_{T,P}^{-1} \tag{3.7}$$

where μ_1 and a_1 is the chemical potential and the activity of water, and is used to determine the KB integrals using the formulae described in Chapter 2: [148]

$$G_{12} = -V_1\left(\frac{\partial \ln n_1}{\partial \ln n_1^{vap}}\right)_{T,P} + kT\kappa_T \tag{2.15}$$

$$G_{11} = \frac{1}{n_1}\left[n_2 V_2\left(\frac{\partial \ln n_1}{\partial \ln n_1^{vap}}\right)_{T,P} - 1\right] \tag{2.16}$$

$$G_{22} = -V_1\left(1 - \frac{1}{n_2 V_2}\right)\left(\frac{\partial \ln n_1}{\partial \ln n_1^{vap}}\right)_{T,P} - \frac{1}{n_2} + kT\kappa_T \tag{2.20}$$

3.2.2 Quantifying the closeness to phase separation

In order to compare quantitatively how close IL–water mixtures are to phase separation (section 1.6.4), the thermodynamic criterion for phase stability, namely $x_2\left(\frac{\partial \ln \gamma_2}{\partial x_2}\right) > -1$ where γ_i is the activity coefficient of the species i has been employed.[300,301,319] Using Eqn. (3.4), this translates to the following condition

$$D = x_2\left(\frac{\partial \mu_2}{\partial x_2}\right)_{T,P} > 0 \tag{3.8}$$

The D parameter summarizes the change in chemical potential of a given species with respect to its composition within a defined mixture. Using the Gibbs–Duhem equation, the single parameter accounts for the thermodynamic behaviour of the species within a multicomponent system (in our case, the IL and water). This *D* can also be measured by scattering experiments; by straightforward algebra, this *D* can be linked directly to the

variance of mole fraction related to the zero wave vector value of the concentration–concentration structure factor, $S_{cc}(0)$ as [303,320–325]

$$D = \frac{x_1 x_2}{S_{cc}(0)} - 1 \quad (3.9)$$

3.2.3 Water activity and density data

The calculation of KB integrals requires experimental data as input: vapor pressure and density of IL–water mixtures. Water activity data on three IL–rich mixture systems have been taken from the literature, [66,326] which include [Ch][NTf_2], [HDMEtA][NTf_2] and [HDMEtA][Pr].[49] The structures of the ILs vary both the anion and cation structure, as well as featuring both protic and aprotic ILs. Density data of the binary mixtures featuring the above ILs was taken from the PhD thesis of Dr. Richard Gammons, University of York (2015).[149,327]

Table 3.1: Parameters for the fitting function $\rho = \frac{ax_2+b}{x_2+c}$ where ρ is the density of mixture and x_2 is the mole fraction of IL, necessary for the calculation of partial molar volumes following a well–established procedure.[138,169–171] Density data taken from Refs 309 and 310 for [BMIm][BF_4], [EMIm][BF_4] and [EMIm][OTf]

IL/water system	a	b	c	R^2
[BMIm][BF_4]	1.223	0.1243	0.1244	0.9997
[EMIm][BF_4]	1.338	0.2097	0.2103	0.9999
[EMIm][OTf]	1.423	01058	0.1060	1.0000
[DMEtA][Pr]*	–0.02876	0.09512	0.998197	1.0000
[DMEtA][NTf_2]	1.655	0.08242	0.08251	1.0000
[Ch][NTf_2]	1.596	0.1206	0.1038	1.0000

*The density of the system [DMEtA][Pr] and water was better fitted using a polynomial expression of the form $\rho = ax_2^2 + bx_2 + c$

Table 3.2: Fitting parameters for the calculation of $\left(\frac{\partial \ln a_1}{\partial \ln x_1}\right)_{T,P}$ necessary for Eqn. (3.4) and all subsequent Kirkwood Buff Integral calculations. To this end, the experimental data (taken from Refs. [66] and [326] for [DMEtA][Pr], [DMEtA][NTf_2] and [Ch][NTf_2] and Refs [307] and [308] for [BMIm][BF_4], [EMIm][BF_4] and [EMIm][OTf]) in Figure 3.1 is fitted against the equation $\ln a_1^{vap} = a + b \ln x_1 + c(\ln x_1)^2$.

IL/water system	a	b	c	R^2
[BMIm][BF_4]	0.3214	0.6993	–0.0381	0.9999
[EMIm][BF_4]	0.4207	0.7453	–0.0264	0.9993
[EMIm][OTf]	0.3235	0.8834	–0.0300	0.9998
[DMEtA][Pr]	–0.2591	1.0715	0.0327	0.9997
[DMEtA][NTf_2]	0.3969	0.5624	–0.0245	0.9997
[Ch][NTf_2]	–0.4646	–0.7199	–0.3445	0.9983

In addition, data sets of water activity[307,308] and density [309,310] of the three IL–water mixtures featuring the ILs 1–butyl–3–methylimidazolium tetrafluoroborate ([BMIm][BF_4]), 1–ethyl–3–methylimidazolium tetrafluoroborate ([EMIm][BF_4]) and 1–ethyl–3–methylimidazolium trifluoromethanesulfonate ([EMIm][OTf]) studied in Chapter 2 are utilized. The experimental water activity and density data have been utilized in Figure 3.1, with subsequent differentiation producing the D value (Eqn (3.4)) as will be shown in section 3.3.3, which is used to calculate all KB integrals (Eqn (3.1)–(3.3)).

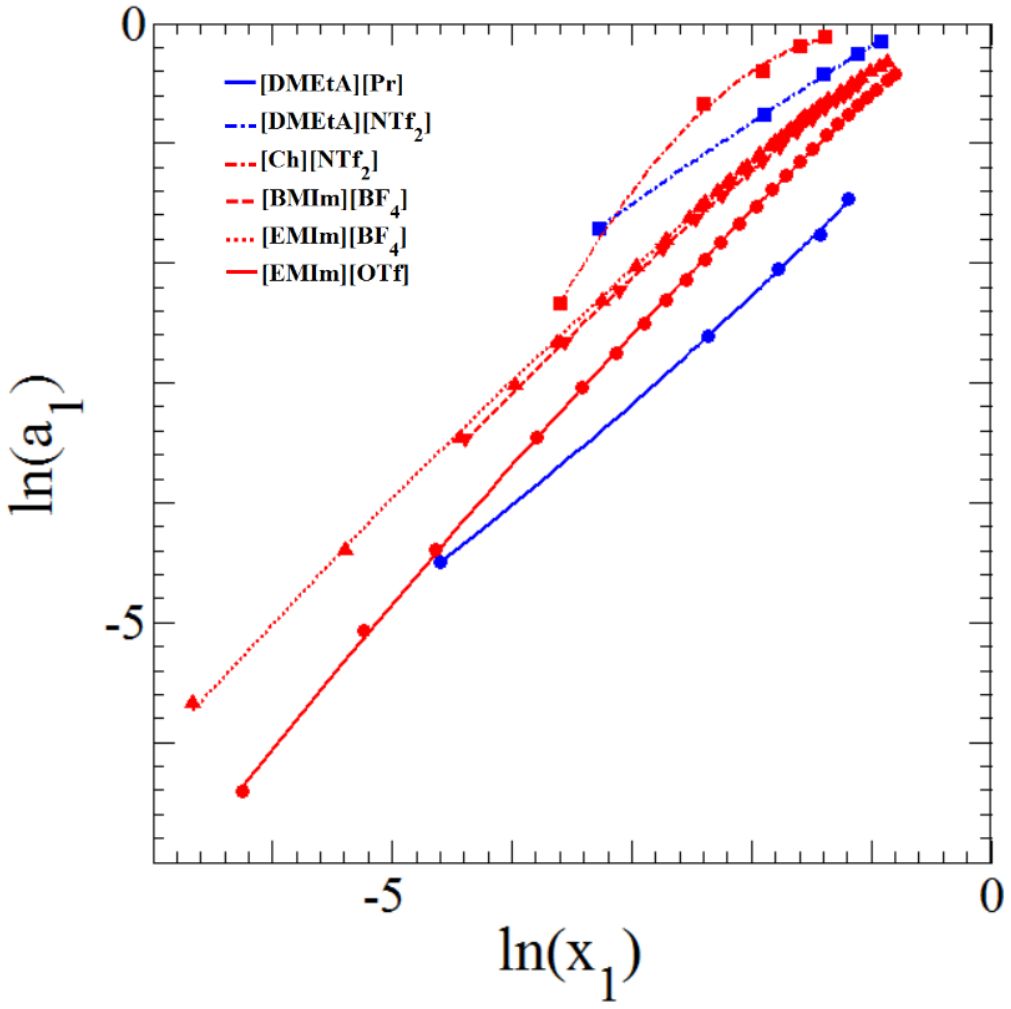

Figure 3.1 Dependence of the activity of water ($\ln a_1$) on the mole fraction of water dissolved in IL ($\ln x_1$). Fitting functions of the plots are used to calculate the KB parameters. Coefficients of the fitting functions are summarized in Table 3.2.

3.3 Results and Discussion

3.3.1 Does water interact more strongly with protic or aprotic ILs? (Question 1)

To answer this question, the values of the ion–water interaction parameter, G_{21}, for all six systems are utilized. Two pairs of ILs have been selected to compare the ion–water interactions in protic and aprotic ILs; one representing hydrophobic ILs, the other representing the hydrophilic ILs from this study.

3.3.1.1 Hydrophobic ILs

Both the [Ch][NTf_2] and [HDMEtA][NTf_2] feature the bis(trifluoromethanesulfonyl)imide anion, near–universally regarded as extremely hydrophobic, ammonium cation (quaternary for the aprotic, tertiary for the protic) and hydroxyl functional group on the cation. (The similarity in ion structure results in comparable average ion size, which can be inferred roughly by the partial molar volume of the ILs at $n_1 \rightarrow 0$, i.e., 169.45 $cm^3\ mol^{-1}$ for [HDMEtA][NTf_2] and 176.47 $cm^3\ mol^{-1}$ for [Ch][NTf_2]). Despite the similarity in structure, the two ILs exhibit distinctly different degrees of interaction with water. At the lowest comparable measured concentration of water ($x_1 = 0.073$), The AIL [Ch][NTf_2] shows more favorable ion–water interactions than the PIL [HDMEtA][NTf_2] (Figure 3.2). Both ILs feature hydroxyl functional groups on the cation, which are expected to act as hydrogen bond donors towards water, as well as with the anion.[328,329] Protic ionic liquids have often been described as having strong, directional hydrogen–bonding networks present as a result of the charge transfer formation of ions, in some cases also being compared to water.[218] This can create strong differences in the local structure of analogous protic and aprotic ILs.[330] As a result, it is likely that the availability of the hydroxyl groups on the cation to form hydrogen bonds with, at low water concentrations, is restricted. As the ion–ion interactions in AILs are typically dependent on

diffuse electrostatic interactions, there is less restriction to the ion–water mode of interaction through hydrogen bonding.

With increasing water concentration, ion–water interactions become less preferential in both systems; however, for the [Ch][NTf_2] system G_{21} decreases more drastically, eventually becoming more negative than for [HDMEtA][NTf_2] at around $x_1 \approx 0.20$. This implies more preferential ion–water interactions in the PIL than in the analogous AIL at $x_1 > 0.20$. At these higher water concentrations, it is likely that a reorganization of water in the AIL takes place, resulting in an increase in the strength of water–water interactions. This is supported by an increase in G_{11} (Figure 3.3) from large and negative values at low water concentration (as discussed in the previous chapter[148]) to large and positive values, larger than in [HDMEtA][NTf_2] at around $x_1 \approx 0.20$. (Note that, due to the inherent difficulties in measuring low water activity, the values of G_{11} should be considered only indicative of qualitative trend at this end.)

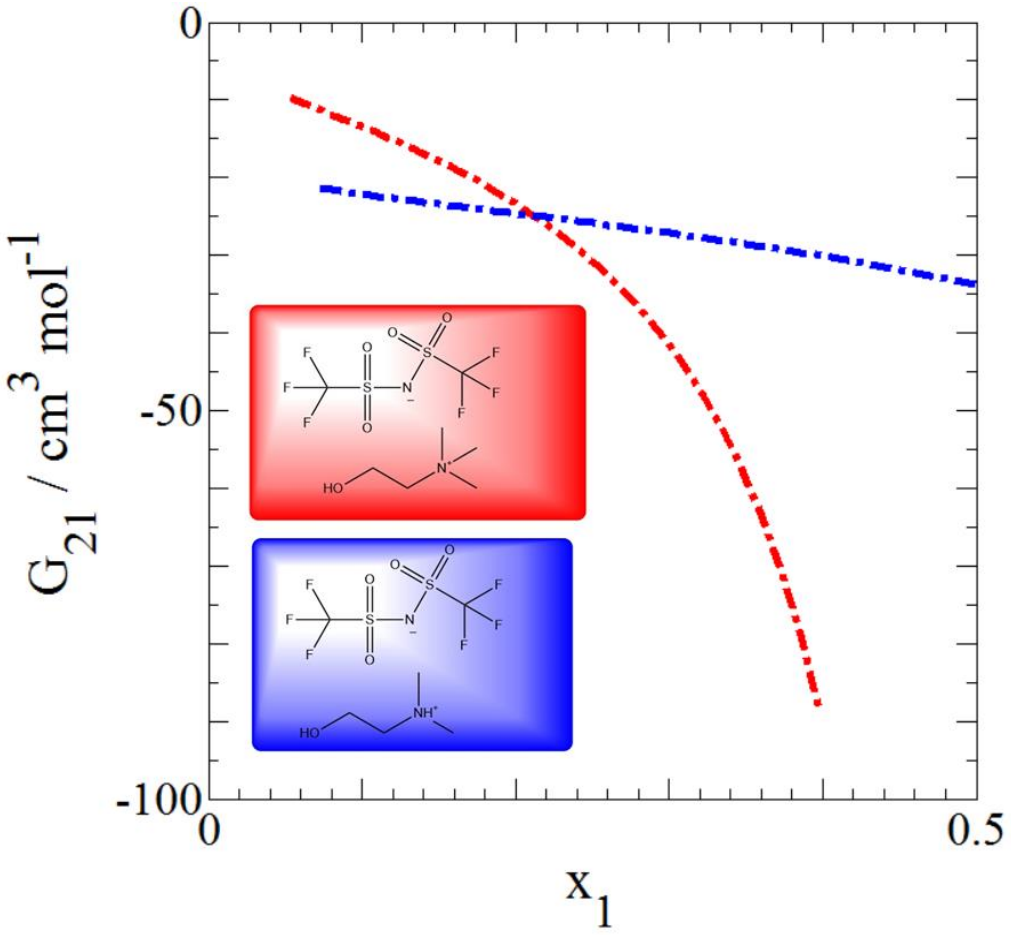

Figure 3.2 The dependence of water–ion Kirkwood Buff Integral G_{21} (cm^3 mol^{-1}) on water mole fraction (x_1) for the two hydrophobic ionic liquid systems studied as calculated by Eqn. (3.1).

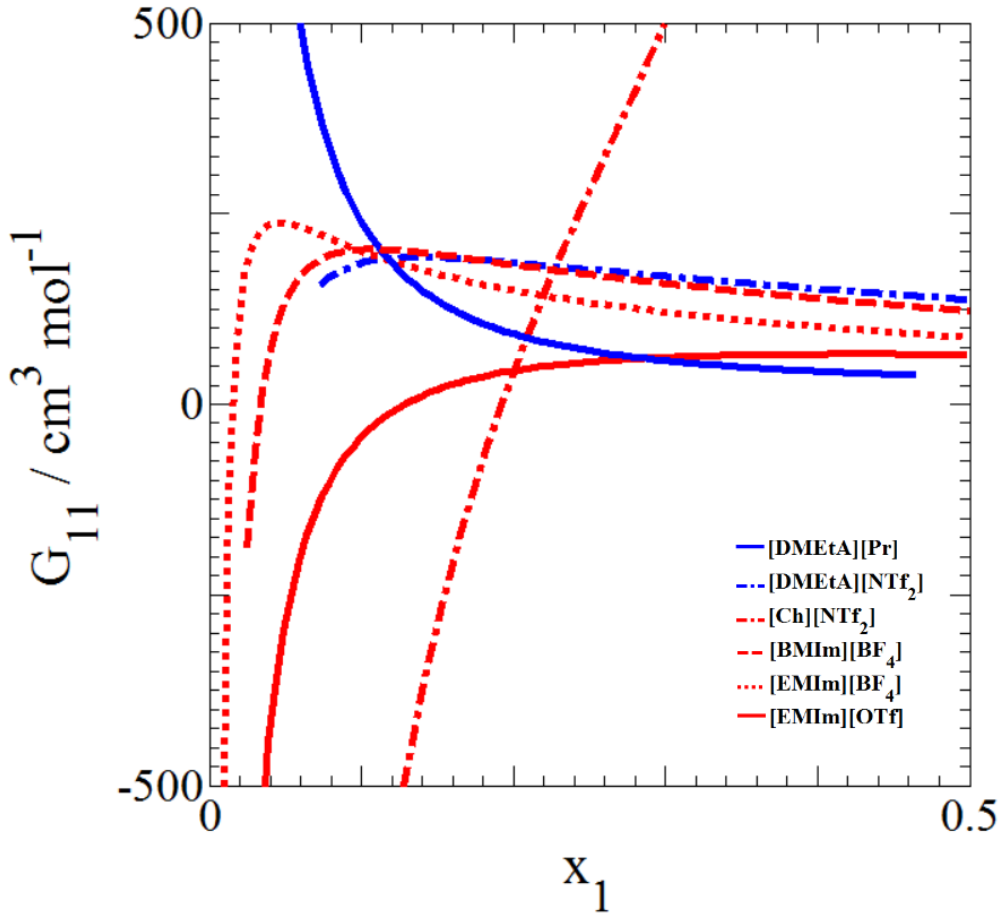

Figure 3.3 The dependence of water–water Kirkwood Buff Integral G_{11} (cm^3 mol^{-1}) on water mole fraction (x_1) for the six systems studied as calculated by Eqn (3.2).

3.3.1.2 Hydrophilic ILs

While not analogous in structure, the PIL [HDMEtA][Pr] and the AIL [EMIm][OTf], represent the most hydrophilic of the ILs from this study. Here, note that [EMIm][OTf] is larger in size than [HDMEtA][Pr] (which can be inferred roughly by their respective pure–phase partial molar volumes, namely 94.13 $cm^3\ mol^{-1}$ for [EMIm][OTf] and 76.69 $cm^3\ mol^{-1}$ for [HDMEtA][Pr]). Over the entire comparable compositions, [EMIm][OTf] exhibits greater G_{21} values than [HDMEtA][Pr] (Figure 3.4). This result conveys that water–ion interactions are more favorable in [EMIm][OTf] than in [HDMEtA][Pr] at the concentration range studied. While the structures of these two ILs are distinctly different, they both feature anions and cations that could form hydrogen bond interactions with water (The hydrogen at the C_2 position of the imidazolium ring of the cation and the oxygen atoms on the triflate anion for [EMIm][OTf]; the hydroxyl and tertiary ammonium groups on the cation and the oxygen atoms on the propionate anion for [HDMEtA][Pr]). The triflate anion has been shown from classical MD simulations to able to form strong hydrogen bonds with water at low concentrations through the oxygen atoms.[331,332] Even at greater water concentrations, the anions of aprotic ILs such as [BMIm][BF_4] and [EMIm][OTf] have shown to significantly interact with water, resulting in a picture of water–anion networks.[315,333] Note that the stronger water–ion interaction of the PIL is observed over the entire concentration range studied here, unlike the case of the hydrophobic ILs, for which the relative strength of ion–water interaction was shown to depend strongly on water concentration.

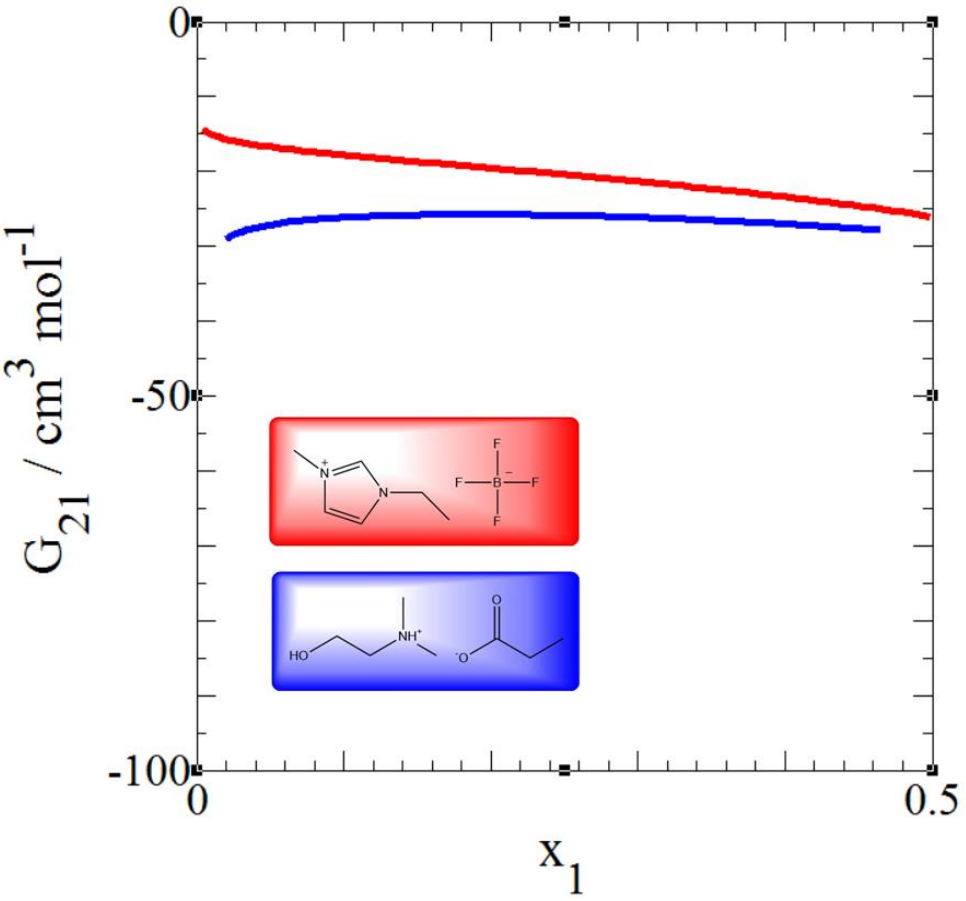

Figure 3.4 The dependence of water–ion Kirkwood Buff Integral G_{21} (cm^3 mol^{-1}) on water mole fraction (x_1) for the two hydrophilic ionic liquid systems studied as calculated by Eqn (3.1).

3.3.2 Does water weaken ion–ion interactions in PILs? (Question 2)

To answer this question, the dependence of water mole fraction on the ion–ion KB parameter, G_{22} (Figure 3.5) can be used. For all but one of the IL–water systems (that of [Ch][NTf_2]), there is a slight decrease of G_{22} with increasing water content. The degree of weakening of ion–ion interactions is seemingly comparable for these systems, despite the wide variety of IL structures present. This relatively small decrease in G_{22} suggests that ion–ion interactions are relatively unchanged by the presence of water. This is in agreement with previous studies into the liquid structure and interactions in PIL systems upon addition of water. [162,163] In Chapter 2, the conclusion was that G_{22} has little impact on the chemical potential of water, which in turn is reinforced by the relatively small change observed for the preferential solvation of ions ($G_{21} - G_{22}$) (Figure 3.6).[148] As well as establishing that ion–ion interactions are relatively unaffected by the presence of water, Figure 3.6 demonstrates that ion–water interactions are preferable to ion–ion interactions over the studied concentration range.

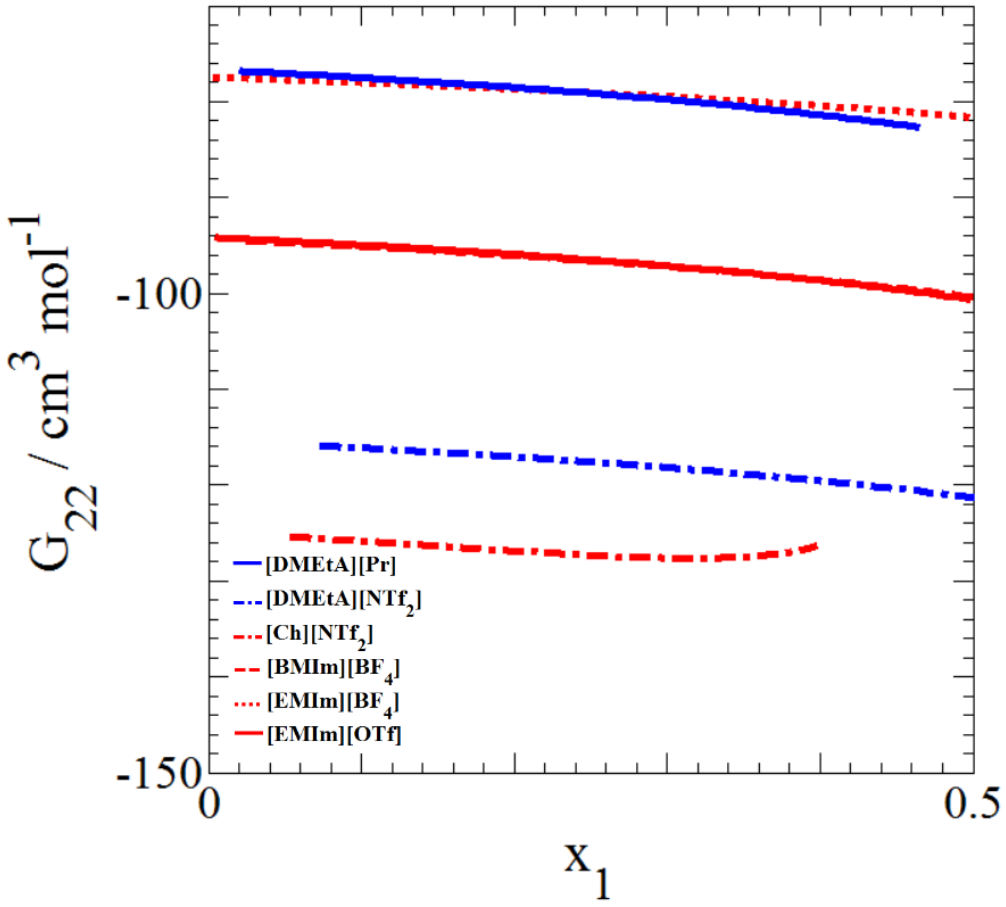

Figure 3.5 The dependence of ion–ion Kirkwood Buff Integral G_{22} (cm^3 mol^{-1}) on water mole fraction (x_1) for the six systems studied as calculated by Eqn (3.3).

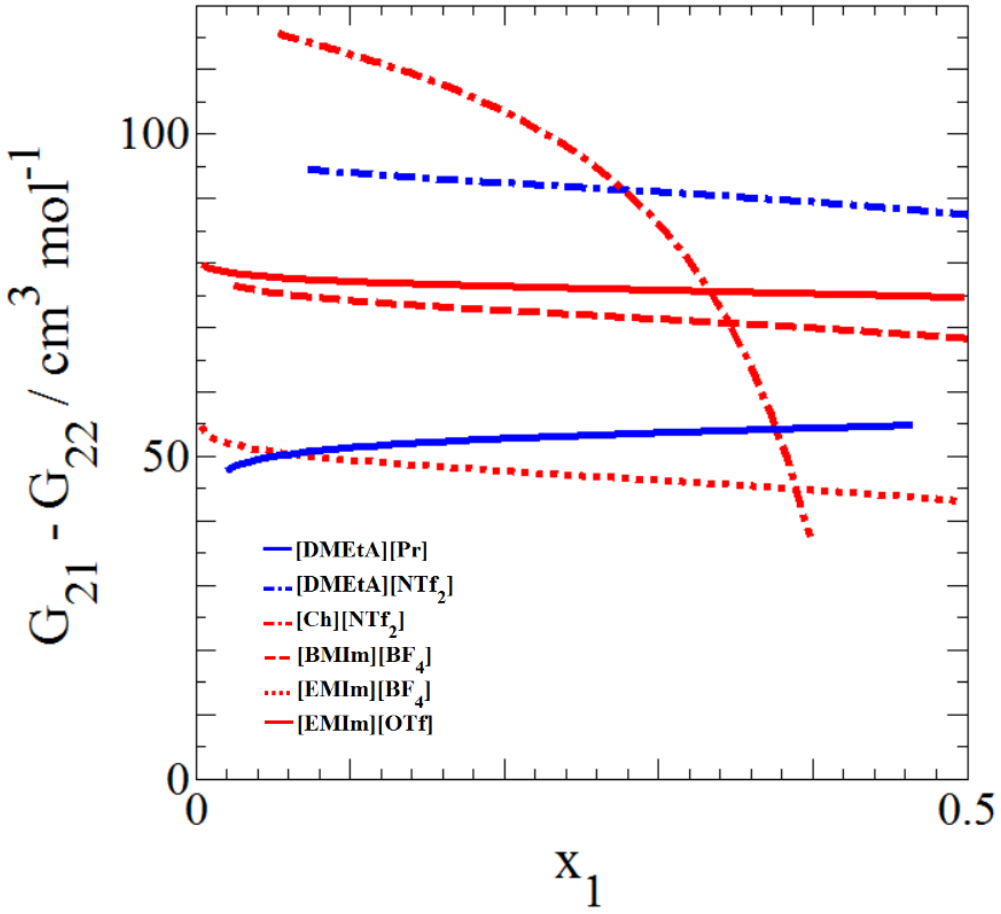

Figure 3.6 Dependence of preferential solvation of ions, (G_{21} – G_{22}) on the mole fraction of water (x_1) for each system.[148]

3.3.3 Does the structure of PIL–water systems reflect homogeneous mixing or the formation of heterogeneous structures? (Question 3)

From G_{22} it is shown that there is little change in the ion–ion interaction strength (Figure 3.5) in PILs in the presence of water, implying that the structure of the PIL remains relatively unchanged. If the water–water interactions for these systems are considered, it is found that for both PILs, G_{11} is large and positive at the concentration range of this study (Figure 3.4). This behaviour of water–water interactions is distinctly different than observed in any of the AILs in this study. Despite this, strong aggregation of water at low concentrations has been observed in other systems using KB theory, such as sucrose–water[334] and dimethyl sulfoxide (DMSO)–water mixtures.[335] (Note that large positive and negative KB integrals have been reported in the past to contribute to discussion on binary systems.[336,337])

To clarify the effect of such strong self–association on the mixing behavior of PIL–water systems, the well–established thermodynamic criterion for phase separation based on Eqn. (3.8) has been employed (Figure 3.7). This parameter has been used to clarify the phase behavior of numerous binary systems which are close to phase separation. [303,320,322–325,338] For the PIL [HDMEtA][Pr], the values of D increase with increasing water concentration, implying an increased stability in the system. As a result, the lowest values of D occur at the lowest water concentrations, which is rationalized by the presence of strong water association at low water concentrations (Figure 3.3). The PIL [HDMEtA][NTf_2] shows a weak dependence of D on water concentration. The values of D for this system are markedly lower than for [HDMEtA][Pr], suggesting a more heterogeneous structure of the system. This could be rationalized by the greater degree of water–water interactions in [HDMEtA][NTf_2], as shown by G_{11}. This is to be expected, as the [NTf_2] anion is widely regarded as being more hydrophobic than the [Pr] anion. For

both PILs the values of *D* are away from phase separation (*D* = 0), suggesting that the PIL–water system is stable despite the presence of water–rich clusters (Figure 3.3).

The three dialkylimidazolium ILs show similar trends, with variation of anion having a greater effect on *D* than variation of cation. Within the concentration range studied, all systems are away from phase separation; [EMIm][OTf] is close to ideal mixing. The only system showing a tendency towards phase separation (D = 0) is [Ch][NTf_2]. This is consistent with the phase separation behavior of the [Ch][NTf_2]–water system at certain temperature and compositions,[339,340] however our values of *D* suggest that the system is stable within the composition range studied.

Nonetheless, the KB interaction parameters in the [Ch][NTf2] IL–water system are distinctly different to that of any other in this study. One hypothesis is that this is due to a combination of two different aspects of IL–water mixtures. The first is a difference in the ability to form heterogeneous liquid structures within the pure IL to form polar and non–polar domains. The resultant liquid structure can then accommodate water within the polar, hydrophilic domains, while being excluded from the non–polar, hydrophobic domains.[341,342]

The second is the ability to form hydrogen–bonding interactions with water. While there has been no study on the liquid structure of this pure IL to the best of our knowledge, the absence of a long, lipophilic functional group on either the anion or cation of the IL suggests a more homogeneous structure of pure [Ch][NTf2]. Additionally, the [NTf2] anion has been shown before now to interact weakly with water through hydrogen bonds,[167,168] while only the hydroxyl group of the cholinium cation is likely to form hydrogen bonds with water. The result is an IL with apparent low compatibility with water at high concentrations, as has been shown in this chapter. However further experimental evidence of the specific molecular interactions and the mesoscopic structure of [Ch][NTf2] and its mixtures with water are required to confirm this hypothesis.

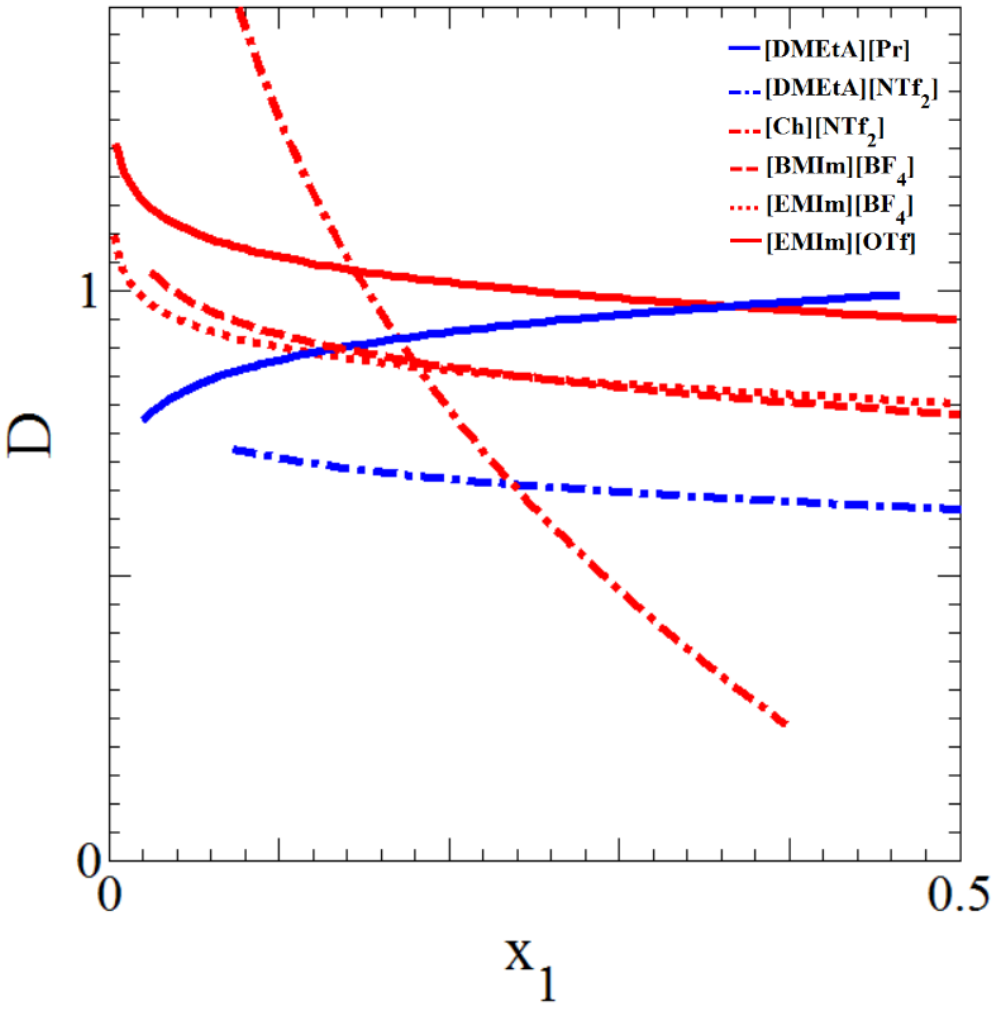

Figure 3.7 The D factor for each system as calculated from Eqn (3.4).

3.3.4 Partial Molar Volume Considerations

Partial molar volumes and excess molar volumes are widely used to probe intermolecular interactions in IL–water mixture. V_1 and V_2, as well as the excess volumes, have been employed in the literature to characterize the interactions between the species. The connection between intermolecular interactions and partial molar volumes has not been well rationalized, leading to misinterpretation of the origin of the thermodynamics of these systems. V_1 and V_2 actually contain several KB integrals, demonstrating that it is hard to separate one type of intermolecular interaction from the other simply by using the volumetric data alone. It is shown here that these quantities are a combination of intermolecular interactions defined via the KB theory. This can be demonstrated easily by solving the simultaneous equations consisting of the following (that can be derived from the Gibbs–Duhem equations or directly from the grand partition function):

$$(n_1 G_{11} + 1)V_1 + n_2 G_{12} V_2 = kT\kappa_T \tag{3.10}$$

and the isobaric isothermal Gibbs–Duhem equation:

$$n_1 V_1 + n_2 V_2 = 1 \tag{3.11}$$

Thus obtaining

$$V_1 = \frac{RT\kappa_T - G_{12}}{[1+n_1(G_{11}-G_{12})]} \tag{3.12}$$

$$V_2 = -\frac{n_1(RT\kappa_T - G_{11})}{n_2[1+n_1(G_{11}-G_{12})]} \tag{3.13}$$

Swapping the indices 1 and 2 also yields a pair of equations which describes V_1 and V_2 in terms of G_{12} and G_{22}. Thus V_1 and V_2 do not correspond to any one single KB integral, especially away from dilute concentration range of 1 or 2, showing that they contain different interactions (water–water and water–IL) at the same time.

3.4 Conclusions

Based upon the rigorous statistical thermodynamic theory, the interactions in IL–water binary mixtures at low water concentrations in both AIL and PIL systems have been determined. By using the Kirkwood–Buff (KB) theory of solutions, [148,287–289,291,293,303,304] interactions between solvent species within six IL–water mixtures have been calculated using only density and water activity data of the mixtures.

For analogous ILs, the AIL [Ch][NTf_2] has greater preference of ion–water interactions at low concentrations, with the PIL [HDMEtA][NTf_2] exhibiting greater preference of ion–water interactions at higher water concentrations (question 1) (Figure 3.2). This is rationalized by a strong increase in the water–water interaction strength with increasing water concentration in [Ch][NTf_2] (Figure 3.3). In contrast, the AIL [EMIm][OTf] exhibits stronger ion–water interactions than the PIL [HDMEtA][Pr] over the studied concentration range (question 1) (Figure 3.4). This potentially is due to the relative difference of the ionic nature betwee [EMIm][OTf] and [HDMEtA][Pr].

The ion–ion interaction strength is not greatly affected by the presence of water for either PIL (question 2). The significance of this result is that while water–ion interactions in the example PILs are preferential to the ion–ion interactions at the concentrations studied (Figure 3.6), the structure of the IL portion of the mixture strongly resembles that of the pure system for both PILs in this study (Figure 3.5).

The mixing behavior of the two PIL–water systems is described using the "closeness to phase separation" parameter (question 3). For both [HDMEtA][NTf_2] and [HDMEtA][Pr], it is found that the systems are closer to stable phase behavior than phase separation (Figure 3.7), despite the strong water–water interactions observed in both PILs (Figure 3.3) and the relatively unchanged ion–ion interactions in the presence of water. The stark contrast between the analogous PIL and AIL is further shown, with [Ch][NTf_2] showing a decrease of phase stability with increasing water concentration.

Chapter 4: On the Structure–Property Relations in Protic Ionic Liquids

4.1 Introduction

Utilising Statistical Thermodynamic theory, it has been suggested that long range solution structure in ionic liquid–water binary mixtures may contribute to the bulk solution properties through the factor of $4\pi r^2$.[148,149] Regardless of the specific components, this is a universal phenomenon across liquid solutions in general. However, from the chemistry perspective, it would be ideal if the bulk properties can be rationalized solely from the short–range interactions. With the understanding gained from the previous chapter on how water interacts with PILs at low concentrations, attention is turned towards studying neat PILs.

Understanding how variation in function corresponds to the change in the properties of PILs, particularly pertaining to their use as solvents, is crucial for their continued application. As discussed in section 1.7, there are many ways of experimentally characterizing the physicochemical properties of neat PILs.[50,52] However, the knowledge of how structure influences the properties of PILs, pertaining to their use as solvents, remains limited. Additionally, the connection between macroscale characteristics and molecular interactions in pure PILs remains unclear. To address this, the questions of how and why the inclusion of additional hydrogen bonding functionality mediates the molecular energetics and solvation properties in model PIL systems will be investigated in this chapter. As discussed in section 1.7.1, by quantifying the energetics of a PIL, aspects such as the vaporization mechanism and the strength of the solvent–solvent interactions can be determined. These intrinsic characteristics of solvents are as important as rationalizing specific solvent–solute interactions as described in section 1.8, yet are often overlooked.

Three tertiary ammonium acetate PILs with varying precursor amine functionality have been chosen; *N*,*N*–dimethylbutylammonium acetate ([HDMBuA][OAc]), 2–(dimethylamino)–*N*,*N*–dimethylethylammonium acetate ([HTMEDA][OAc]) and *N*,*N*–dimethylethanolammonium acetate ([HDMEtA][OAc]) as model PIL systems. In this Chapter, the following questions will be addressed; (1) How does PIL functionality influence the vaporization mechanism of PILs under reduced pressure? (2) Can changes in the energetics of PILs be rationalized by the molecular interactions in PILs? (3) Can the same molecular interactions explain how variation of PIL cation structure influences the solvent properties of PILs?

By using a combination of Calvet–drop microcalorimetry, solution calorimetry and *ab–initio* calculations, $\Delta_{\mathrm{vap}}H_m^{\circ}$ of each PIL was determined using two independent techniques. The agreement of these two values of $\Delta_{\mathrm{vap}}H_m^{\circ}$ will confirm the vaporization mechanism (question 1).[343]

In assessing the molecular basis for variations in the quantified energetics of PILs, comparisons to the properties and structures of the precursors are shown.[343] Based on these connections, a molecular level rationalization for the variation in energetics is obtained using attenuated total reflectance infrared (ATR–IR) spectroscopy (question 2).[344]

Based on the insight gained from thermochemistry and spectroscopy, a molecular basis of key solvent properties of these three PILs is connected to experimental quantities of viscosity and Kamlet–Taft solubility parameters. Using these quantities, connection of specific and non–specific solvent–solute and net solvent–solvent interactions to the ionic nature of a tertiary ammonium acetate PIL can be established (question 3).[344]

4.2 Experimental

4.2.1 NMR Characterization

^{1}H and ^{13}C NMR analysis of the pure PILs were performed using a Bruker 700 MHz NMR instrument at 700 MHz and 176 MHz, respectively.[245] A Wilmad coaxial inset contained a solution of D_2O with 1.0 % w/w *tert*–butyl alcohol was used to generate a reference signal for both the ^{1}H and ^{13}C NMR.[345]

4.2.2 Materials and Synthesis of PILs.

The acetic acid (HAc, ≥99.5%) and amines (DMBuA, 99.0%; TMEDA, ≥99.5%; DMEtA, ≥99.5%,) used in the preparation of the protic ionic liquids were supplied by Sigma Aldrich UK, and were not further purified.

The three PILs in this study were prepared following the procedure outlined by Walker.[49] All sample preparation was performed within a fume cupboard. Into a two–necked round bottom flask equipped with a dropping funnel attached vertically and a magnetic stirrer bar, the predetermined quantity of precursor amine is weighed. The vessel is then purged with nitrogen, cooled in an ice bath above a magnetic stirrer, set at a steady mixing speed. The predetermined quantity of acetic acid is weighed into the dropping funnel. Once the amine has been sufficiently chilled, add the acid dropwise taking consideration to not allow the temperature of the system to rise above 30°C. After complete addition, remain stirring the mixture for at least one hour to ensure the mixture has reached equilibrium. Remove the vessel from the ice bath and allow the mixture to gradually reach room temperature. Transfer the mixture to a pre–weighed, labelled brown glass bottle.

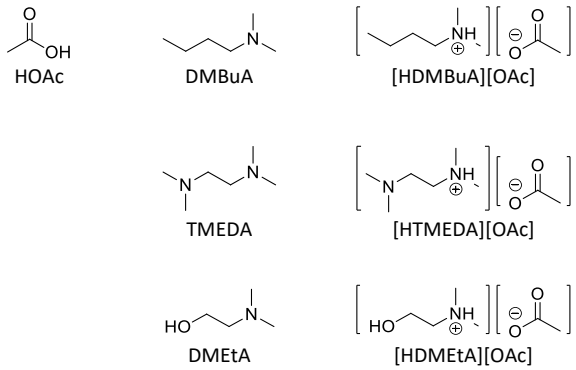

Figure 4.1. Molecular structures and abbreviations of the three PILs and their corresponding precursor materials studied in this chapter.

4.2.2.1 Synthesis of [HDMBuA][OAc]

Mass of DMBuA: 5.1158 g (50.6 mmol), mass acetic acid: 3.0961 g, (51.6 mmol). Molar percentages of components as determined from the above masses: 50.5% (acid), 49.5% (amine). ^{1}H NMR (700 MHz, D_2O) δ/ppm 2.98–2.96 (t, *J* = 7.8 Hz, 2H), 2.81 (s, 6H), 2.29 (s, 3H), 1.97–1.92 (q (tt)[(a)], *J* = 7.8,7.6 Hz, 2H), 1.78–1.72 (hx (qt)[(b)], *J* = 7.6, 7.4) 1.34 (t, *J* = 7.4). ^{13}C NMR (176 MHz, D_2O) δ 174.63, 58.24, 43.62, 28.34, 22.22, 20.56, 13.88.

4.2.2.2 Synthesis of [HTMEDA][OAc]

Mass TMEDA: 4.6541 g (40.1 mmol), mass acetic acid: 2.4377 g (40.6 mmol). Molar percentages of components as determined from the above masses: 50.3% (acid), 49.7% (amine). ^{1}H NMR (700 MHz, DMSO–d6) δ/ppm 2.98 (s, 4H), 2.71 (t, 12H), 2.29 (s, 3H). ^{13}C NMR (176 MHz, D_2O) δ 174.47, 56.14, 44.90, 22.36.

4.2.2.3 Synthesis of [HDMEtA][OAc]

Mass DMEtA: 4.4747 g (50.2 mmol), mass acetic acid: 3.0404 g (50.6 mmol). Molar percentages of components as determined from the above masses: 50.2% (acid), 49.8% (amine). ^{1}H NMR (700 MHz, D_2O) δ/ppm 4.00–3.98 (t, *J* = 5.0 Hz, 2H), 3.19–3.17

(t, *J* = 5.0 Hz, 2H), 2.88 (s, 6H), 2.11 (s, 3H). ^{13}C NMR (176 MHz, DMSO) δ 176.63, 59.89, 57.10, 43.50, 23.42.

(a) non-equivalent hydrogen environments have very similar coupling constants, producing a multiplicity pattern indicative of a single 4H environment (pentet) as opposed to two 2H environments (triplet of triplets).

(b) non-equivalent hydrogen environments have very similar coupling constants, producing a multiplicity pattern indicative of a single 5H environment (hextet) as opposed to a 3H and a 2H environments (quartet of triplets).

4.2.3 Karl Fischer Titration

Measurements were performed with a Metrohm 890 Titrando with 803 Ti Stand apparatus. Hydranal–Composite 5 was used as the titrating agent and methanol as the baseline solvent. The instrument was calibrated with Hydranal Water Standards 10.0, 1.0 and 0.1, which correspond to weight percentage water contents of 10.0%, 1.0% and 0.1%. Approximately 1 cm^3 of sample was used in the determinations. The water contents in the amines were: 230 ppm (x_w: 0.001295203) for DMBuA, 895 ppm (x_w: 0.005737812) for TMEDA, and 270 ppm (x_w: 0.001334204) for DMEtA. The water contents in the PILs studied were: 645 ppm (x_w: 0.002876844) for [HDMBuA][OAc], 1057 ppm (x_w: 0.005140561) for [HTMEDA][OAc] and 900 ppm (x_w: 0.003712974) for [HDMEtA][OAc].

4.2.4 Calvet Microcalorimetry

Direct measurements of the standard molar enthalpies of vaporization of the studied PILs and their constituent amines were carried out by Calvet–drop microcalorimetry, following a procedure previously described by Vitorino *et al.*[204] A sample with a mass between 6–12 mg was inserted into a capillary under an N_2 atmosphere. The capillary was sealed using Parafilm ''M'' tape and weighed in a Mettler UMT2 ultra–micro balance, with a precision of 0.1 μg. The Parafilm seal was removed and the capillary with the sample was immediately dropped into the calorimetric cell, held at 297.9±0.1 K under a N_2 atmosphere. After the drop, the system was evacuated to 0.13 Pa. The specific enthalpy of the calorimetric process, $\Delta_{\mathrm{vap}}h$ (J·g^{-1}), was obtained from:

$$\Delta_{\mathrm{vap}}h = \frac{1}{m}\left[\frac{A - A_b}{\varepsilon} - \frac{M_{\mathrm{H_2O}}}{m_{\mathrm{H_2O}}}\Delta_{\mathrm{vap}}H_m^{\circ}(\mathrm{H_2O})\right] \quad (4.1)$$

where m is the mass of the sample, $m_{\mathrm{H_2O}}$ is the mass of water given by Karl Fischer titration, $M_{\mathrm{H_2O}}$ = 18.015 g·mol^{-1} is the molar mass of water, $\Delta_{\mathrm{vap}}H_m^{\circ}(\mathrm{H_2O})$ = 44.004±0.002 kJ·mol^{-1} is the standard molar enthalpy of vaporization of water,[346] A is the area of the measured curve corresponding to the overall experiment, A_b is the area of the background contribution for the observed process due to dropping and to the evacuation of the cell, and ε is the energy equivalent of the calorimeter obtained by electrical calibration.[347] Background values were determined by replicating the above described experiment using an empty capillary. Results are summarized in Table 4.1.

Table 4.1 Standard specific enthalpy of vaporisation, $\Delta_{vap}h^0$/J·g^{-1}, of amines and PILs obtained by Calvet–drop microcalorimetry at 297.93 K.

Amines/PILs	DMBuA	TMEDA	DMEtA	[HDMBuA][OAc]	[HTMEDA][OAc]	[HDMEtA][OAc]
M / g·mol^{-1}	101.190	116.209	89.138	161.245	176.260	149.190
$\Delta_{vap}h^0$ / J·g^{-1}	349.586	370.895	526.250	663.648	663.648	796.545
	354.331	366.870	534.395	667.617	663.599	795.269
	342.641	376.427	529.967	673.758	665.108	804.606
	343.631	368.116	528.869	688.508	660.580	796.614
$<\Delta_{vap}h^0>$ / J·g^{-1}	347.55 ± 2.73[a]	370.58 ± 2.12 [a]	529.87± 1.70 [a]	673.38 ± 5.45 [a]	663.23 ± 0.95 [a]	798.26 ± 2.14 [a]
$<\varepsilon>$ / mV·W^{-1}	64.112 ± 0.034					
σ(over–all) / J·g^{-1}	2.74	2.13	1.72	5.46	1.01	2.18
$\Delta_{vap}H^0_m$ / kJ·mol^{-1}	35.2 ± 0.6	43.1 ± 0.5	47.2 ± 0.3	108.6 ± 1.8	116.9 ± 0.4	119.1 ± 0.7

[a] The assigned uncertainties are twice the combined standard uncertainty, u_c,[348] of four determinations, which includes contributions from the main experiment and calibration.

4.2.5 Solution Calorimetry

Solution calorimetry measurements were performed with an electrically calibrated isoperibol Thermometric Precision Solution Calorimeter (model 2225) adapted to a Thermal Activity Monitor thermostatic jacket (TAM 2227) with a temperature stability better than 0.1 mK. The procedure has been previously detailed.[204,205] In a typical experiment a thin walled glass ampule was loaded with sample, under N_2 atmosphere, and weighed with a precision of 10 μg in a Mettler Toledo XS205 balance. The dissolution process was started by breaking the ampule inside the calorimetric vessel containing 100 cm^3 of the appropriate solution, under stirring. The standard molar enthalpy of the solution process, $\Delta_{sol}H_m^\circ$, was calculated from:

$$\Delta_{sol}H_m^\circ = \frac{M\varepsilon\Delta T_{ad}}{m} \quad (4.2)$$

$$\varepsilon = \frac{VIt}{\Delta T_{ad}} \quad (4.3)$$

where *m* and *M* are the mass and the molar mass of the sample, respectively; ε is the calibration constant determined by dissipating an known amount of heat $Q = VIt$ inside the calorimetric solution, where *V* is the potential difference applied to the calibration resistance, *I* the resulting current and *t* the duration of the heat input; and ΔT_{ad} is the adiabatic temperature change in the calibration or main experiment calculated from the experimental temperature *vs.* time curves by using the Regnault–Pfaundler method[349] as implemented in the SolCal 1.2 program from Thermometric under the designation dynamics of break. The heat associated with ampoule breaking was not taken into account, since it was previously shown that when empty ampoules were broken in 100 cm^3 of water, it corresponded to a temperature change of less than 0.1 mK. The solution calorimetry measurements are summarized in Table 4.2.

Table 4.2 Standard molar enthalpies of solution, $\Delta_{sol}\boldsymbol{H_m^0}$ / kJ·mol^{-1}, of amines and PILs at 298.15 K.

Amines/PILs	DMBuA	TMEDA	DMEtA	[HDMBuA][OAc]	[HTMEDA][OAc]	[HDMEtA][OAc]
		Eq. (4.9)			Eq. (4.7)	
$-\Delta_{sol}H^0_m$ / kJ·mol^{-1}	–60.427	–79.659	–55.303	–46.102	–59.810	–31.849
	–62.267	–71.636	–57.848	–47.607	–55.999	–32.757
	–60.798	–78.774	–60.894	–46.733	–56.870	–36.698
	–57.873	–79.585	–57.966	–47.839	–61.472	–35.078
	–66.439	–80.105	–55.623	–45.862	–60.000	–35.613
	–64.712	–73.882				–32.400
$< -\Delta_{sol}H^0_m >$ / kJ·mol^{-1}	62.09 ± 2.53[a]	77.27 ± 2.93 [a]	57.53 ± 2.01[a]	46.83 ± 0.79 [a]	58.83 ± 2.06 [a]	34.07 ± 1.62 [a]

[a] The assigned uncertainties are twice the combined standard uncertainty, u_c,[348] of four determinations, which includes contributions from the main experiment and calibration.

4.2.6 Density

Density measurements by the oscillating U–tube method were performed at 298.15 K, in an Anton–Parr DSA5000 apparatus. Calibration of the density meter was carried out by using freshly boiled de–ionized water with a known density of 0.997048±0.000001 g cm^{-3} at 298.15 K.[350] Care was taken to avoid the formation of air bubbles within the measurement chamber. The estimated accuracy of the results was 0.000001 g cm^{-3}. Density values were used to calculate the molar volumes of each PIL based on the corresponding molar masses (Table 4.3).

Table 4.3 Experimental densities and molar volumes at 298.15 K of the three PILs under study.

PIL	Density / g·cm^{-3}	Molar Mass / g·mol^{-1}	Molar Volume / cm^3·mol^{-1}
[HDMBuA][OAc]	0.879215	161.24	183.39
[HTMEDA][OAc]	0.915760	176.26	192.47
[HDMEtA][OAc]	1.044627	149.19	142.82

4.2.7 Viscosity

Viscosity measurements by the tuning–fork vibration method were performed using an A&D SV–10 Vibro Viscometer. The estimated accuracy of the determinations was 0.01 mPa·s. Temperature control to 298.15± 0.01 K was achieved using a water circulator located on the floor so as not to disturb the measurements. The absolute viscosities of each of the three PILs were recorded once the instrument was brought to equilibrium and a stable value was obtained.

4.2.8 Attenuated Total Reflectance Infrared Spectroscopy (ATR–IR)

The ATR–IR spectra of all precursor materials and mixtures were recorded at room temperature using an A_2 Technologies (Agilent) ExoScan Fourier–Transform Infrared Spectrometer fitted with a germanium crystal attenuated total reflectance interface. All measurements were performed within the infrared region between 3500 and 800 cm^{-1}. A background signal was recorded 32 times to produce a single averaged background spectrum. The sample was then placed directly on to the interface for immediate measurement of 32 scans and then averaged to produce a single sample spectrum. The interface was cleaned using a dry paper towel and propan–2–ol. Once the interface was cleaned sufficiently to return the beam to the background baseline, the instrument was ready for subsequent measurements. Each sample was recorded three times for a total of 96 scans, averaged to produce the final ATR–IR spectrum.

4.2.9 Solvatochromic Parameters from UV–Visible Spectroscopy

The solvatochromic parameters α, β and π^* [2,260,261,351,352] were calculated based on the observed wavelength of maximum absorption, λ_{max}, of three solvatochromic dyes: 4–nitroaniline (NA), *N*,*N*–diethyl–4–nitroaniline (DE), and 2,6–dichloro–4–(2,4,6–triphenylpyridinium–1–yl)phenolate (BD). The 2,6–dichloro derivative of the betaine dye was chosen because of its stability in strong hydrogen bond donating media, such as water and protic ionic liquids.[261,351,352]

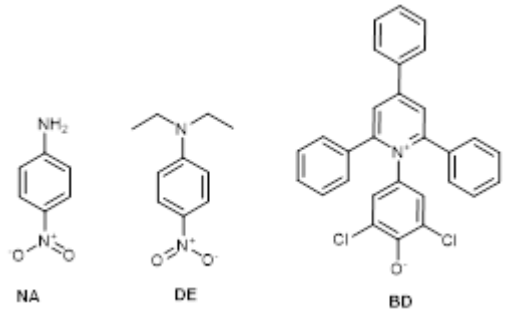

Figure 4.2. Structures and abbreviations of the three solvatochromic dyes used.

The UV–Visible spectra in the region of 300 – 800 nm, with a 0.1 nm resolution, were recorded using a Thermo Scientific Evolution 60S UV–Visible Spectrophotometer, at 298.15 K, using quartz silica 1 cm path length cuvettes. A small quantity of a specific dye (c.a. 2–5 mg) was dissolved in 1 cm^3 of PIL, and was subsequently diluted to achieve a relative absorption value between 1 – 1.5. The wavelength was converted from nm to kKayser (10^3 cm^{-1}) for all necessary calculations. To calculate the solvatochromic parameters, the following equations were used: [2,260,261,351,352]

$$\alpha = \lambda_{\max}(\mathrm{BD}) - \ 0.72\pi^* - 1.54 \quad (4.4)$$

$$\beta = \ 0.370(\lambda_{max}(\mathrm{DE})) \ - \ 0.357(\lambda_{max}(\mathrm{NA})) + \ 0.943 \quad (4.5)$$

$$\pi^* = - \ 0.314(\lambda_{max}(\mathrm{DE})) + 8.64 \quad (4.6)$$

4.3 Results and Discussion

4.3.1 The Vaporization Mechanism of Protic Ionic Liquids

As discussed in section 4.1, the vaporization mechanism of some PILs under reduced pressure has been shown to proceed via reverse proton transfer followed by vaporization of the discrete precursor materials.[204] Insights into the most likely mechanism of [HDMBuA][OAc], [HTMEDA][OAc], and [HDMEtA][OAc] vaporization were provided by a comparison of the enthalpy of reaction scheme (4.1) (dissociation of the PIL into its gaseous acid and base precursors) obtained from solution calorimetry experiments, with the $\Delta_{\mathrm{vap}}H_m^{\circ}$ values directly measured by Calvet microcalorimetry. [343]

$$[BH][A](l) \rightarrow B(g) + HA(g) \qquad (4.1)$$

The enthalpy of vaporization of the PILs according to reaction scheme 4.1, $\Delta_{\mathrm{vap}}H_m^{\circ}(\mathrm{indirect})$, was determined using an adaptation of the procedure previously described by Vitorino *et al*.,[204,205] and involved the following steps:

(*i*) The enthalpies, $\Delta_{\mathrm{sol}}H_{\mathrm{m}}^{0}$(4.7), $\Delta_{\mathrm{sol}}H_{\mathrm{m}}^{0}$(4.8), $\Delta_{\mathrm{sol}}H_{\mathrm{m}}^{0}$(4.9), corresponding to the solution processes (B represents the amine precursors of the PILs):

$$[HB][OAc](l) + n H_2O(l) \rightarrow \{[HB][OAc]{:}n H_2O\}(aq) \qquad (4.7)$$

$$HOAc(l) + n H_2O(l) \rightarrow (HOAc{:}n H_2O)(aq) \qquad (4.8)$$

$$B(l) + (HOAc{:}n H_2O)(aq) \rightarrow \{[HB][OAc]{:}n H_2O\}(aq) \qquad (4.9)$$

were firstly measured by solution calorimetry or, in the case of $\Delta_{\mathrm{sol}}\mathrm{H}_{\mathrm{m}}^{0}$(4.8), obtained from data in the NBS Tables.[353] Then (*ii*) the enthalpy of the mixing process:

$$B(l) + HOAc(l) \rightarrow [HB][OAc](l) \quad (4.10)$$

was calculated as:

$$\Delta_{mix}H^0_m = \Delta_{sol}H^0_m(4.8) + \Delta_{sol}H^0_m(4.9) - \Delta_{sol}H^0_m(4.7) \quad (4.11)$$

and (*iii*) subsequently used to derive the enthalpy of formation of the PIL according to:

$$\Delta_f H^0_m\,([HB][OAc], l) = \Delta_{mix}H^0_m + \Delta_f H^0_m\,(B, l) + \Delta_f H^0_m\,(HOAc, l) \quad (4.12)$$

Finally (*iv*), $\Delta_{vap}H^0_m(\text{indirect})$ could be obtained as:

$$\Delta_{vap}H^0_m(\text{indirect}) = \Delta_f H^0_m\,(B, g) + \Delta_f H^0_m\,(HOAc, g) - \Delta_f H^0_m\,([HB][OAc], l) \quad (4.13)$$

The multiple measurements of $\Delta_{sol}H^0_m(4.7)$ and $\Delta_{sol}H^0_m(4.9)$ and the mean average used in all subsequent calculations are summarized in Table 4.2. The The values of $\Delta_f H^0_m$ (HOAc, l) (-483.66 ± 0.18 kJ.mol^{-1}) used in Eq. (4.12) and $\Delta_f H^0_m$ (HOAc, g) (-432.84 ± 0.62 kJ.mol^{-1}) in Eq. (4.13) were taken from the literature.[354] The results are summarized in Table 4.4. It should be mentioned that the calculations of $\Delta_f H^\circ_m$ ([HB][OAc], l) and $\Delta_{vap}H^\circ_m(\text{indirect})$ relied on the enthalpies of formation of the amines, which were calculated using *ab initio* calculations. The computational details of how these calculations were performed are summarized in the appendix of this Chapter.

Table 4.4 Enthalpies of solution and vaporization obtained in this work (see text). All data in kJ·mol^{-1}.[a]

	[HDMBuA][OAc]	[HTMEDA][OAc]	[HDMEtA][OAc]
$\Delta_{sol}H_m^0$(4.7)	46.83±0.79 (5)	58.83±2.06 (5)	34.07±1.62 (6)
$\Delta_{sol}H_m^0$(4.8)	1.27±0.08 [b]	1.27±0.08 [b]	1.26±0.08 [b]
$\Delta_{sol}H_m^0$(4.9)	62.09±2.53 (6)	77.27±2.93 (6)	57.53±2.01 (5)
$-\Delta_{vap}H_m^\circ$	16.53±2.65	19.71±3.58	24.72±2.58
$-\Delta_f H_m^\circ$(PIL, l)	626.6±3.9	555.7±4.5	763.4±3.2
$\Delta_{vap}H_m^\circ$(indirect)	102.6±4.8	113.7±5.3	122.8±3.7
$\Delta_{vap}H_m^\circ$(direct)	108.6±1.8 (4)	116.9±0.4 (4)	119.1±0.7 (4)

[a] The reported uncertainties correspond to twice the standard error of the mean. Where appropriate, the number of independent determinations is given in parenthesis. [b] Reference [353].

Table 4.4 also includes the enthalpies of vaporization of the PILs directly measured by Calvet microcalorimetry, $\Delta_{vap}H_m^\circ$(direct), which are in excellent agreement with the corresponding $\Delta_{vap}H_m^\circ$(indirect) values. As has been previously demonstrated for 1–methylimidazolium acetate,[204] the good agreement between these two independently determined values gives a good indication that [HDMBuA][OAc], [HTMEDA][OAc], and [HDMEtA][OAc] preferentially vaporize under reduced pressure as their neutral acid and base precursors.[343]

4.3.2 Structure–Property Relations on the Thermochemistry of PILs

4.3.2.1 Connection between Precursor and PIL Cohesive Energy

From Table 4.4, it is found that the substitution of the alkyl functional group with either a hydrogen bond acceptor (HBA) or donor (HBD) functional group on the cation of these PILs studied increases its $\Delta_{\mathrm{vap}}H_m^{\circ}$. However, the introduction of a HBA or HBD functional group in the PIL backbone is also expected to affect the proton transfer equilibrium involving the ionic (HB^+, OAc^-) and neutral species (B, HOAc) present in the condensed state and the number of strong directional intermolecular interactions between them.[193,194,218,355]

For example, when [HTMEDA][OAc] is compared to [HDMBuA][OAc], the presence of the additional hydrogen bond acceptor dimethylamino group in the $TMEDAH^+$ cation, is likely to lead to further hydrogen bonding interactions within the system. NMR analysis of the neat PIL (see Experimental Section) showed only a single peak for the $–CH_3$ environment and a single peak for the $–CH_2–$ environment. This suggests that at the temperatures studied, the two nitrogen centers in $TMEDAH^+$ are equivalent due to a low barrier for proton transfer between them.[356] As such, both nitrogen atoms could be engaged in intermolecular hydrogen bonding to the acetate anion.

Furthermore, the presence of an hydroxyl group may also have a significant influence on the cohesive energy of [HDMEtA][OAc] when compared to [HDMBuA][OAc], since additional intramolecular hydrogen bonds with the acetate anion or intermolecular interactions within the system may be formed.[357] An intramolecular hydrogen bond with oxygen atoms of the acetate anion has, for example, been suggested to exist in the aprotic analogue of [HDMEtA][OAc], choline acetate.[329]

It is therefore interesting to evaluate whether or not this causes the cohesive energies of the studied PILs (measured by their $\Delta_{\mathrm{vap}}H_m^{\circ}$ values) to significantly deviate

from the typical bond or group additivity behavior often observed for many families of organic molecules[357,358] including aprotic ionic liquids.[359] To do this, the $\Delta_{\mathrm{vap}}H_m^{\mathrm{o}}$ of the precursor amines to the corresponding PILs is reported.[343] The standard molar enthalpies of vaporization of the three precursor amines, at 298.15 K, obtained by Calvet–drop microcalorimetry, are summarized in Table 4.5. The assigned uncertainties are twice the combined standard uncertainty, u_c,[348] of four determinations, which includes contributions from the main experiment and calibration. The calorimetric results for TMEDA and DMEtA in Table 1 are not significantly different from the previously reported $\Delta_{\mathrm{vap}}H_m^{\circ}(\mathrm{TMEDA})$ = 42.2±0.2[360] and $\Delta_{\mathrm{vap}}H_m^{\circ}(\mathrm{DMEtA})$ = 46.5±0.4[361], at 298.15 K, obtained from temperature-dependent vapor pressure data.

Table 4.5 Standard Molar Enthalpies of Formation and Vaporization of DMBuA, TMEDA, and DMEtA, at 298.15 K, obtained in this work.

Compound	$\Delta_{\mathrm{vap}}H_m^{\circ}$/kJ·mol^{-1} [a]	$-\Delta_{\mathrm{f}}H_m^{\circ}$/kJ·mol^{-1}	
		(g) [b]	(l) [c]
DMBuA	35.2±0.6	91.2±2.7	126.4±2.8
TMEDA	43.1±0.5	9.2±2.8	52.3±2.8
DMEtA	47.2±0.3	207.8±1.8	255.0±1.8

[a] Calvet microcalorimetry. [b] Obtained through quantum chemistry calculations (W1–F12 procedure, see appendix). [c] Derived from the corresponding $\Delta_{\mathrm{vap}}H_m^{\circ}$ and $-\Delta_{\mathrm{f}}H_m^{\circ}(\mathrm{g})$ values.

Also listed in Table 4.5 are the standard molar enthalpies of formation of the amines in the gas phase calculated by the W1–F12 procedure. The details of the computations and equations used to calculate $\Delta_{\mathrm{f}}H_m^{\circ}(\mathrm{g})$ of each amine are summarized in the Appendix. Finally, the standard molar enthalpies of formation of the amines in the liquid state (Table 4.5), needed for the solution calorimetry studies, can then be derived from the corresponding $\Delta_{\mathrm{vap}}H_m^{\circ}(\mathrm{g})$ and $\Delta_{\mathrm{f}}H_m^{\circ}(\mathrm{g})$ data presented in Table 4.5.

Despite these possible differences in hydrogen–bonding ability, the enthalpies of vaporization of the studied PILs follow, to a good approximation, a group additivity rule. Indeed, as shown in Figure 4.3, a linear least squares fit to a plot of the enthalpies of vaporization of the PILs, $\Delta_{\mathrm{vap}}H_m^{\circ}(\mathrm{PIL})$, against the enthalpies of vaporization of the corresponding precursor amines, $\Delta_{\mathrm{vap}}H_m^{\circ}(\mathrm{amine})$ led to:

$$\Delta_{\mathrm{vap}}H_m^{\circ}(\mathrm{PIL}) = (0.968\pm0.145)\,\Delta_{\mathrm{vap}}H_m^{\circ}(\mathrm{amine}) + 74.1\pm6.1 \qquad (4.14)$$

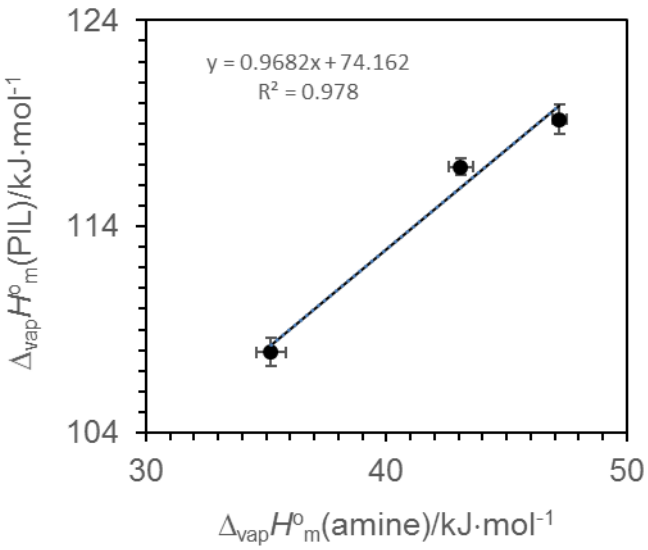

Figure 4.3. Correlation between the enthalpies of vaporization of the studied PILs and of their precursor amines.

with a correlation coefficient $R^2 = 0.978$, and where the uncertainties of the slope and the intercept represent standard deviations of the mean for 95% probability. Eq. (4.14) is able to reproduce the $\Delta_{\mathrm{vap}}H_m^{\circ}(\mathrm{PIL})$ values with deviations in the range 0.4–1.0 kJ·mol^{-1}.

4.3.2.2 Rationalizing the Ionicity of Protic Ionic Liquids

The additive contribution of functional groups to $\Delta_{vap}H_m^o$ of a PIL as inferred from Figure 4.3 suggests that functional groups do not influence the proton transfer equilibrium, and subsequently the ionic nature of a PIL. As the vaporization mechanism proceeds via the reverse proton transfer between cation and anion, the cohesive energy of PILs must also be influenced by a PILs ionicity. Although it has been recognized that aqueous data may not be appropriate for the nonaqueous PIL environment,[36,52,194,232,362] different physical properties of PILs have shown regular trends with ΔpK_a.[50,52]

As shown in Figure 4.4, this does not seem to be the case for the enthalpies of vaporization of the PILs studied in this work for which ΔpK_a([DMBuAH][OAc]) = 5.26, ΔpK_a([TMEDAH][OAc]) = 4.38, and ΔpK_a([DMEtAH][OAc]) = 4.87.[363–366] This reinforces the importance of understanding the effect of functionality on the properties of PILs; a combination of both the proton transfer mediated interactions and the contributions from the cation functional groups clearly govern the cohesive energy in PILs.

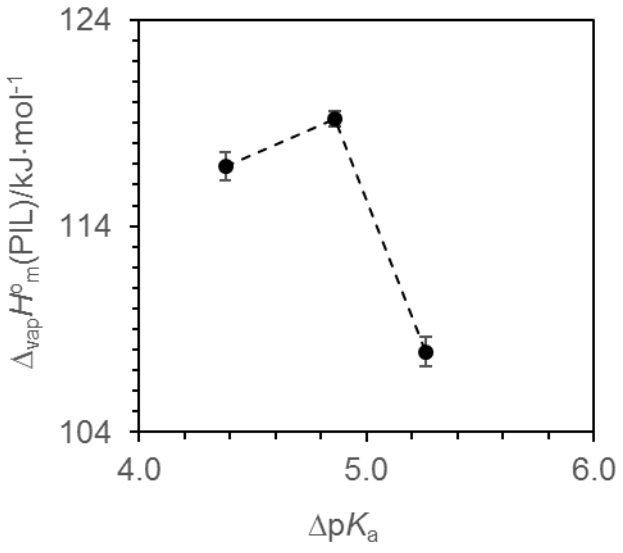

Figure 4.4. Enthalpies of vaporization of the studied PILs as a function of ΔpK_a (see text).

Since ΔpK_a does not account for the possible effects of additional functional groups to the ionicity of the PILs in this study, an approach that is more appropriate for these systems is required. One way this can be achieved for the three PILs selected is the use of infrared spectroscopy to characterize the relative absorptions of neutral and ionic species. This is because peaks can be seen corresponding to neutral acetic acid (HOAc) at approximately 1710 cm^{-1}, and to acetate anion (OAc^-) at approximately 1570 cm^{-1}.[247,367] The ATR–IR spectra of [HDMBuA][OAc], [HTMEDA][OAc], and [HDMEtA][OAc] in the range 1500–1800cm^{-1} are shown in Figure 4.5. For reference, the spectra of neat acetic acid and of the PILs precursor amines are also included.[344]

It is apparent from Figure 4.5 that the absorbance at ~1570 cm^{-1} is greater for [HDMEtA][OAc] than for either [HDMBuA][OAc] or [HTMEDA][OAc]. Simultaneously, the peak corresponding to neutral acetic acid is less intense in [HDMEtA][OAc] than in the other two PILs. This implies that the molar ratio of acetate to acetic acid and, consequently, the ionic nature, is greater for [HDMEtA][OAc] than for [HDMBuA][OAc] or [HTMEDA][OAc]. In contrast, the ionicity order given by the ΔpK_a values is [HDMBuA][OAc] > [HDMEtA][OAc] > [HTMEDA][OAc].[344] The larger ionicity of [HDMEtA][OAc] suggested by the ATR results may reflect a stabilization of the acetate ion through hydrogen bonding involving the hydroxyl group of the $DMEtAH^+$ cation, which is not possible in the cationic moieties of the other two PILs. Similar interactions have been suggested in the aprotic analogue of [HDMEtA][OAc], choline acetate.[329] Such function–specific factors influencing the ionic nature of PILs cannot, therefore, be rationalized through ΔpK_a alone.

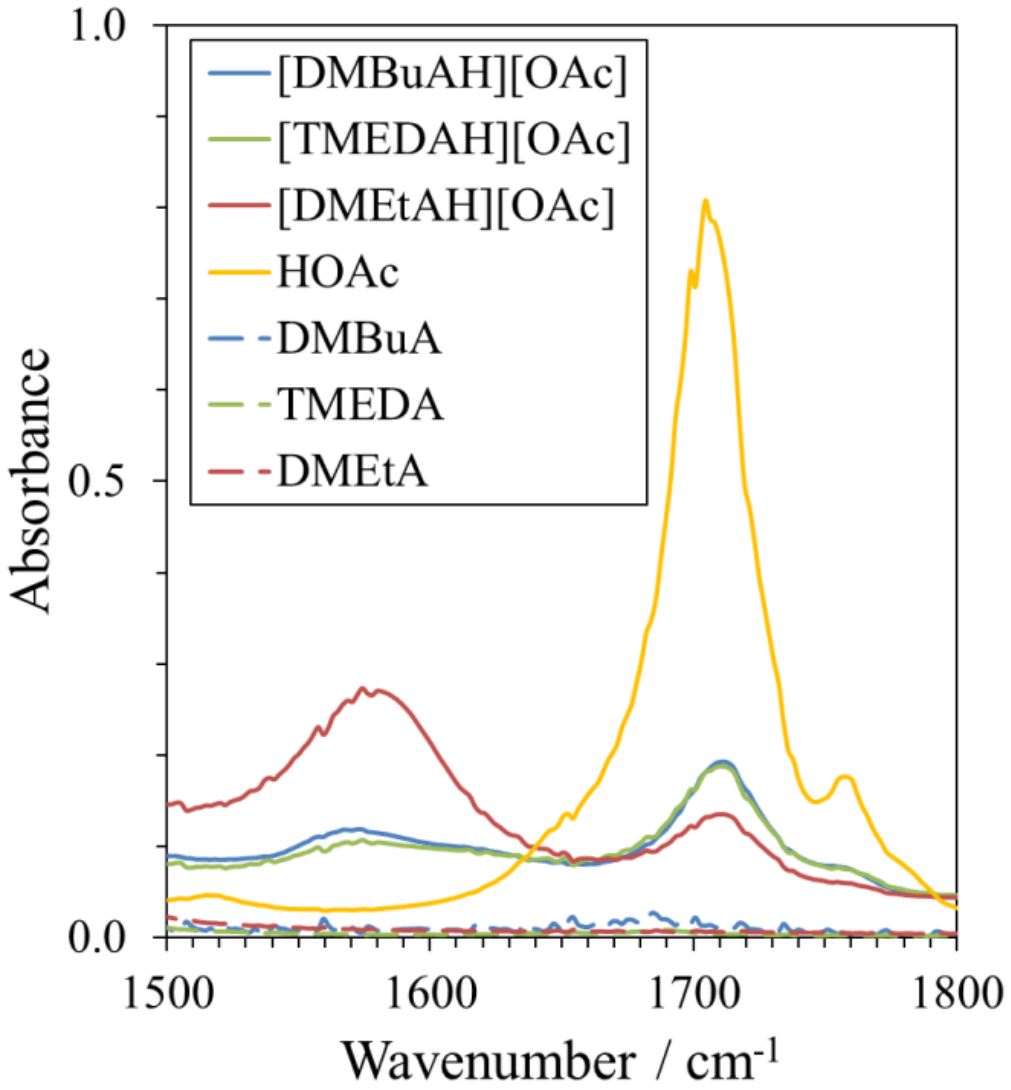

Figure 4.5. ATR–IR spectra of the three PILs and of their corresponding precursors in the region of 1500–1800 cm^{-1}. The spectrum of [HDMEtA][OAc] shows a significantly greater absorbance for the acetate species (~1570 cm^{-1}) than for the neutral species (~1710 cm^{-1}) when compared with the spectra of either [HDMBuA][OAc] or [HTMEDA][OAc].

4.3.2.3 Correlating the Ionicity and Cohesive Energy

How does this expression of ionicity relate with the cohesive energy of the PILs? Based on the calculated values of $\Delta_{\mathrm{vap}}H_m^{\mathrm{o}}$ for each PIL, there is still no clear correlation between ionicity as inferred from spectroscopy and PIL energetics. However, if the cohesive energy density, CED, of each PIL is considered, the observation is different. The CED of a solvent takes into consideration not just the enthalpy of vaporization but also the molar volume, V_{m}, of the solvent (as calculated from its density and molecular weight), and is defined by the equation;

$$\mathrm{CED} = \sqrt{\frac{\Delta_{\mathrm{vap}}U_{\mathrm{m}}^{\circ}}{V_{\mathrm{m}}}} = \sqrt{\frac{\Delta_{\mathrm{vap}}H_{\mathrm{m}}^{\circ} - RT}{V_m}} \qquad (4.15)$$

where $\Delta_{\mathrm{vap}}U_{\mathrm{m}}^{\circ}$ is the standard molar internal energy of vaporization, T is the absolute temperature (298.15 K) and R is the gas constant (8.3144598 J mol^{-1}·K^{-1}).[368]

The observed trends of CED for the three PILs suggest significantly stronger solvent–solvent interactions in [HDMEtA][OAc] than in [HDMBuA][OAc] and [HTMEDA][OAc], as shown in Table 4.6.[344]

Table 4.6 Cohesive energy densities (CED) of each PIL studied as determined from the directly measured standard molar enthalpy of vaporization and their molar volume, at 298 K.

	[HDMBuA][OAc]	[HTMEDA][OAc]	[HDMEtA][OAc]
V_{m} (cm^3·mol^{-1})	183.39	192.47	142.82
$\Delta_{\mathrm{vap}}H_{\mathrm{m}}^{\circ}$ (kJ·mol^{-1}) [a]	107.9±1.7	116.9±0.4	119.2±0.7
CED (J cm^{-3})	574.8	594.5	817.3

[a] Reference [343]

The latter two show fairly comparable CED values, which is consistent with the observed low ionic character in their IR spectra, while [HDMEtA][OAc] exhibits both a higher CED and greater ionicity based on its IR spectra. In contrast, the values of ΔpK_a show no correlation with CED, further highlighting the incapability of ΔpK_a to describe the ionicity in functionalized PILs. This excellent correlation between ionicity inferred from spectroscopy and molecular cohesion shows that hydrogen bond donor groups can significantly influence the ionicity of a PIL, and as a result influence its bulk properties.

4.3.3 Structure–Property Relations on the Solvent Properties of PILs

With this newfound appreciation of how cation functionality can alter the ionic nature and molecular cohesion of the three PILs studied in this chapter, the question of how PIL properties may also be rationally tuned by variation in functionality will be addressed. Here it is shown that the degree of ionicity, as influenced by cation functionality, plays an important role in describing the solvation environment in PILs.

Solvation behaviour depends on both solvent–solute and solvent–solvent interactions. These multiple contributions to solvation can be characterized independently from one another utilising experimentally determined solvation parameters as outlined by Kamlet and Taft.[260] Specific solvent–solute interactions i.e. hydrogen bond donor acidity (α) and hydrogen bond acceptor basicity (β), as well as non–specific solvent–solute interactions such as dipolarity/polarizability (π^*), can be parameterized using selected solvatochromic probes. While best practice for accurately characterising α, β, and π^* is by using multiple solvatochromic probes per parameter, there are limited datasets in the literature for cross comparison, and none for PILs. Three solvatochromic probes were selected to determine α, β, and π^*: 4–nitroaniline (NA), *N*,*N*–diethyl–4–nitroaniline (DE) and 2,6–dichloro–4–(2,4,6–triphenylpyridinium–1–yl)phenolate (BD).[258,260,326,351,352,369] The net contribution of solvent–solvent interactions to solvation behaviour, also considered

by Kamlet and Taft,[260] is weighted by the Hildebrand solubility parameter (δ), which is accessed through cohesive energy density values (CED).[267] Using these parameters, it is possible to quantify how specific and non–specific solvent–solute and net solvent–solvent interactions correlate to the ionic nature of a tertiary ammonium acetate PIL.[260,266,267,370]

Table 4.7 Solvatochromic parameters for the three PILs in this study.

Parameter	[HDMBuA][OAc]	[HTMEDA][OAc]	[HDMEtA][OAc]
α	0.95	0.98	0.95
β	0.95	1.01	0.69
π^*	0.69	0.69	0.94

The three solvent–solute parameters are summarized in Table 4.7.[344] The α values for the three PILs are all relatively similar, regardless of the cation functionality. [HDMEtA][OAc] may have been expected to exhibit a higher α value due to the presence of an additional hydrogen bond donor functional group, but this was not observed. The obtained values are comparable to those previously reported for acetate PILs,[261] which are greater than those typical of similarly–sized short chain alcohols.[260] These high α values are indicative of the extensive hydrogen bonding network and amphiproticity that are common features of PILs.[211]

The β value for [HDMEtA][OAc] is noticeably lower in comparison to the other two PILs (Table 4.7). It is possible this may be a result of hydrogen bonding between the hydroxyl group on the cation and the acetate anion, reducing the hydrogen bond acceptor capacity of the anion. [HTMEDA][OAc] exhibits the highest β value, which was expected due to the presence of an additional tertiary amino function on the cation. This may be anticipated to significantly alter the hydrogen bonding environment due to the formal equivalence of both amino functions in terms of their ability to interact with acetic acid.

Interestingly, the increase of β by only 0.06 on going from [HDMBuA][OAc] to [HTMEDA][OAc] further suggests a small influence of the second amino function on the hydrogen bond acceptor ability of the PIL. It is likely that a low barrier hydrogen bond exists between the two nitrogen atoms, resulting in rapid proton exchange between the two nitrogen centres on the (formally singly–charged) $[TMEDA]^+$ cation.[356] The presence of this low barrier hydrogen bond will result in a lower proton affinity of the monoprotonated $[HTMEDA]^+$ cation compared to the unprotonated amine.

In contrast, the value of π^* is highest in [HDMEtA][OAc], with [HTMEDA][OAc] and [HDMBuA][OAc] showing similar values (Table 4.7). This implies that the hydroxyl functionalized PIL has a greater dipolarity/polarizability effect on the DE dye than the alkyl or the tertiary amino functionalized PILs. With an increased ionic nature, it is to be expected that the permanent dipole moment will also increase. This is consistent with the ionicity trend observed in the ATR–IR spectra (Figure 4.5).

The δ parameter is equivalent to the square root of the CED of each PIL based,[267] and the values of δ calculated in this work are listed in Table 4.8. Due to this relation, the observations of how δ changed with functionality are consistent with observed changes in CED amongst the studied PILs: [HDMEtA][OAc] displays the highest values for both properties, with [HTMEDA][OAc] having a comparable δ to [HDMBuA][OAc]. While equivalent observations for $\Delta_{vap}H_m^\circ$ have been rationalized for variations within alkane, amine and alcohol series, through the formation of intermolecular hydrogen bonds, [357] the observed trends of δ (and corresponding CED) for the three PILs suggest significantly stronger solvent–solvent interactions in [HDMEtA][OAc] than in [HDMBuA][OAc] and [HTMEDA][OAc].

The observed differences in δ correlate well with the ionic nature of the PILs as implied by their ATR–IR spectra (Figure 4.3) but not from their ΔpK_a values. Furthermore,

the relative viscosities of these three PILs here determined were also found to correlate well with δ (Table 4.8) and the ionicity order inferred from ATR–IR spectroscopy: the viscosity of [HDMEtA][OAc] is far higher than those of the other two PILs, despite the fact that the corresponding ΔpK_a is lower than that of [HDMBuA][OAc].

Table 4.8 Molar volumes (V_m), enthalpies of vaporization, $\Delta_{vap}H^\circ_m$, cohesive energy densities (CED), viscosities (η) and Hildebrand parameter (δ) for the three PILs in this study.

	[HDMBuA][OAc]	[HTMEDA][OAc]	[HDMEtA][OAc]
CED (J cm^{-3})	574.8	594.5	817.3
δ_H (J$^{0.5}$ cm$^{-1.5}$)	24.0	24.4	28.6
η (mPa·s)	1.89	2.59	42.10
ΔpK_a [b]	5.26	4.38	4.86

[a] Reference [344]. [b] References [344,363–366].

The variation of cation functionality can influence the solvation environment in PILs as inferred from solvent–solute and solvent–solvent Kamlet–Taft solubility parameters, as well as the bulk viscosity. While there are likely many interactions occurring in these PILs, it is the extent of proton transfer as shown from ATR–IR spectroscopy that correlates well with the change in solvent properties observed. This connection, between the variation of cation functionality, the ionic nature of the PIL and the properties pertaining to their use as solvents, rationalizes the molecular origin of how solvation properties change with molecular structure of PILs.

4.4 Conclusions

The analysis of the $\Delta_{vap}H^\circ_m$(PIL) data suggested that the predominant vaporization mechanism of the three PILs under reduced pressure involves a reverse proton transfer from the cationic to the anionic moiety in the liquid state to give the neutral amine and acetic

acid precursors in the gas phase. Variation of the cation functional group does not influence the vaporization mechanism, thus further reinforcing the previously proposed vaporization mechanism (question 1).

A good linear correlation between $\Delta_{\mathrm{vap}}H_m^{\circ}(\mathrm{PIL})$ and $\Delta_{\mathrm{vap}}H_m^{\circ}(\mathrm{amine})$ is found, which initially implied group additive contributions of functional groups to the cohesive energy of PILs. As the vaporization mechanism proceeds via proton transfer, it would imply that the ionicity of a PIL would also correlate to its cohesive energy. While there is a lack of trend between $\Delta_{\mathrm{vap}}H_m^{\circ}$ and the $\Delta\mathrm{p}K_{\mathrm{a}}$ of the PILs, an excellent correlation between the CED and the apparent ratio of acetate and acetic acid species for each of the PILs as described from the IR spectra of the PILs is observed. The PIL *N,N*–dimethylethanolammonium acetate exhibited far greater CED and ionicity (inferred from infrared spectroscopy) than the other two PILs, rationalized by the hydroxyl functional group stabilizing the acetate anion (question 2). This result not only shows that functional groups can influence the ionicity of PILs, but also that the $\Delta\mathrm{p}K_{\mathrm{a}}$ is not an appropriate relation to describe the ionicity of functionalized PILs.

The ionicity of the PILs inferred from infrared spectroscopy also correlates very well with specific solvent–solute (β), non–specific solvent–solute (π^*) and solvent–solvent (δ) computed interaction parameters, as well as with the experimental viscosity (η) (question 3). The variation in bulk thermodynamic properties and Kamlet–Taft solubility parameters with cation structure can be rationalized through the ionicity of PILs inferred from ATR–IR spectroscopy. In this chapter, the ionicity of a PIL is shown to significantly impact properties relevant to its application as a solvent, and it can be used for tuning solvent–solute and solvent–solvent interactions which mediate both cybotactic and bulk properties of foremost importance to numerous PILs applications.

Chapter 5: Relating Precursors to Protic Ionic Liquids: Mixing behaviour of Acid–Amine Binary Mixtures.

5.1 Introduction

The correlation between short–range interactions and macroscopic properties shown in chapter four is valuable in rationalizing structure–property relationships. Yet in the context of a PIL being an equimolar mixture of a Brønsted acid and base, the systems studied in chapter 4 represent one composition within an acid–amine binary mixing scheme. An appreciation of the non–equimolar compositions of acid and base will bridge the understanding of how precursor structure influences PIL properties. In thermodynamics, by studying the composition derivative of properties one can yield the interactions at a molecular level.[287,299,371] Therefore, to understand the interactions in the equimolar composition (i.e. the PIL), it is necessary to study the non–equivalent mixtures of acid and amine precursors.

Furthermore, maintaining a strictly equimolar composition of acid and amine adds a further constraint to the application of PILs in industrial applications. A more practical approach would be to comprehend how slight deviations from the equimolar composition truly influences bulk properties and molecular interactions in acid–amine binary systems. Expanding from this further, understanding the applicability of non–equivalent acid–amine binary mixtures as solvents over the entire composition range may lead to additional tunability and control of processes taking place in these binary systems. Is the 50:50 anything more than just a point on the continuum?

To study the mixing behaviour of non–equivalent acid–amine binary mixtures, an experimentally practical methodology is required. While the insight may be less robust than what can be obtained from statistical thermodynamic theory, the advantage of an experimentally practical study is that it can be readily applied to other systems for future

work. In light of the success from chapter four, where energetic and solvation parameters were rationalized by short–range interactions, a similar methodology was applied to non–equivalent acid–amine binary mixtures. The same three acid–amine binary mixtures studied in chapter four will likewise be considered here, to explore how variation of the amine functionality influences the relation between bulk properties and molecular interactions.

By characterizing the density and subsequently the average molar volume of species, the trend of these bulk properties with composition can be established. By comparing these trends to additive mixtures (i.e. the weighted sum of contributions from the precursors assuming no change in the intermolecular interactions) hypotheses concerning the mixing behaviour of these systems can be made (see sections 1.7.1). It is emphasized that volumetric data alone cannot account for the specific interactions (see section 3.3.4). To rationalize the mixing behaviour at the molecular level, two aspects of the short–range interactions will be discussed: (1) the intermolecular hydrogen bonding interactions and (2) the effect of the intermolecular interaction on both the acid and the amine species. To describe the intermolecular interactions, far infrared (FIR) spectroscopy has been used successfully for a number of PILs and hydrogen bonding mixtures (see section 1.7.2). Rationalizing the nature of intermolecular hydrogen bond interactions i.e. between neutral or ionic species, will surely better explain at a molecular level the observed trends in bulk properties. This can be addressed by characterizing the ionic nature of both the acid/anion species and the amine/cation species using a combination of ^{13}C NMR, ^{15}N NMR and ATR–IR spectroscopy (see section 1.7.3).

5.2 Experimental

5.2.1 Materials and Sample Preparation

The precursor materials acetic acid (HOAc), *N*,*N*–dimethylbutylamine (DMBuA), *N*,*N*,*N'N'*–tetramethylethan–1,2–diamine (TMEDA) and *N*,*N*–dimethylethanolamine (DMEtA) were all purchased from Sigma Aldrich and used without further purification (Figure 5.1). The same procedure as outlined in section 4.2.2 was used to prepare all acid–amine binary mixtures. The mass of each precursor used to prepare each mixture is summarized in Tables 5.1–5.3.

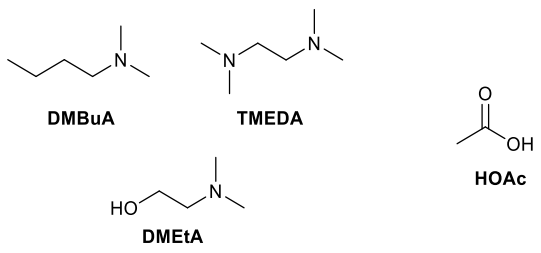

Figure 5.1. Structures of the precursor amines and acid used to prepare the non-equivalent mixtures in this chapter

5.2.2 Karl–Fischer Titration

To determine the water content of all materials studied, one component Karl–Fischer titrations were performed utilising a Metrohm 890 Titrando titration unit with a Metrohm 803 Ti Stand unit using Hydranal–Composite 5 as the titrating agent and methanol as the baseline solvent. The instrument was calibrated utilising Hydranal Water Standards 10.0, 1.0 and 0.1, which correspond to the calibrated weight percentage of water in the samples of 10.0%, 1.0% and 0.1%. Approximately 1 cm^3 of each sample was used to determine total water content. All determined water quantities of the samples studied are summarized in the tables below.

Table 5.1 Mass of precursors used for preparation of binary mixtures of acetic acid and *N*,*N*–dimethylbutylamine. Water content was determined from Karl Fischer titration.

X_{Ac}	X_{Am}	Mass Acid / g	Mass Amine / g	Moles Acid	Moles Amine	Water Content	
						ppm	X_W
0.00	1.00	–	–	–	–	231	0.001295
0.05	0.95	0.1330	4.2560	0.0022	0.0421	291	0.001598
0.10	0.90	0.2659	3.8648	0.0044	0.0382	295	0.001584
0.15	0.85	0.4143	3.7892	0.0069	0.0375	341	0.001795
0.20	0.80	0.5627	3.7135	0.0094	0.0367	331	0.001702
0.25	0.75	0.7352	3.6445	0.0122	0.0360	315	0.001586
0.30	0.70	0.9077	3.5754	0.0151	0.0354	340	0.001674
0.35	0.65	1.1631	3.4579	0.0194	0.0342	362	0.00174
0.42	0.58	1.4185	3.3404	0.0236	0.0330	396	0.001843
0.45	0.55	1.6305	3.2198	0.0272	0.0318	414	0.001896
0.50	0.50	1.8425	3.0991	0.0307	0.0306	404	0.002877
0.55	0.45	2.1552	2.9268	0.0359	0.0289	467	0.002032
0.60	0.40	2.4680	2.7544	0.0411	0.0272	515	0.00218
0.65	0.35	2.8214	2.5200	0.0470	0.0249	556	0.002292
0.70	0.30	3.1748	2.2856	0.0529	0.0226	508	0.002036
0.75	0.25	3.5747	1.9805	0.0595	0.0196	418	0.001629
0.80	0.20	3.9746	1.6754	0.0662	0.0166	316	0.001196
0.85	0.15	4.4134	1.2959	0.0735	0.0128	399	0.001464
0.90	0.10	4.8521	0.9163	0.0808	0.0091	420	0.001494
0.95	0.05	5.1691	0.4582	0.0861	0.0045	135	0.000465
1.00	0.00	–	–	–	–	105	0.000350

Table 5.2 Mass of precursors used for preparation of binary mixtures of acetic acid and *N,N,N',N'*–tetramethylethan–1,2–diamine. Water content was determined by Karl Fischer titration.

x_{Ac}	x_{Am}	Mass Acid / g	Mass Amine / g	Moles Acid	Moles Amine	Water Content	
						ppm	x_W
0.00	1.00	–	–	–	–	895	0.005738
0.05	0.95	0.1675	6.1560	0.0028	0.0530	900	0.005631
0.10	0.90	0.3349	4.8739	0.0056	0.0420	931	0.005631
0.15	0.85	0.5456	4.3087	0.0091	0.0371	832	0.004951
0.20	0.80	0.7562	3.7434	0.0126	0.0322	850	0.004715
0.25	0.75	0.7740	3.6592	0.0129	0.0315	759	0.004285
0.30	0.70	0.7918	3.5749	0.0132	0.0308	721	0.003960
0.35	0.65	0.9789	3.4780	0.0163	0.0299	704	0.003758
0.40	0.60	1.1659	3.3811	0.0194	0.0291	772	0.004000
0.45	0.55	1.4384	3.3406	0.0240	0.0288	731	0.003675
0.50	0.50	1.7109	3.3000	0.0285	0.0284	689	0.003358
0.55	0.45	1.9134	2.9937	0.0319	0.0258	627	0.002960
0.60	0.40	2.1158	2.6874	0.0352	0.0231	501	0.002289
0.65	0.35	2.4868	2.5317	0.0414	0.0218	667	0.002942
0.70	0.30	2.8577	2.3760	0.0476	0.0205	718	0.003056
0.75	0.25	3.2579	2.0785	0.0543	0.0179	748	0.003066
0.80	0.20	3.6581	1.7810	0.0609	0.0153	780	0.003079
0.85	0.15	4.1341	1.3901	0.0688	0.0120	521	0.001976
0.90	0.10	4.6100	0.9992	0.0768	0.0086	616	0.002242
0.95	0.05	4.9073	0.4996	0.0817	0.0043	413	0.001439
1.00	0.00	–	–	–	–	105	0.000350

Table 5.3 Mass of precursors used for preparation of binary mixtures of acetic acid and *N*,*N*–dimethylethanolamine. Water content was determined by Karl Fischer titration.

x_{Ac}	x_{Am}	Mass Acid / g	Mass Amine / g	Moles Acid	Moles Amine	Water Content ppm	x_W
0.00	1.00	–	–	–	–	270	0.001334
0.05	0.95	0.1330	3.7510	0.0022	0.0421	281	0.001366
0.10	0.90	0.2659	3.8711	0.0044	0.0434	330	0.001577
0.15	0.85	0.4952	3.7722	0.0082	0.0423	342	0.001607
0.20	0.80	0.7245	3.6732	0.0121	0.0412	418	0.001930
0.25	0.75	0.8639	3.5663	0.0144	0.0400	389	0.001765
0.30	0.70	1.0033	3.4593	0.0167	0.0388	516	0.002297
0.35	0.65	1.2154	3.3172	0.0202	0.0372	441	0.001929
0.40	0.60	1.4275	3.1751	0.0238	0.0356	499	0.002142
0.45	0.55	1.6682	3.0047	0.0278	0.0337	452	0.001904
0.50	0.50	1.9088	2.8343	0.0318	0.0318	387	0.001600
0.55	0.45	2.1808	2.6288	0.0363	0.0295	309	0.001253
0.60	0.40	2.4527	2.4232	0.0408	0.0272	421	0.001672
0.65	0.35	2.7251	2.1715	0.0454	0.0244	417	0.001623
0.70	0.30	2.9975	1.9198	0.0499	0.0215	399	0.001522
0.75	0.25	3.2930	1.6301	0.0548	0.0183	432	0.001602
0.80	0.20	3.5885	1.3404	0.0598	0.0150	412	0.001505
0.85	0.15	3.9196	1.0173	0.0653	0.0114	378	0.001350
0.90	0.10	4.2507	0.6941	0.0708	0.0078	451	0.001573
0.95	0.05	4.4429	0.3471	0.0740	0.0039	225	0.000768
1.00	0.00	–	–	–	–	105	0.000350

5.2.3 Density

As all samples were liquid at the studied temperature of 293.15 K, all density measurements were recorded using an Anton–Parr DSA5000 density meter. Density measurements are made based on the oscillating U–tube technology. Calibration of the density meter was performed using freshly boiled, de–ionized water with a known density of 0.998199 ± 0.000001 g cm^{-3}.[350] Care was taken to avoid the formation of air bubbles within the measurement chamber. Density results were measured to an accuracy of 0.000001 g cm^{-3}.

Table 5.4 Density (ρ) and molar volume (V_m) of the acetic acid–*N*,*N*–dimethylbutylamine binary system over the complete composition range. Additive quantities are denoted by (Id). All values were recorded at 293 K.

x_{Acid}	x_{Amine}	ρ / g cm^{-3}	$x_{Acid}.m_{Acid} + x_{Amine}.m_{amine}$ / g mol^{-1}	V_m / cm^3 mol^{-1}	V_m (Id) / cm^3 mol^{-1}
1.00	0.00	1.049631	60.05	57.21	57.21
0.95	0.05	1.046978	62.11	59.32	61.37
0.90	0.10	1.037763	64.16	61.83	65.53
0.85	0.15	1.025568	66.22	64.57	69.69
0.80	0.20	1.012445	68.28	67.44	73.85
0.75	0.25	0.997277	70.34	70.53	78.01
0.70	0.30	0.980262	72.39	73.85	82.17
0.65	0.35	0.959256	74.45	77.61	86.33
0.60	0.40	0.937941	76.51	81.57	90.49
0.55	0.45	0.90865	78.56	86.46	94.65
0.50	0.50	0.885413	80.62	91.05	98.81
0.45	0.55	0.855005	82.68	96.70	102.97
0.40	0.60	0.836901	84.73	101.25	107.13
0.35	0.65	0.815526	86.79	106.42	111.29
0.30	0.70	0.799727	88.85	111.10	115.45
0.25	0.75	0.778861	90.91	116.72	119.61
0.20	0.80	0.766929	92.96	121.21	123.77
0.15	0.85	0.754049	95.02	126.01	127.93
0.10	0.90	0.742178	97.08	130.80	132.09
0.05	0.95	0.732618	99.13	135.31	136.25
0.00	1.00	0.720672	101.19	140.41	140.41

Table 5.5 Density (ρ) and molar volume (V_m) of the acetic acid–*N*,*N*,*N*,*N*–tetramethylethan–1,2–diamine binary system over the complete composition range. Additive quantities are denoted by (Id). All values were recorded at 293 K.

x_{Acid}	x_{Amine}	ρ / g cm^{-3}	$x_{Acid}.m_{Acid} + x_{Amine}.m_{amine}$ / g mol^{-1}	V_m / cm^3 mol^{-1}	V_m (Id) / cm^3 mol^{-1}
1.00	0.00	1.049631	60.05	57.21	57.21
0.95	0.05	1.07534	62.86	58.45	61.84
0.90	0.10	1.083696	65.67	60.59	66.48
0.85	0.15	1.076351	68.47	63.62	71.11
0.80	0.20	1.049496	71.28	67.92	75.75
0.75	0.25	1.033168	74.09	71.71	80.38
0.70	0.30	1.011782	76.90	76.00	85.01
0.65	0.35	0.992304	79.71	80.32	89.65
0.60	0.40	0.968241	82.51	85.22	94.28
0.55	0.45	0.945794	85.32	90.21	98.92
0.50	0.50	0.921284	88.13	95.66	103.55
0.45	0.55	0.899202	90.94	101.13	108.18
0.40	0.60	0.879277	93.75	106.62	112.82
0.35	0.65	0.863279	96.55	111.85	117.45
0.30	0.70	0.845119	99.36	117.57	122.09
0.25	0.75	0.830166	102.17	123.07	126.72
0.20	0.80	0.818019	104.98	128.33	131.35
0.15	0.85	0.805401	107.79	133.83	135.99
0.10	0.90	0.793327	110.59	139.41	140.62
0.05	0.95	0.784195	113.40	144.61	145.26
0.00	1.00	0.775299	116.21	149.89	149.89

Table 5.6 Density (ρ) and molar volume (V_m) of the acetic acid–*N*,*N*–dimethylethanolamine binary system over the complete composition range. Additive quantities are denoted by (Id). All values were recorded at 293 K.

x_{Acid}	x_{Amine}	ρ / g cm^{-3}	$x_{Acid}.m_{Acid} + x_{Amine}.m_{amine}$ / g mol^{-1}	V_m / cm^3 mol^{-1}	V_m (Id) / cm^3 mol^{-1}
1.00	0.00	1.049631	60.05	57.21	57.21
0.95	0.05	1.079095	61.50	57.00	59.37
0.90	0.10	1.088896	62.96	57.82	61.52
0.85	0.15	1.091576	64.41	59.01	63.68
0.80	0.20	1.090058	65.87	60.43	65.83
0.75	0.25	1.088145	67.32	61.87	67.98
0.70	0.30	1.086639	68.78	63.29	70.14
0.65	0.35	1.083411	70.23	64.82	72.29
0.60	0.40	1.075198	71.69	66.67	74.45
0.55	0.45	1.064694	73.14	68.70	76.60
0.50	0.50	1.049876	74.60	71.05	78.76
0.45	0.55	1.037091	76.05	73.33	80.91
0.40	0.60	1.019884	77.50	75.99	83.07
0.35	0.65	1.004901	78.96	78.57	85.22
0.30	0.70	0.987666	80.41	81.42	87.38
0.25	0.75	0.969143	81.87	84.47	89.53
0.20	0.80	0.950941	83.32	87.62	91.69
0.15	0.85	0.932582	84.78	90.91	93.84
0.10	0.90	0.921021	86.23	93.63	96.00
0.05	0.95	0.905436	87.69	96.84	98.15
0.00	1.00	0.888661	89.14	100.31	100.31

5.2.4 Absorbance Far Infrared Spectroscopy (FIR)

The Far Infrared (FIR) spectra were recorded using a Bruker 66 V Michelson interferometer equipped with a 3 μm thick Mylar beam splitter and a Pyroelectric detector.[372] The spectral resolution was 2 cm^{-1} and data points were collected between 50–500 cm^{-1} . The liquid mixture was contained in an optical cell closed by silica windows with a 25 μm polyethylene terephthalate spacer. The cell was maintained at a temperature of 293.15 K for the duration of the measurements using a recirculating water heater. The absorption coefficient was calculated using the equation

$$A = -\left(\ln\left(\frac{I_v}{I_v^0}\right) - \ln\left(\frac{I_v^{w1}+I_v^{w2}}{I_v^0}\right)\right) \quad (5.1)$$

where I_v is the transmitted light intensity at wavelength v of the sample, I_v^{w1} and I_v^{w2} are the corresponding transmitted light intensities of each silica window used and I_v^0 is the corresponding transmitted light intensity of the background signal.

5.2.5 Attenuated Total Reflectance Mid Infrared Spectroscopy (ATR–IR)

The ATR–IR spectra of all precursor materials and mixtures were recorded at room temperature using an A_2 Technologies (Agilent) ExoScan Fourier–Transform Infrared Spectrometer fitted with a germanium crystal attenuated total reflectance interface. All measurements were performed between 3500–800 cm^{-1}. A background signal was recorded 32 times to produce a single averaged background spectrum. The sample was then placed directly on to the interface for immediate measurement of 32 scans and then averaged to produce a single sample spectrum. The interface was then cleaned using a dry paper towel and propan–2–ol. Once the interface was cleaned sufficiently to return the beam to the background baseline, the instrument was then ready for following measurements. Each sample was recorded three times for a total of 96 scans, averaged to produce the final infrared spectra of the given sample.

5.2.6 Nuclear Magnetic Resonance Spectroscopy (NMR)

NMR characterisations (^{1}H, ^{13}C and ^{15}N) of all neat samples were recorded using a Bruker 700 MHz instrument. In order to record NMR spectra of the pure liquids, a Wilmad coaxial insert with a reference lock solution 1% (w/w) *t*–butanol in D_2O was used to generate a standard lock signal in the spectra. The ^{1}H and ^{13}C NMR results were internally referenced to *t*–butanol, and the ^{15}N NMR results were externally referenced.

5.3 Results and Discussion

5.3.1 Profiling the Bulk Properties.

By measuring bulk properties, a macroscopic profile of a given binary liquid mixture is obtained, that is dependent on the interactions at the molecular level. By systematically varying the composition, both the macroscopic property and the microscopic interactions change. By comparing how the macroscopic properties change from experiment with an additive mixing scheme, which assumes zero change in the molecular interactions upon mixing, it is possible to understand what effects of molecular interactions have on the bulk properties. This will allow for potential hypotheses to be suggested on how amine functionality and composition variation change the interactions at the molecular level.

The experimental density, ρ, and the corresponding average molar volume, V_m, have been determined for the three acid–amine binary mixtures over the entire composition range at 0.05 mole fraction intervals. While these quantities are inversely related to one another, deviations from additive mixing of these two quantities can highlight slightly different attributes of the binary mixture: density fluctuations correspond to the change in molecular packing of the whole system, while changes in molar volume correspond to the variation in average size of all species in a given binary mixture. [276,373–375]

5.3.1.1 Molar Volume

The average molar volume of a binary mixture is the volume occupied per mole of said binary mixture, and is scalable with the average molecular volume of all species in the binary mixture. Using density, ρ, the average molar volume of species in a binary mixture, V_m, can be calculated utilising the mole fraction (x_1 for acetic acid and x_2 for the given amine) and molar mass of the pure precursors (m_{ac} for acetic acid, m_{am} for the given amine):

$$V_{\mathrm{m}} = \frac{(x_{\mathrm{acid}}.\mathrm{m}_{\mathrm{acid}})+(x_{\mathrm{amine}}.\mathrm{m}_{\mathrm{amine}})}{\rho} \quad (5.1)$$

This can then be compared to an additive approximation of the selected system, V_m^I, using the pure precursor molar volumes (V_{ac}^0 for acetic acid and V_{am}^0 for the given amine) giving the excess molar volume for that composition, V_m^E.

$$V_{\mathrm{m}}^{\mathrm{E}} = V_{\mathrm{m}} - (V_{\mathrm{acid}}x_{\mathrm{acid}} + V_{\mathrm{amine}}x_{\mathrm{amine}}) \quad (5.2)$$

This difference between the experimental and additive molar volumes provides a qualitative insight into how the net strength of interactions between species changes with composition in binary mixtures.[276,373–375] Note that the values of $V_{\mathrm{m}}^{\mathrm{E}}$ are also relative to the precursor V_{m} i.e. the larger the V_{m} of the pure amine, the expected greater value of $V_{\mathrm{m}}^{\mathrm{E}}$. Therefore, the deviation from additivity of molar volume relative to the additive quantity, $V_{\mathrm{m}}^{\mathrm{E}}(rel.)$ was determined for each of the acid–amine binary systems:

$$V_{\mathrm{m}}^{\mathrm{E}}(rel.) = \left(\frac{V_{\mathrm{m}}^{\mathrm{E}}}{V_{\mathrm{m}}}\right) \times 100 \quad (5.3)$$

This can allow for a fairer comparison on the effect of amine functionality on the mixing behaviour of the three systems studied.

For all three systems, each composition exhibited negative values varying in magnitude with composition (Figure 5.2). This is similar to previously published observations for similar binary mixtures of carboxylic acids and amines.[274–276,281] Negative values of $V_{\mathrm{m}}^{\mathrm{E}}$ imply an increase in the net strength of interactions between species. Coincidentally, the $V_{\mathrm{m}}^{\mathrm{E}}$ at the equimolar composition for all three systems are almost equivalent to one another. This would imply that a similar increase in interaction strength has occurred as a result of forming the equimolar mixture in each of the three systems. However, each system shows a different relation between composition and $V_{\mathrm{m}}^{\mathrm{E}}$, suggesting that the trends of how the interactions change with composition are different for all three systems.

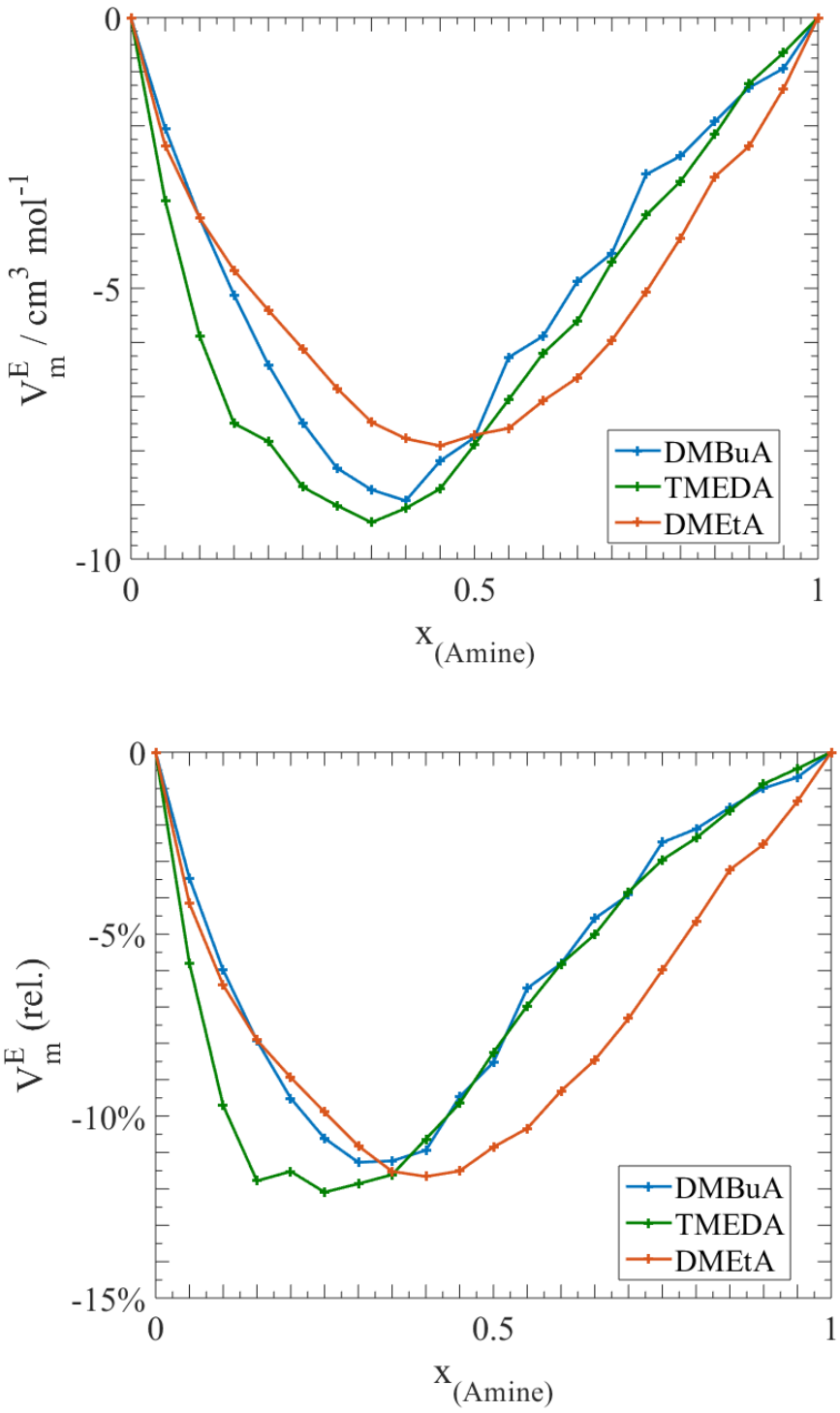

Figure 5.2 Dependence of the excess molar volume (V_m^E) (top) and the relative excess molar volume ($V_m^E(rel.)$) (bottom) on the mole fraction of amine for each of the three acid–amine binary mixtures.

In general, the most negative values of V_m^E are observed in the acid–rich compositions, as has been seen before for ammonium carboxylate binary systems.[274–276,281] All three systems show a similar most negative $V_m^E(rel.)$ value of around –10%, with the compositions varying between system. The compositions of most negative V_m^E, have been suggested to correlate with the compositions of the most stable association products of a binary mixture (e.g. for DMBuA, this would imply an aggregate of Am_2HAc_3 being the most stable). [274–276,281,376] However, there is no further evidence to support the formation of such aggregates, and as such remains simply as a hypothesis. In the amine–rich compositions, the DMEtA system shows the greatest values of $V_m^E(rel.)$, with the DMBuA and TMEDA systems having similar values in this region. This result for the DMEtA system indicates that the hydroxyl functional group significantly influences the mixing behaviour with acetic acid.

5.3.1.2 Hypotheses on the mixing behaviour of the acid–amine binary mixtures

In chapter 4, it was suggested that the increased ionicity of the PIL *N,N*–dimethylethanolammonium acetate may be due to hydrogen bonding between the acetate anion and the hydroxyl group of the cation. This stabilising hydrogen bond interaction could also be a more robust description as to why acid–rich compositions show greater deviations from additivity. Therefore, there should be a correlation between $V_m^E(\mathrm{rel})$ and the extent of hydrogen bonding interactions taking place.

The large deviations indicating increased interaction strength, particularly in the acid–rich compositions, are much greater than those typically observed in binary liquid mixtures of hydrogen bonding solvents.[373,374] This may be the direct result of the proton transfer reaction taking place, thus increasing the strength of the hydrogen bond interactions between species.[377] Therefore there should also be a correlation between the concentration of ionic species and $V_m^E(\mathrm{rel})$.

5.3.2 Characterising the short–range intermolecular interactions: hydrogen bonding and proton transfer between species.

The effect of composition and amine functionality on the intermolecular hydrogen bonding interactions between species in the three studied systems will now be considered. The FIR spectra of each system was recorded in the region of 50 – 300 cm^{-1}. While this region of the infrared spectrum has been well documented for showing intermolecular hydrogen bonding interactions,[156,162,184,210,218,220,223,236,355,378–385] there are numerous hydrogen bond interactions that could be described – for example, there will likely be some contribution from acetic acid hydrogen bonding with itself,[380,381] particularly in acid–rich compositions. Additionally, due to the different strength of molecular and ionic hydrogen bonds,[377] it is likely that there will be contributions of both acid–amine and anion–cation hydrogen bonding interactions to the observed band shape. Finally, the hydroxyl functional group on *N*,*N*–dimethylethanolamine is expected to undergo hydrogen bonding with itself,[386] which will also contribute to the FIR spectra of the DMEtA series. With these interactions in mind, the discussion focuses on how the FIR peak shape changes with both composition and amine functionality. For the sake of showing the results clearly, the FIR spectra was recorded at 10% mole percentage intervals.

5.3.2.1 Acid–Rich mixtures

The FIR of acetic acid at 293 K showed a broad peak with a maximum around 187 cm^{-1}, which is in good agreement with previously reported values of 184 cm^{-1} (Figure 5.3.[380] For the acid–rich compositions, significant changes in the peak shape in comparison to acetic acid are seen. For all systems, an increase in intensity of the peak at 187 cm^{-1} with increasing amine mole fraction is observed, as well as the emergence of a second peak at higher frequency. This suggests that an additional intermolecular interaction with an absorption around 187 cm^{-1} exists which overlays the absorption seen for pure acetic acid. All binary systems also show the emergence of a broad peak at around 235 cm^{-1}, implying that there is a second intermolecular interaction occurring as a result of mixing acid and amine. A third, broad peak of much lower intensity is observed in the range of 100–150 cm^{-1}, which appears to have greater absorbance in the DMEtA binary system.

The change in intensity of the FIR peak with respect to composition is different for each system. In fact, the compositions with maximum absorption for each system (70% HOAc for DMBuA, 80% HOAc for TMEDA and 60% HOAc for DMEtA) appear to correlate well with the compositions with the most negative V_m^E(rel) values. In addition, the equimolar composition (50% HOAc) for the DMEtA system shows a much larger absorbance than for either the DMBuA or TMEDA system. The same trend can be observed for V_m^E(rel) in Figure 5.2, further showing the connection between the relative excess molar quantity and the change in intermolecular interactions from FIR.

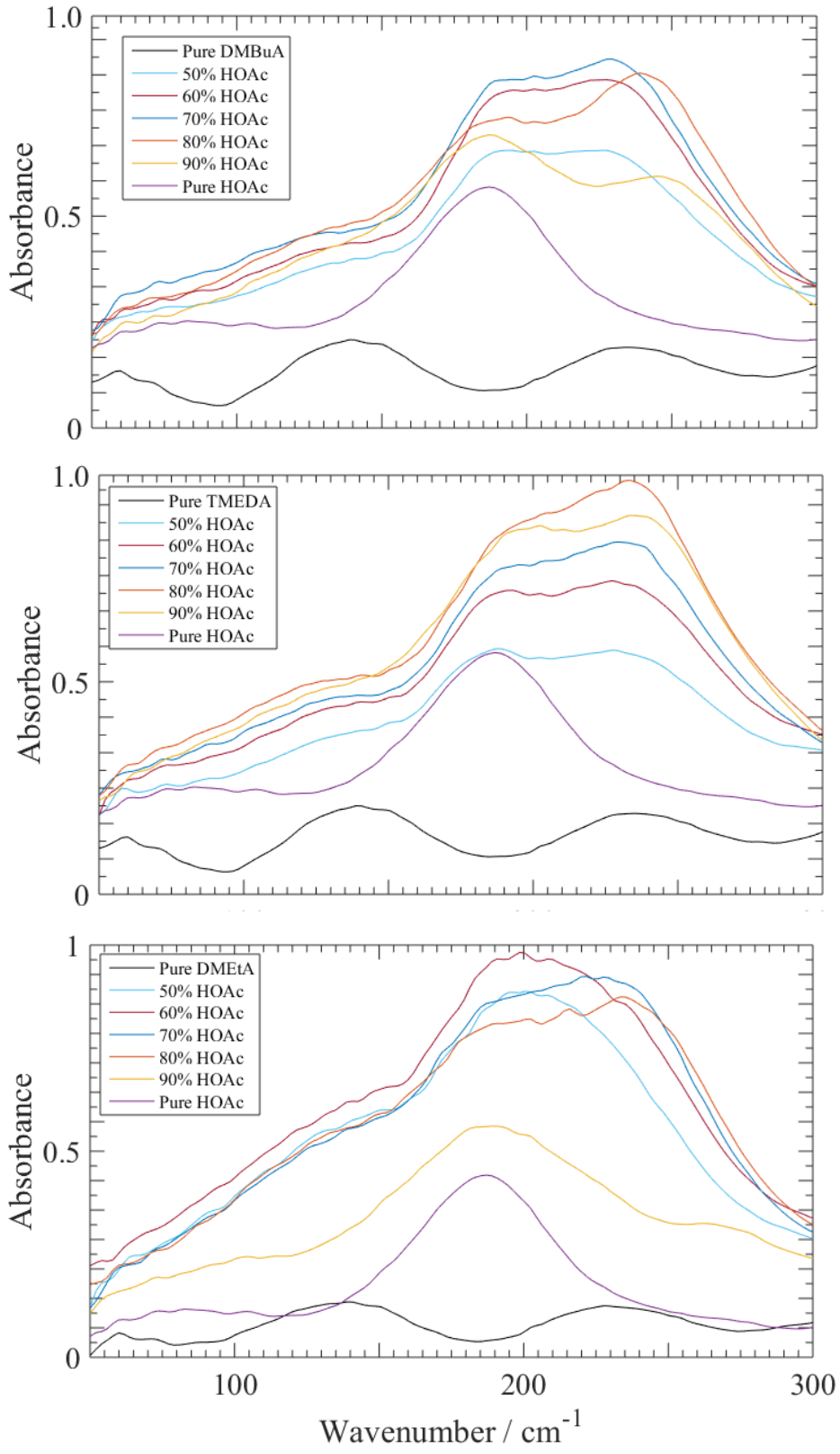

Figure 5.3 Far infrared (FIR) spectra of the acid–rich mixtures of each acid–amine binary mixture in the region of 50 – 300 cm^{-1} as a function of acetic acid mole fraction.

5.3.2.2 Amine–Rich mixtures

The pure amines all showed no evidence of a prominent absorbance peak in the FIR region studied (Figure 5.4). The DMBuA and TMEDA systems both exhibited peaks in a similar position to the acid rich compositions, however the peak in the region 100 – 150 cm^{-1} was not very well resolved in these compositions. The DMEtA system showed more clearly the emergence of this broad peak in the region 100 – 150 cm^{-1} with increasing acetic acid mole fraction, however the peak at around 230 cm^{-1} was not as well resolved as the peak at around 187 cm^{-1}.

For both the DMBuA and TMEDA binary systems, there was a comparatively similar increase in the overall absorbance of the FIR spectra as a function of increasing mole fraction of acetic acid (Figure 5.4). The DMEtA system however showed a much greater increase in the overall absorbance in the FIR region with increasing mole fraction of acetic acid. Both these trends indicate an increase in the intermolecular interactions that take place upon mixing acetic acid and amine. It also highlights that the hydroxyl–functionalized amine has a greater increase in the number of intermolecular interactions upon mixing with acetic acid than the corresponding alkyl–functionalized and dimethylamino–functionalized amines.

In comparison, all three binary systems showed negative values of $V_{\mathrm{m}}^{\mathrm{E}}(\mathrm{rel})$ in all amine–rich compositions (Figure 5.2), which correlates with the increased intensity in the FIR region (Figure 5.4). Furthermore, the DMEtA system showed a much greater negative value of $V_{\mathrm{m}}^{\mathrm{E}}(\mathrm{rel})$ for all amine–rich compositions, again consistent with the observations found here. These correlations, both in the acid–rich and amine–rich compositions, between $V_{\mathrm{m}}^{\mathrm{E}}(\mathrm{rel})$ and the total absorbance in the FIR region, give evidence for the correlation between the large negative deviations from additivity of molar volume and an increase in the intermolecular interactions between species.

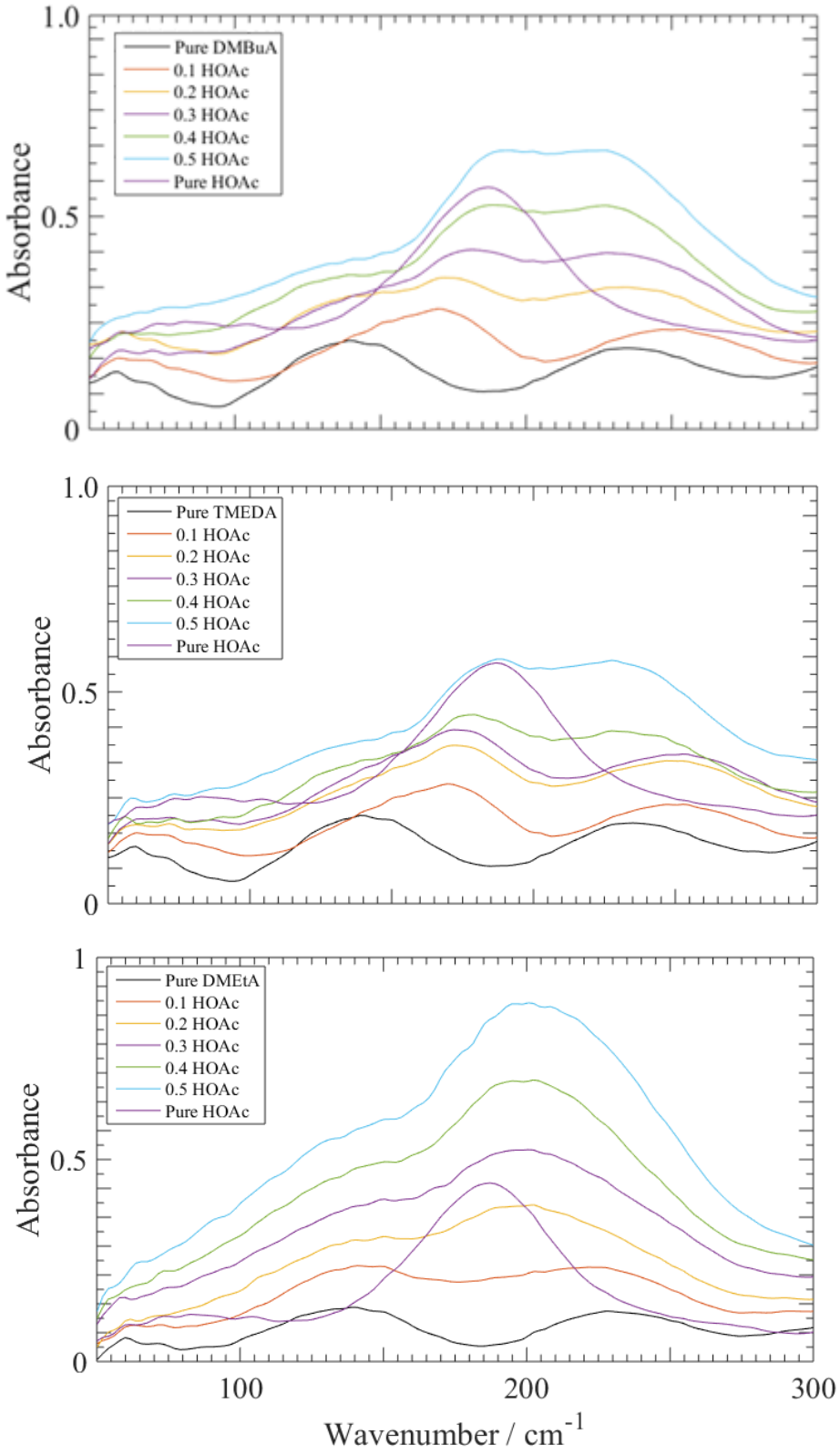

Figure 5.4 Far infrared (FIR) spectra of the amine–rich mixtures of each acid–amine binary mixture in the region of 50 – 300 cm^{-1} as a function of acetic acid mole fraction.

A disadvantage of using experimental FIR results in isolation is the lack of understanding regarding individual underlying contributions to the spectra, and therefore the level of specific molecular and ionic hydrogen bond interactions between species. To address this issue, the ionic nature of the acid/anion and amine/cation species can be inferred indirectly using multiple spectroscopic techniques. By characterizing the ionic nature of these species, the trends both in bulk properties and in intermolecular interactions may be better understood.

5.3.3 Intramolecular bonding to clarify the ionic nature of individual species.

To better comprehend how the change in amine functionality and composition mediate the change in bulk property and intermolecular interaction, the ionic nature of the acid/anion and amine/cation species was investigated. Using multiple experimental techniques to characterize both the acid/anion and amine/cation species provided a better understanding of how the ionic nature of species changed as a function of both composition and amine functionality. This ultimately helped to rationalize the trends in both molar volume and FIR absorption for these same systems, and supported the connection between bulk property and molecular interactions.

As already shown in chapter four, the ATR–IR spectra of the three acetate PILs can describe the ratio of anion:acid species. [247,283,367,387,388] This same approach was used here. Additionally, ^{13}C NMR was employed to describe the change in electron localization on both the carboxylate carbon (C_1) and the methyl carbon (C_2) of the acid/anion species. To study the mixing behaviour of the amine species in each system, ^{15}N NMR was used to understand how the electron density of the nitrogen centres varies with respect to change in composition. Cross comparisons were made with the changes in the ^{13}C NMR signal of the adjacent methyl (C_3) and methylene (C_4) groups of each amine.

5.3.3.1 Acetic acid (HOAc) species

In the acid–rich composition region, all systems showed the presence of both neutral (peak at ~1710 cm^{-1}) and ionic species (peak at ~ 1570 cm^{-1}) of HOAc as indicated by ATR–IR (Figure 5.5). This correlated well with the C_1 carbon signal shifting upfield in a comparable manner up to an amine mole fraction of 0.2 (Figure 5.6), and the C_2 carbon signal shifting downfield in a complementary manner to the observed trend for C_1 (Figure 5.7). A similar trend of the ^{13}C NMR had been observed in binary mixtures of HOAc and water, which was rationalized by the shift of electron density from the methyl group towards the C_1 carbon upon mixing as inferred from wide angle X–ray scattering.[389] For our systems, this corresponds to the formation of a hydrogen bond between acid and amine upon mixing.

At higher amine mole fractions, a decrease is observed in the absorbance of the peak for the acetate anion relative to the peak for the neutral acetic acid in the ATR–IR spectra for either of the DMBuA or TMEDA systems (Fig 5.8). In parallel, an upfield shift for the C_2 signal was observed for the DMBuA and TMEDA systems, indicating an increase in electron density on the C_2 carbon with increasing amine mole fraction (Figure 5.7). This observed upfield shift for these two systems suggests a weakening of the hydrogen bonding between HOAc and amine, resulting in a shift of electron density from C_1 back to C_2 with increasing amine mole fraction. The DMBuA and TMEDA systems both exhibited a continual shift upfield of the C_1 signal, suggesting that there are still interactions between acid and base in these amine–rich compositions, but more characteristic of a hydrogen bond interaction between neutral molecules than between ion pairs (Figure 5.6).

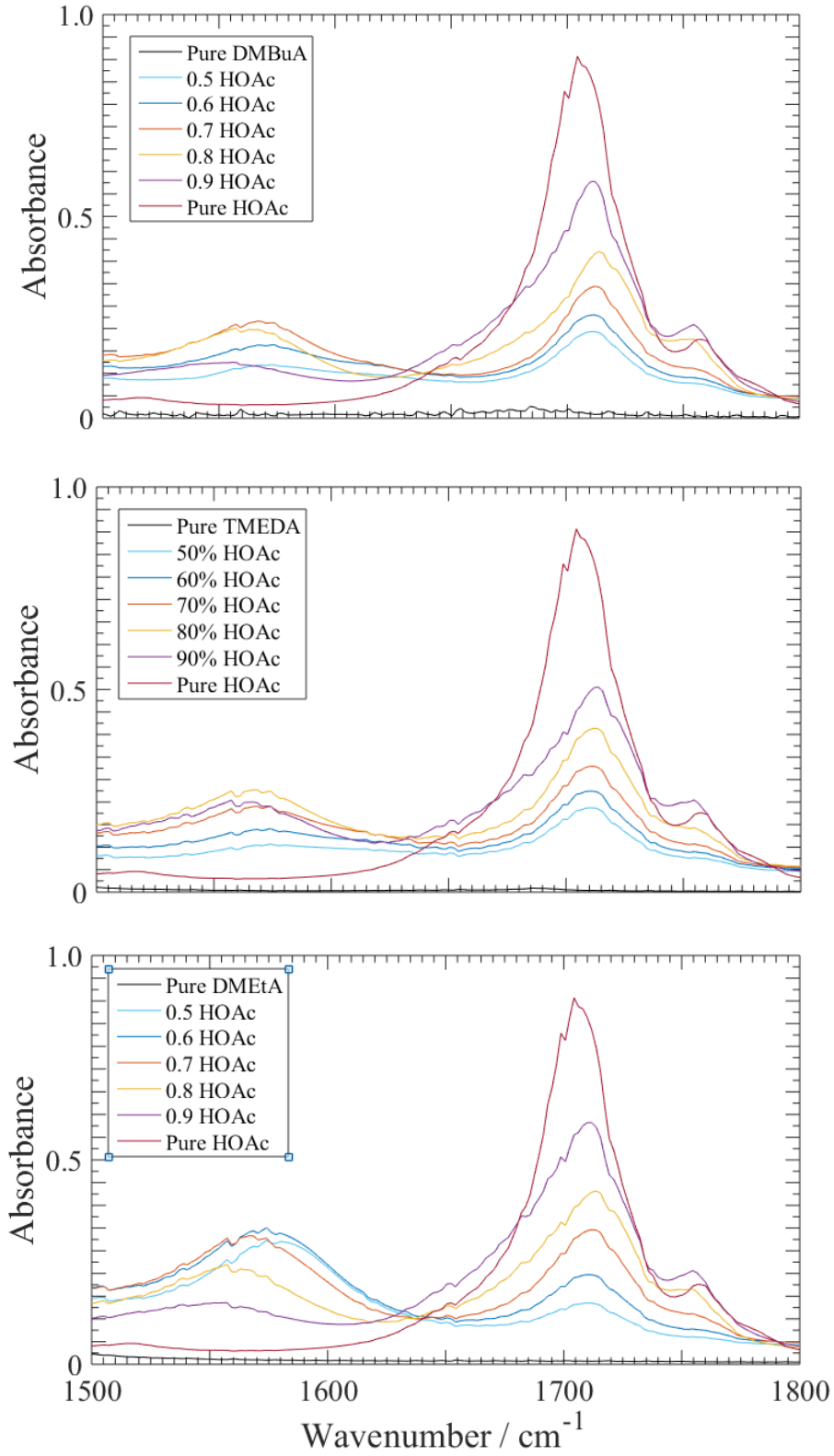

Figure 5.5 ATR–IR spectra of the acid–rich compositions of the three acid–amine mixtures in the region of 1500–1800 cm^{-1}. The peak for the acetate species occurs at ~1570 cm^{-1} and the peak corresponding to HOAc species is at ~1710 cm^{-1}.

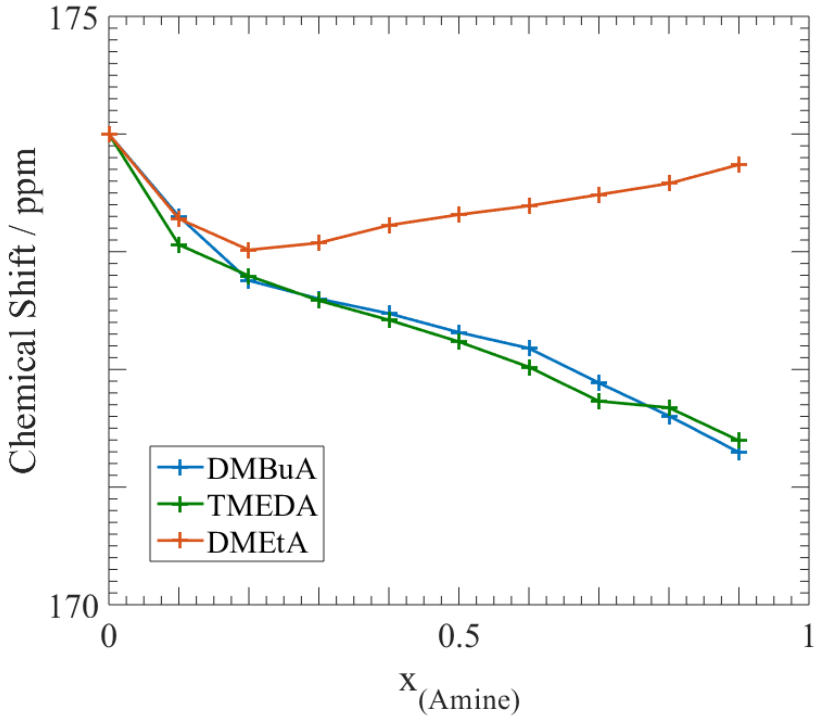

Figure 5.6 Dependence of the ^{13}C chemical shift of the C_1 carbon on the mole fraction of the amine of acetic acid for the three binary mixtures.

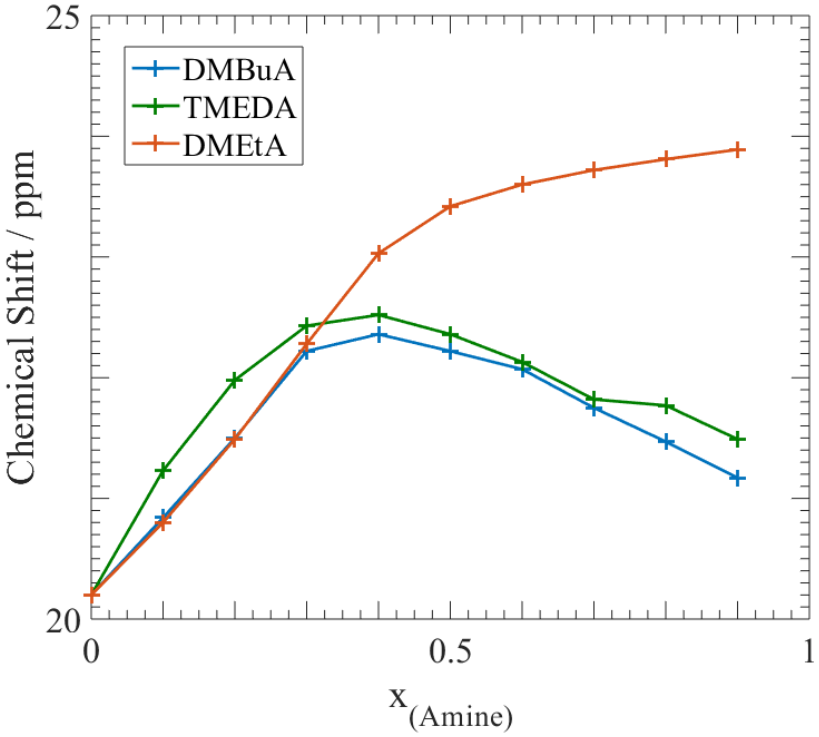

Figure 5.7 Dependence of the ^{13}C chemical shift of the C_2 carbon on the mole fraction of the amine of acetic acid for the three binary mixtures.

For the DMEtA system, the C_2 carbon signal continued to shift downfield with increasing amine concentration, showing that the electron density was decreasing (Figure 5.7). This suggests a continued increase in the shift of electron density from C_2 to C_1, consistent with an increase in the extent of hydrogen bond interactions between HOAc and DMEtA at increasing amine concentrations. However, the DMEtA system showed a downfield shift of the C_1 signal with increasing amine mole fraction (Figure 5.6). This was in contrast to the trend observed for the DMBuA and TMEDA systems, which indicated the formation of hydrogen bond interactions between the neutral acid–amine species. One explanation for this could be that proton transfer occurs at a greater extent in the DMEtA system than in the other two studied systems. Deprotonation of acetic acid would be expected to induce a net deshielding effect as a result of delocalisation of the negative charge around the COO^- group. This is supported by what is seen from ATR–IR of DMEtA; only in the DMEtA system can signals for the acetate anion be observed in amine–rich compositions (Figure 5.7).

Mixing HOAc with a molar excess of an amine with a conjugate acid with a substantially greater $p\mathrm{Ka}_{(\mathrm{aq})}$ value might reasonably be expected to result in deprotonation of HOAc to produce the acetate anion; however, only the DMEtA system exhibited deprotonation of HOAc in a molar excess of amine. This may be the result of the capability of the excess amine to solvate the ionic species upon proton transfer. The fact that the amine–rich region of the DMEtA system was so drastically different implies that hydrogen bond donor (HBD) capability is very important in increasing the ionic nature of a mixture. This observation further supports the idea that HBD interactions can stabilize the acetate anion, and thus provide a driving force for the formation of ionic species. The interactions between acid and base in the DMEtA system are characteristic of an increase in hydrogen bonding between ionic species.

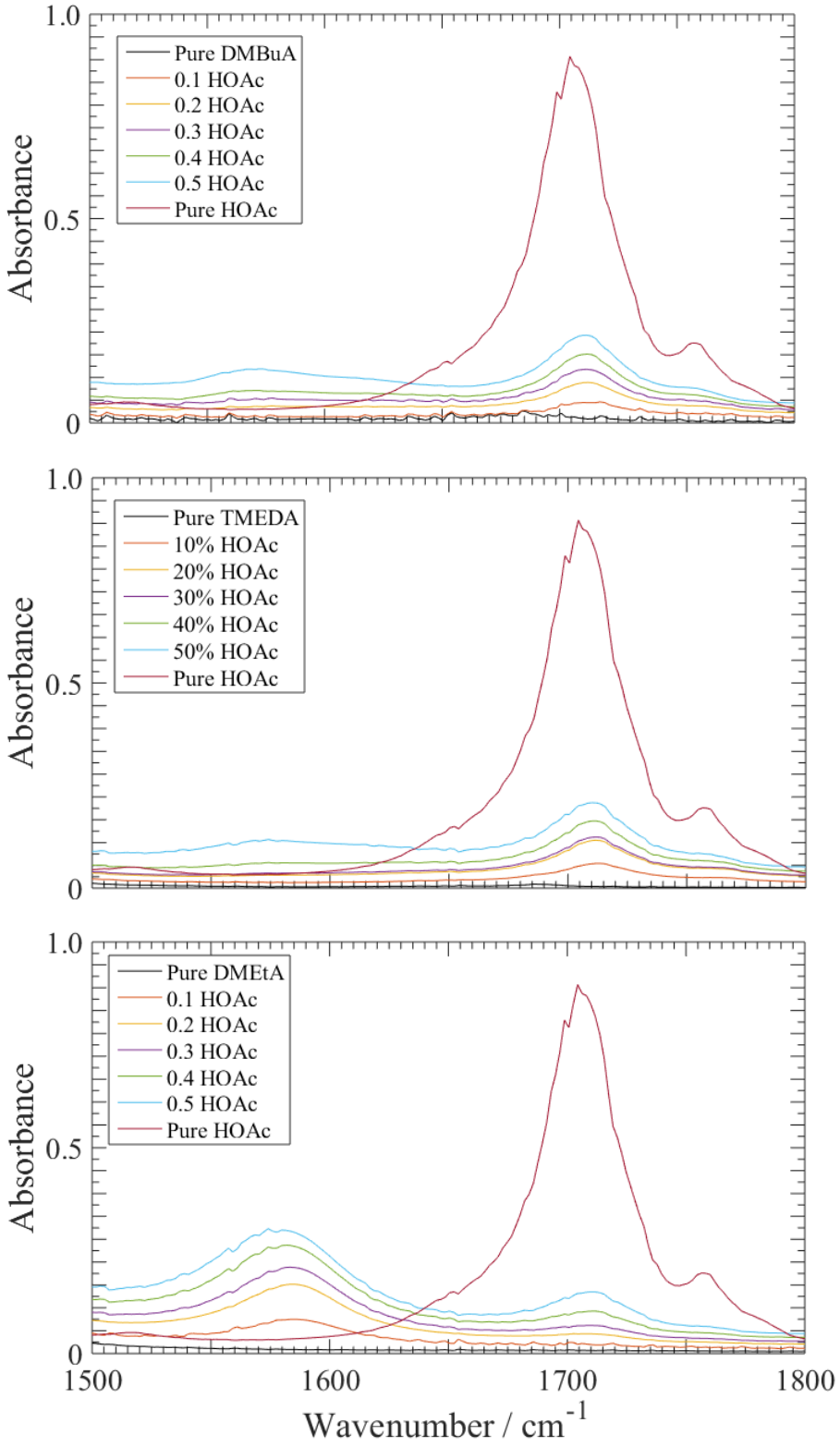

Figure 5.8 ATR–IR spectra of the acid–rich compositions of the three acid–amine mixtures in the region of 1500–1800 cm^{-1}. The peak for the acetate species occurs at ~1570 cm^{-1} and the peak corresponding to acetic acid species is at ~1710 cm^{-1}.

5.3.3.2 Amine (Am) species

In all ^{15}N NMR spectra, only a single peak could be resolved, due to the rate of proton transfer being greater than the timescale of the NMR experiment (Figure 5.9). As a result, the distinction between a neutral and the protonated form of the amine could not be made from the ^{15}N NMR. From the pure amine to the equimolar composition, a gradual shift of the ^{15}N signal downfield was observed, indicating a net deshielding of the nitrogen centre of the amine (Figure 5.9). This trend has been previously reported for the ^{15}N NMR of different acid–amine binary mixtures.[245,286] This deshielding shift corresponds to a reduced electron density on the nitrogen centre of the amine, as could occur when the nitrogen lone pair interacts with the labile proton of HOAc, either as a hydrogen bond or as a result of formal proton transfer (or indeed any intermediate state). This correlated well with an upfield shift of both the C_3 and C_4 carbon signals with decreasing amine mole fraction, indicating an increase in the electron density on these two carbon environments (Figure 5.10).

The downfield change of chemical shift was noticeably less for the TMEDA systems, as a result of two degenerate nitrogen centres exhibiting identical proton affinities in the pure amine (Figure 5.9). For monoprotonated diamines, a low barrier hydrogen bond (LBHB) between the two nitrogen atoms will occur, resulting in a single degenerate peak.[356] Surprisingly, this trend was not reciprocated with the ^{13}C signals for either the methyl or methylene groups, which seemed to move in a similar trend to the same signals for both the DMBuA and DMEtA systems (Figure 5.10).

The DMBuA and DMEtA system appeared to have similar downfield chemical shift changes, however considering the chemical shift change relative to that of the pure amine, the DMEtA system had a slightly greater relative downfield shift in amine rich compositions (Figure 5.9). This was nonetheless surprising, as the ATR–IR spectra for the DMBuA and DMEtA systems showed distinctly different ionic nature of the acetate/anion

species, suggesting practically no charge transfer taking place in the amine–rich compositions of DMBuA. This lack of correlation raises a significant question as to the true interpretation of the change in ^{15}N chemical shift with composition. [245,286] As such, it becomes much more important to cross–compare the trends from the cation/amine species with that of the anion/acid species.

In the acid–rich compositions, all three systems exhibited distinctly different trends of ^{15}N chemical shift dependence on composition (Figure 5.9). The DMBuA system still showed a downfield shift in signal, however at a lesser rate of change between than in the acid rich compositions giving a sigmoidal shape of the trend overall. For both the C_3 and C_4 signals in the ^{13}C NMR, the signals appeared to shift upfield at amine mole fractions of 0.3 and lower (Figure 5.10). This change in trend was not consistent with a continued increase in the deshielding of the nitrogen centre at the lowest amine mole fractions as inferred from ^{15}N NMR (Figure 5.9). A recent study into the NMR spectra of binary mixtures of 1,3–dimethyl–2–imidazolidinone with sulfuric acid and methanesulfonic acid found that changes in the trend in the ^{15}N NMR in acid–rich composition correlated with the Lewis basicity of the anion interacting with a protonated cation.[286] As such, the ^{13}C signals of the adjacent carbons on 1,3–dimethyl–2–imidazolidinone shifted upfield and the nitrogen signals shifted downfield, which is consistent with the observation in the DMBuA system.

The TMEDA system exhibited a greater rate of change of the ^{15}N signal in the same region, although exhibited a lesser change in both relative and absolute ^{15}N chemical shift than the DMBuA system (Figure 5.9). This is consistent with the continual upfield shift of both the C_3 and C_4 ^{13}C NMR signals, indicating an increase in electron density on the carbon nuclei adjacent to the nitrogen centres, until the lowest measured amine mole fraction (Figure 5.10). These effects were presumably mostly due to the interaction of both tertiary amine functionalities with HOAc becoming more favourable in acid–rich compositions.

This is consistent with the ATR–IR results indicating the greatest relative intensity of ionic species in the TMEDA system occur around the 0.8–0.9 acid mole fractions.

The DMEtA system appeared to reach a maximum downfield chemical shift of the ^{15}N signal at an amine mole fraction of 0.3 (Figure 5.9). At lower amine mole fractions, the ^{15}N signal appeared to shift upfield indicating a net increase in the shielding of the nitrogen centre. Over the same composition range, the ^{13}C chemical shifts for the methyl groups of the DMEtA system started to shift downfield (Figure 5.10). The net shift of the ^{15}N signal upfield in the DMEtA system at the lowest amine mole fractions suggests a stronger effect of the anion basicity on the anion–cation interactions, stronger than what is observed in the DMBuA system.[286] However, the lack of complementary trends in both the C_3 and C_4 signals in ^{13}C NMR did not support this (Figure 5.10). An alternative explanation could be that the DMEtA system at the lowest amine mole fractions studied has less ionic character than the DMBuA system. This is consistent with the nature of acetic acid at these compositions as shown from the ATR–IR spectra (Figure 5.5), showing relatively little ionic character at the lowest amine mole fractions.

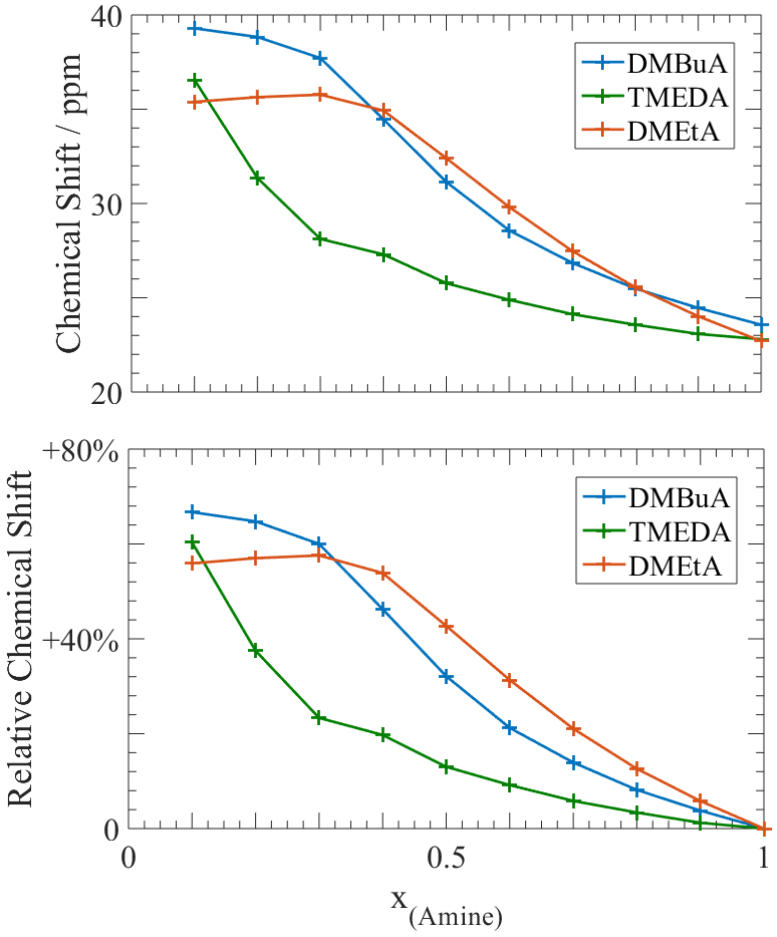

Figure 5.9 Dependence of the absolute (top) and relative (bottom) change in ^{15}N chemical shift of the nitrogen centre signal for the three binary mixtures on the amine mole fraction.

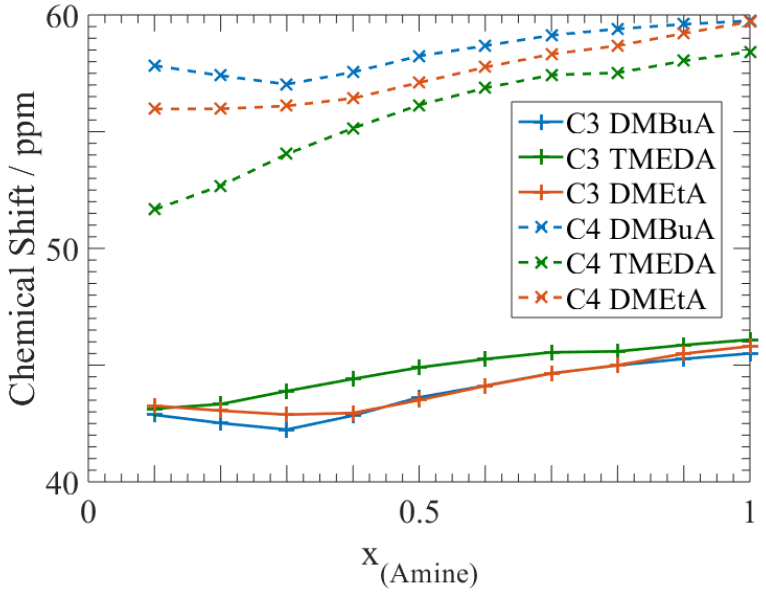

Figure 5.10 Dependence of the ^{13}C chemical shift of the C_3 and C_4 carbon environments of each amine on the mole fraction of the amine for the three binary mixtures.

5.3.4 Correlation between bulk properties and short–range interactions.

The ATR–IR spectra indicated that significant contributions from acetate species existed in all acid–rich compositions for all three systems (Figure 5.4). The compositions that had the largest intensity of the acetate species (0.7 HOAc for DMBuA, 0.8 for TMEDA and 0.6 for DMEtA) suggested that these compositions also exhibited the greatest degree of ionic character. These same compositions showed the greatest absorption in the FIR region, as well as the most negative values of $V_m^E(\mathrm{rel})$. The correlation of these three characteristics further supports the connection between short range interactions at the molecular level and bulk properties. Compositions which exhibit highly ionic characteristics appear to also exhibit greater intermolecular interactions (from FIR) and therefore greater deviations from additive mixing of the two precursors. This observation is of profound importance when considering the possibilities of "designing" PILs with specific desired properties.

Rationalizing why these compositions show the largest deviations from additivity and the greatest extent of both intermolecular interactions and ionic nature requires an appreciation of the entire composition range. In the amine–rich compositions, there were no significant intensities in the ATR–IR spectra for the acetate species in the DMBuA and TMEDA system, while the DMEtA system showed predominant intensity of the acetate species (Figure 5.7). This was despite the similar downfield shift of the nitrogen centre ^{15}N NMR signal (Figure 5.8) and the upfield shift of the C_3 and C_4 ^{13}C NMR signals (Figure 5.9) for all three binary systems. This was further supported by the distinctly different trends of the C_1 (Figure 5.5) and C_2 (Figure 5.6) signals of the DMEtA system and the other two binary systems. This implies that while acid–amine hydrogen bond interactions take place in the amine–rich compositions in all three systems (Figure 5.3), only in the DMEtA system does extensive proton transfer take place in amine–rich compositions.

This supports the hypothesis that additional hydrogen bond interactions with the acetate anion can stabilize the ionic species in an acid–base binary mixture. This hypothesis was proposed in chapter 4 to rationalize how hydroxyl–functionalized PILs can have such a distinct impact on the cohesive energy density and solvent–solute interactions. In amine–rich mixtures, this stabilization comes from the hydroxyl group of the amine species donating a proton to the acetate anion. In the acid–rich compositions, this stabilization is due to acetic acid–acetate hydrogen bond interactions. This interaction between acid and anion to form a stabilized dimer anion has been suggested before, [274,275,280,376] however it was defined as an explicit stoichiometric adduct as opposed to a less specific stabilization mechanism. The concept of explicit stoichiometric adduct formation in these systems does not appreciate the complex proton transfer equilibria and re–orientation dynamics that can take place in liquids in contrast to crystalline solids of acid–amine binary mixtures with well–defined stoichiometry.[390–392]

5.4 Conclusions

The comparison between experimental and additive molar volume of the three acid–amine binary mixtures as shown by the $V_{\mathrm{m}}^{\mathrm{E}}(\mathrm{rel})$ shows that strong, negative deviations occur. These negative deviations were much larger than typically found for hydrogen bond donor/acceptor binary mixtures, suggesting the formation of ionic species with strong intermolecular hydrogen bond interactions. The largest deviations for all three systems occur in acid–rich compositions, however the DMEtA system exhibited noticeably greater deviations from additivity than either the DMBuA or TMEDA system.

Intermolecular interactions as inferred from the FIR spectra of the binary mixtures appeared to have similar dependence on composition than $V_{\mathrm{m}}^{\mathrm{E}}(\mathrm{rel})$. In general, all binary mixtures exhibited an increase in the extent of intermolecular interactions in comparison to the pure precursor materials. Compositions with the largest absorbance in the FIR region

correlated well to compositions with the greatest deviations from additive mixing. The DMEtA system exhibited a much greater FIR absorbance than the corresponding DMBuA and TMEDA systems in the amine–rich compositions.

The nature of the short–range intermolecular interactions was rationalized by spectroscopy by describing the change in the acid/anion and amine/cation species separately as a result of mixing. By considering both types of species, distinctly different mixing behaviour in each of the three binary systems can be appreciated. In the TMEDA system, both the acid/anion and amine/cation species only showed evidence of significant proton transfer taking place in acid–rich compositions. The DMBuA system showed a similar continued downfield shift of the ^{15}N NMR signal as the DMEtA system with increasing acid mole fraction, which had previously been suggested to represent systematic increase in extent of proton transfer. However, compared to the ATR–IR and ^{13}C NMR spectra of the acid/anion species, distinctly different behaviour was shown between these two systems; the DMBuA system also only showed significant proton transfer taking place in acid–rich compositions, whereas the DMEtA system showed evidence implying proton transfer takes place in amine–rich compositions as well.

For all three systems, the ATR–IR peak of the acetate species showed maxima at the same compositions as observed in both the FIR absorbance and the $V_{\mathrm{m}}^{\mathrm{E}}(\mathrm{rel})$. This correlation between bulk property deviations and the change in short–range interactions was surprising, given the long–ranged interactions that can occur in binary liquid systems. However, it is widely reported in literature that hydrogen bond interactions are dominant in such binary systems, which is perhaps why the correlation between bulk property and spectroscopy was so strong. Further application of such correlations to a wider variety of acid–amine binary systems may yield a much deeper understanding of the molecular basis of bulk properties, which would be invaluable in establishing rational structure–property relationships in PILs.

Chapter 6: Towards the Application of Acid–Amine Binary Mixtures as Solvents

6.1 Introduction

To understand the solvation capacity (i.e. will a solute dissolve in a given solvent?) requires some rudimentary empirical data directly relevant to an industrial application. At this stage, it is not essential to have rigorous theory to rationalize the results quantitatively; qualitative trends can yield valuable insights. The capability to relate these trends to the interactions in the solvent as inferred indirectly using spectroscopic techniques is notably useful.[4,5] With specific regard to the acid–amine binary mixtures studied in chapter five, the relationship of solvation capacity to (1) the formation of ionic species and (2) the increase in the extent of intermolecular hydrogen bonding interactions will prove valuable in rationalizing how composition and amine functionality can tune the solvation properties of acid–amine binary mixtures. Indeed, such a connection between short range interactions and solvation capability has already been shown for the equimolar acid–amine binary mixtures in chapter four.

In this chapter, there are two primary objectives: (1) to characterize the solvation capacity of acid–amine binary mixtures and (2) to rationalize the variance of solvation behaviour with both amine functionality and composition.

The change in solvation environment will be reflected in the change in solubility of a solute with respect to composition. Based on characteristics of the solute, such as induced dipolarity, permanent dipole moment and hydrogen bonding capability, one could probe how the solvation environment changes. A deeper understanding can be achieved when multiple solutes with varying characteristics are screened, providing a more detailed insight into how the solvation environment changes with composition and amine functionality. This follows similar principles to using multiple solvation parameters to

describe the solvation environment as established by Kamlet, Taft and Abraham,[255,258,260] albeit in a more qualitative manner.

These changes can then be compared to the trends in short–range interactions as discussed in chapters four and five. By doing so, a qualitative yet rational interpretation of how the ionic nature and the extent of intermolecular hydrogen bonding interactions influence the solvation capacity of acid–amine binary mixtures may be obtained. The failure to connect these short–range interactions to the solvation capability of these binary mixtures will provide support to the hypothesis of significant contributions of long–range interactions to the solvation properties of these systems.

6.2 Experimental

6.2.1 Materials and Samples

The same precursor materials as used in chapters four and five (acetic acid, *N*,*N*–dimethylbutylamine, *N*,*N*–dimethylethanolamine and *N*,*N*,*N'*,*N'*–tetramethylethan–1,2–diamine) were used in this chapter. Binary mixtures of acid and amine were prepared following the same procedure outlined in chapter five.[49] The experimental details (mass of precursors, water content from volumetric Karl–Fischer titration) are summarized in Tables 6.1–6.3. All probe solutes were obtained from Sigma Aldrich and used without further purification.

Table 6.1 Mass of precursors used for the preparation of the binary mixtures of acetic acid and *N*,*N*–dimethylbutylamine. Water content was determined from Karl Fischer titration (see section 4.2.3).

x_{Ac}	x_{Am}	Mass Acid / g	Mass Amine / g	Moles Acid	Moles Amine	Water Content / ppm
0	1	–	–	–	–	230
0.10	0.90	1.4731	18.8481	0.0245	0.1864	320
0.20	0.80	2.8698	17.9620	0.0478	0.1776	366
0.30	0.70	4.4575	17.2969	0.0742	0.1710	460
0.40	0.60	6.4583	16.2799	0.1075	0.1610	451
0.50	0.50	8.9371	15.0914	0.1488	0.1492	687
0.60	0.40	12.016	13.5883	0.2001	0.1344	603
0.70	0.30	15.5162	11.0702	0.2584	0.1095	932
0.80	0.20	19.3485	8.2890	0.3222	0.0820	804
0.90	0.10	23.8295	4.4628	0.3968	0.0441	1265
1	0	–	–	–	–	105

Table 6.2 Mass of precursors used for the preparation of the binary mixtures of acetic acid and *N,N,N',N'*–tetramethylethan–1,2–diamine. Water content was determined from Karl Fischer titration (see section 4.2.3).

x_{Ac}	x_{Am}	Mass Acid / g	Mass Amine / g	Moles Acid	Moles Amine	Water Content / ppm
0	1	–	–	–	–	895
0.10	0.90	1.2920	22.5081	0.0215	0.1938	993
0.20	0.80	2.8079	21.7332	0.0468	0.1871	942
0.30	0.70	4.5978	20.7569	0.0766	0.1787	966
0.40	0.60	6.7591	19.6208	0.1126	0.1689	921
0.50	0.50	9.8962	19.1512	0.1648	0.1649	1003
0.60	0.40	12.0699	15.5701	0.2010	0.1340	1120
0.70	0.30	16.5934	13.7606	0.2763	0.1185	1022
0.80	0.20	21.2204	10.2659	0.3534	0.0884	1098
0.90	0.10	26.7582	5.7530	0.4456	0.0495	1277
1	0	–	–	–	–	105

Table 6.3 mass of precursors used for the preparation of the binary mixtures of acetic acid and *N,N*–dimethylethanolamine. Water content was determined from Karl Fischer titration (see section 4.2.3).

x_{Ac}	x_{Am}	Mass Acid / g	Mass Amine / g	Moles Acid	Moles Amine	Water Content / ppm
0	1	–	–	–	–	895
0.10	0.90	1.8140	23.3608	0.0302	0.2621	588
0.20	0.80	3.7542	22.1466	0.0625	0.2484	624
0.30	0.70	6.5904	20.9451	0.1097	0.2350	738
0.40	0.60	8.6109	19.1505	0.1434	0.2148	1008
0.50	0.50	11.4918	17.0162	0.1914	0.1909	965
0.60	0.40	14.7380	14.5684	0.2454	0.1634	934
0.70	0.30	18.0844	11.4483	0.3011	0.1284	1105
0.80	0.20	21.6882	8.0633	0.3612	0.0905	1273
0.90	0.10	25.4401	4.1454	0.4236	0.0465	1355
1	0	–	–	–	–	105

6.2.2 Solvent Miscibility Screening

In total, 15 probe solutes were selected to characterize the solvation profile of each acid–amine binary mixture as well as the pure precursor materials. The solutes were rationally chosen on the basis of various characteristics, which describe their dissolution behaviour. Non–specific solute–solvent interactions are discussed on the basis of instantaneously–induced dipolar interactions referred to as the London dispersive forces, permanent dipolar–induced dipolar interactions known as the Keesom forces and the permanent dipolar interactions also known as the Debye forces, which are often grouped together as the van der Waals forces. Specific hydrogen bonding donor and acceptor capability will also significantly influence the solubility of the solute. Finally, the strength of solute–solute interactions will additionally contribute to the likelihood of a solute being solubilized.

The induced dipolar interactions will be discussed on the basis of the dispersive Hansen solubility parameter, δ_D of the solute.[393,394] The permanent dipolar interactions will be considered on the basis of the polar Hansen solubility parameter, δ_P,[393,394] as well as the dipole moment of the solute.[395] Finally, the Kamlet–Taft dipolarity/polarizability parameter (π^*) will be used as a descriptor of the net non–specific van der Waals forces of the solute.[260,396,397] To consider these two separately, the Kamlet–Taft hydrogen bond acidity (α) and basicity (β) are used when available for each solute.[2,4,260,397–399] Finally, cohesive energy of the solute is appreciated on the basis of the Hildebrand solubility parameter, δ.[267] The quantities of the above stated parameters are summarized in table 6.4

Table 6.4 Properties of the solutes used in the miscibility profiling of acid–amine binary mixtures. [2,4,260,267,393–399]

Probe Solvent	δ	δ_D	δ_P	Dipole Moment	π*	α	β
Hexane	14.9	14.9	0.0	0.00	– 0.11	0.00	0.00
Cyclohexane	16.8	16.8	0.0	0.00	0.00	0.00	0.00
Toluene	18.2	18.0	1.4	0.43	0.49	0.00	0.11
Dichloromethane	20.2	18.2	6.3	1.90	0.82	0.13	0.10
Diiodomethane	19.0	17.8	3.9	1.10	1.00	0.00	0.00
Bromotrichloromethane	20.9	18.3	8.1	0.21	0.43	0.00	–
Diethyl ether	15.6	14.5	2.9	1.17	0.24	0.00	0.47
Ethyl acetate	18.2	15.8	5.3	1.88	0.45	0.00	0.45
Acetone	19.9	15.5	10.4	3.11	0.71	0.08	0.48
Acetonitrile	24.4	15.3	18.0	3.39	0.66	0.19	0.40
Dimethyl sulfoxide	26.7	18.4	16.4	3.90	1.00	0.00	0.76
1,3–Bis(trifluoromethyl)benzene	18.3	17.0	6.8	2.43	–	0.00	–
Ethanol	21.0	17.0	3.3	1.65	0.40	0.77	0.81
1–Octanol	26.5	15.8	8.8	1.73	0.54	0.86	0.75
Water	47.8	15.5	16.0	1.82	1.09	1.17	0.47

Due to the qualitative nature of this approach, actual masses were not recorded. Approximately 1 g of each acid–amine binary mixture was measured into a clear glass sample vial. Approximately 100 mg of a probe compound was added to each sample. The sample vial was sealed and shaken for 60 seconds, letting the vial rest for up to 300 seconds to reach a state of equilibrium. After this time, the system in the vial was given a qualitative score based on the phase behaviour of the system:

- A score of **1** was awarded when the system appeared as a single, clear, homogeneous liquid phase.
- A score of **0.5** was awarded when the system became turbid, which cannot be describe as being a single phase or two discrete phases.
- A score of **0** is awarded when there was no visible dissolution of probe molecule in the solvent, resulting in observation of two discrete, immiscible phases.

For each sample studied, a score was assigned based on the mixing behaviour observed with each probe molecule, creating the miscibility profile for that sample. Repeating this for all samples generates a visual guide to the change in miscibility profile with composition for each acid–amine system.

Table 6.5 Miscibility profiles of the *N*,*N*–dimethylbutylamine (DMBuA) – acetic acid (HOAc) binary system at 0.1 mole fraction intervals.

Probe Solute	Pure Amine	0.1 HOAc	0.2 HOAc	0.3 HOAc	0.4 HOAc	0.5 HOAc	0.6 HOAc	0.7 HOAc	0.8 HOAc	0.9 HOAc	Pure Acid
Hexane	1	0.5	0.5	0	0	0	0	0	0	0	1
Cyclohexane	1	1	1	0.5	0.5	0	0	0	0	0	1
Toluene	1	1	1	1	1	1	1	0.5	0	0	1
Dichloromethane	1	1	1	1	1	1	1	1	1	1	1
Diiodomethane	0.5	0.5	1	1	1	1	0.5	0	0	0	0
Bromotrichloromethane	1	1	1	1	1	1	1	0.5	0	1	1
Diethyl ether	1	1	1	1	1	1	1	1	0	1	1
Ethyl Acetate	1	1	1	1	1	1	1	1	1	1	1
Acetone	1	1	1	1	1	1	1	1	1	1	1
Acetonitrile	1	1	1	1	1	1	1	1	1	1	1
Dimethyl sulfoxide	0	0	0	0	0.5	1	1	1	1	1	1
1,3–Bis(trifluoromethyl)benzene	1	1	1	1	1	1	1	1	0	1	1
Ethanol	1	1	1	1	1	1	1	1	1	1	1
1–Octanol	1	1	1	1	1	1	1	1	1	1	1
Water	0	0	0	0	0.5	1	1	1	1	1	1

Table 6.6 Miscibility profiles of the *N,N,N',N'*–tetramethylethan–1,2–diamine (TMEDA) – acetic acid (HOAc) binary system at 0.1 mole fraction intervals.

Probe Solute	Pure Amine	0.1 HOAc	0.2 HOAc	0.3 HOAc	0.4 HOAc	0.5 HOAc	0.6 HOAc	0.7 HOAc	0.8 HOAc	0.9 HOAc	Pure Acid
Hexane	1	1	0.5	0.5	0.5	0	0	0	0	0	1
Cyclohexane	1	1	1	1	0.5	0	0	0	0	0	1
Toluene	1	1	1	1	1	1	1	1	1	1	1
Dichloromethane	1	1	1	1	1	1	1	1	1	1	1
`Diiodomethane	0.5	0.5	0.5	1	1	1	1	0	0	0	0
Bromotrichloromethane	0.5	0.5	0.5	0.5	0.5	1	1	1	1	1	1
Diethyl ether	1	1	1	1	1	1	1	1	1	1	1
Ethyl Acetate	1	1	1	1	1	1	1	1	1	1	1
Acetone	1	1	1	1	1	1	1	1	1	1	1
Acetonitrile	1	1	1	1	1	1	1	1	1	1	1
Dimethyl sulfoxide	1	1	1	1	1	1	1	1	1	1	1
1,3–Bis(trifluoromethyl)benzene	1	1	1	1	1	1	0.5	0.5	0.5	1	1
Ethanol	1	1	1	1	1	1	1	1	1	1	1
1–Octanol	1	1	1	1	1	1	1	1	1	1	1
Water	1	1	1	1	1	1	1	1	1	1	1

Table 6.7 Miscibility profiles of the *N*,*N*–dimethylethanolamine (DMEtA) – acetic acid (HOAc) binary system at 0.1 mole fraction intervals.

Probe Solute	Pure Amine	0.1 HOAc	0.2 HOAc	0.3 HOAc	0.4 HOAc	0.5 HOAc	0.6 HOAc	0.7 HOAc	0.8 HOAc	0.9 HOAc	Pure Acid
Hexane	1	0	0	0	0	0	0	0	0	0	1
Cyclohexane	1	1	0.5	0	0	0	0	0	0	0	1
Toluene	1	1	1	1	1	0	0	0	1	1	1
Dichloromethane	1	1	1	1	1	1	1	1	1	1	1
Diiodomethane	1	1	1	1	1	0	0	0	0	0	0
Bromotrichloromethane	0.5	0.5	0.5	1	1	1	0	0	1	1	1
Diethyl ether	1	1	1	1	1	0.5	0.5	0	0.5	1	1
Ethyl Acetate	1	1	1	1	1	1	1	1	1	1	1
Acetone	1	1	1	1	1	1	1	1	1	1	1
Acetonitrile	1	1	1	1	1	1	1	1	1	1	1
Dimethyl sulfoxide	1	1	1	1	1	1	1	1	1	1	1
1,3–Bis(trifluoromethyl)benzene	1	1	1	1	1	0.5	0.5	0	0	1	1
Ethanol	1	1	1	1	1	1	1	1	1	1	1
1–Octanol	1	1	1	1	1	1	1	1	1	1	1
Water	1	1	1	1	1	1	1	1	1	1	1

6.3 Results and Discussion

6.3.1 Solvent Miscibility

As a whole, each binary system shows a different miscibility profile to the 15 probe solutes, with the change of composition having varying effects on the miscibility with each solute. By comparing probe solutes on the basis of the characteristics outlined above it is possible to explain the change in miscibility score for each probe with composition and functionality on the basis of changing solvent–solute interactions. For the sake of clarity, the solutes are grouped into four categories: hydrocarbons, haloalkanes, dipolar aprotic and amphiprotic.

6.3.1.1 Hydrocarbons: hexane, cyclohexane and toluene

The three hydrocarbon solutes, hexane, cyclohexane and toluene, exhibit little to no hydrogen bonding capability, with only toluene exhibiting a dipole moment (Table 6.4). The predominant interaction between solvent and solute are the London dispersion forces.[400]

For all precursor materials, each of the three hydrocarbon solutes are fully miscible. Upon mixing, there is reduced solubility of the hydrocarbon solutes, particularly in acid–rich compositions. That cyclohexane is comparatively more soluble than hexane in all acid–amine binary mixtures is likely the result of stronger dispersive interactions between the solute and solvent owing to the greater polarizability of the constrained ring electrons. It is easier to induce a dipole in cyclohexane than in hexane, hence the larger value of δ_D (Table 6.4), and therefore is easier to solubilize in solvents which are highly polarizing. In comparison, toluene, which has both greater inducible polarity and a permanent dipole moment (Table 6.4), is much more soluble than both hexane and cyclohexane.

Despite the increased solubility of toluene in comparison to hexane and cyclohexane, toluene is still immiscible in multiple acid–rich mixture of the DMBuA and DMEtA systems. The low solubility of all hydrocarbon solutes in the acid–amine binary mixtures (apart from toluene in the TMEDA system) can be rationalized by competing interactions between species. In general, solute–solvent interactions are competing with solvent–solvent interactions, which would explain the reduced solubility in acid–rich compositions, which showed the greatest extent of intermolecular hydrogen bonding interactions in the binary mixtures as shown in section 5.3.2.1. This would also explain the reduced solubility of hydrocarbon solutes in the DMEtA system over the whole composition range, as this system showed the greatest extent of intermolecular interactions in amine rich compositions as shown in section 5.3.2.2.

The effect of introducing an *N*,*N*–dimethylamino functional group to the amine to increase hydrogen bond acceptor capability of the solvent structure appears to have a counterintuitive effect: over the whole composition range, solubility of hydrocarbon solutes is greater in TMEDA than in DMBuA or DMEtA. Considering the hydrogen bonding contributions, the *N*,*N*–dimethylamino functional group is not a very strong base,[364,401] so may not undergo extensive intermolecular interactions compared to the hydroxyl functional group on DMEtA. Additionally, the *N*,*N*–dimethylamino functional group on TMEDA is more sterically bulky than the linear alkyl group on DMBuA, which has been suggested to positively influence the London forces in molecules.[400]

Table 6.8 Miscibility of Hexane, Cyclohexane and Toluene in the DMBuA–HOAc binary system at 0.1 mole fraction intervals.

Probe Solute	Pure Amine	0.1 HOAc	0.2 HOAc	0.3 HOAc	0.4 HOAc	0.5 HOAc	0.6 HOAc	0.7 HOAc	0.8 HOAc	0.9 HOAc	Pure Acid
Hexane	1	0.5	0.5	0	0	0	0	0	0	0	1
Cyclohexane	1	1	1	0.5	0.5	0	0	0	0	0	1
Toluene	1	1	1	1	1	1	1	0.5	0	0	1

Table 6.9 Miscibility of Hexane, Cyclohexane and Toluene in the TMEDA–HOAc binary system at 0.1 mole fraction intervals.

Probe Solute	Pure Amine	0.1 HOAc	0.2 HOAc	0.3 HOAc	0.4 HOAc	0.5 HOAc	0.6 HOAc	0.7 HOAc	0.8 HOAc	0.9 HOAc	Pure Acid
Hexane	1	1	0.5	0.5	0.5	0	0	0	0	0	1
Cyclohexane	1	1	1	1	0.5	0	0	0	0	0	1
Toluene	1	1	1	1	1	1	1	1	1	1	1

Table 6.10 Miscibility of Hexane, Cyclohexane and Toluene in the DMEtA–HOAc binary system at 0.1 mole fraction intervals.

Probe Solute	Pure Amine	0.1 HOAc	0.2 HOAc	0.3 HOAc	0.4 HOAc	0.5 HOAc	0.6 HOAc	0.7 HOAc	0.8 HOAc	0.9 HOAc	Pure Acid
Hexane	1	0	0	0	0	0	0	0	0	0	1
Cyclohexane	1	1	0.5	0	0	0	0	0	0	0	1
Toluene	1	1	1	1	1	0	0	0	1	1	1

6.3.1.2 Haloalkanes: dichloromethane, diiodomethane and bromotrichloromethane

The incorporation of halogen atoms significantly increased the dispersive forces of the solute as evident by the relatively large values of δ_D for the three haloalkane solutes, dichloromethane, diiodomethane and bromotrichloromethane (Table 6.4). All three haloalkane solutes exhibit little in the way of hydrogen bond donor or acceptor capability as described by their Kamlet–Taft α and β parameters.

In terms of permanent dipole moment, dichloromethane has the largest of the three (1.90) followed by diiodomethane (1.10) and bromotrichloromethane (0.21). What is interesting is that the δ_P does not follow a similar trend as the dipole moment; in fact bromotrichloromethane has the largest δ_P value of the three haloalkanes, while also having the lowest dipole moment. For the sake of discussing the dipolarity of the solute, the dipole moment will be used, as these values are experimentally determined,[395] while the values of δ_P are determined indirectly.[393]

For all three systems, dichloromethane was freely soluble in all binary mixtures. This trend does not yield significant information as to how the solvation environment changes with composition in each binary system. However, that dichloromethane is soluble in all of the precursors and binary mixtures shows that solutes which are both highly dispersive and feature a large dipole moment are likely to be well solvated.

In comparison, diiodomethane is immiscible in acetic acid and many acid–rich compositions, and has sparing solubility in the amine–rich compositions of the DMBuA and TMEDA systems. The immiscibility in pure acetic acid and the acid–rich compositions is possibly due to the preference of solvent–solvent interactions over solvent–solute interactions. The combination of hydrogen bonding and permanent dipole–dipole interactions between acid–acid, acid–amine and amine–amine are hypothetically stronger than the permanent dipole–induced dipole interactions between solvent and diiodomethane, despite its large δ_D and significant dipole moment (Table 6.4). This is supported by the extensive hydrogen bonding interactions observed in the acid–rich compositions as well as pure acetic acid from their FIR spectra as discussed in section 5.3.2.1.

The sparing solubility of diiodomethane in the amine–rich compositions is likely due to the reduced polarization capability of these acid–amine binary mixtures. It is worth noting that the solute–solute in pure diiodomethane is primarily the result of London forces, but the polarizability of the outer electron shells of the iodine atoms make diiodomethane highly susceptible to Keesom forces for solvent–solute interactions (Table 6.4). Considering the pure amines, DMEtA is likely to have the largest permanent dipole, due to the highly electronegative oxygen atom in its molecular structure. As such, it and its amine–rich binary mixtures with acetic acid are expected to have stronger permanent dipolar interactions with a solute. Furthermore, the highly ionic nature of these amine–rich compositions in the DMEtA system, as discussed in section 5.3.2, are likely to have greater polarizability potential in comparison to the other two binary systems.

The solvation behaviour of bromotrichloromethane is different for each acid–amine binary system. In amine–rich compositions, sparing solubility is observed for the TMEDA and DMEtA systems, while fully miscible in the DMBuA system. The full miscibility in the DMBuA system could be due to the formation of nanoscale ordered domains in a similar manner to some alcohols.[402,403] While not as ordered as micelles, these domains could prove to be sufficiently stabilizing for such a highly dispersive solute. This is not likely to occur in either the TMEDA or bond donating DMEtA systems, hence their sparing solubility with bromotrichloromethane.

As the acid mole fraction increases, so does the polarization capability of the binary mixtures, as shown for the equimolar acid–amine binary mixtures in section 4.3.3, resulting in stronger solvent–solute interactions. However, there is reduced immiscibility in some acid–rich compositions in the DMBuA and DMEtA binary systems. This suggests that at these compositions, which also corresponded to compositions showing the greatest ionic character and extent of intermolecular interactions, that solvent–solvent interactions become more favourable than solvent–solute interactions. The fact that this same result was not observed in the TMEDA system suggests again that the solvent–solvent interactions in this binary system are generally weaker than in the other two systems, likely a result of the steric bulk of the dimethylamino functional group.

Table 6.11 Miscibility of Dichloromethane, Diiodomethane and Bromotrichloromethane in the *N*,*N*–dimethylbutylamine (DMBuA) – acetic acid (HOAc) binary system at 0.1 mole fraction intervals.

Probe Solute	Pure Amine	0.1 HOAc	0.2 HOAc	0.3 HOAc	0.4 HOAc	0.5 HOAc	0.6 HOAc	0.7 HOAc	0.8 HOAc	0.9 HOAc	Pure Acid
Dichloromethane	1	1	1	1	1	1	1	1	1	1	1
Diiodomethane	0.5	0.5	1	1	1	1	0.5	0	0	0	0
Bromotrichloromethane	1	1	1	1	1	1	1	0.5	0	1	1

Table 6.12 Miscibility of Dichloromethane, Diiodomethane and Bromotrichloromethane in the *N*,*N*,*N'*,*N'*–tetramethylethan–1,2–diamine (TMEDA) – acetic acid (HOAc) binary system at 0.1 mole fraction intervals.

Probe Solute	Pure Amine	0.1 HOAc	0.2 HOAc	0.3 HOAc	0.4 HOAc	0.5 HOAc	0.6 HOAc	0.7 HOAc	0.8 HOAc	0.9 HOAc	Pure Acid
Dichloromethane	1	1	1	1	1	1	1	1	1	1	1
Diiodomethane	0.5	0.5	0.5	1	1	1	1	0	0	0	0
Bromotrichloromethane	0.5	0.5	0.5	0.5	0.5	1	1	1	1	1	1

Table 6.13 Miscibility of Dichloromethane, Diiodomethane and Bromotrichloromethane in the *N*,*N*–dimethylethanolamine (DMEtA) – acetic acid (HOAc) binary system at 0.1 mole fraction intervals.

Probe Solute	Pure Amine	0.1 HOAc	0.2 HOAc	0.3 HOAc	0.4 HOAc	0.5 HOAc	0.6 HOAc	0.7 HOAc	0.8 HOAc	0.9 HOAc	Pure Acid
Dichloromethane	1	1	1	1	1	1	1	1	1	1	1
Diiodomethane	1	1	1	1	1	0	0	0	0	0	0
Bromotrichloromethane	0.5	0.5	0.5	1	1	1	0	0	1	1	1

6.3.1.3 Dipolar aprotic: diethyl ether, ethyl acetate, acetone, acetonitrile, dimethyl sulfoxide and 1,3–Bis(trifluoromethyl)benzene

The dipolar aprotic solutes chosen exhibit moderate to high dipole moments, with varying London dispersive forces and hydrogen bond acceptor capability and practically no hydrogen bond donor capability. Much as was seen with the haloalkanes, solutes which are highly dipolar are more readily dissolved in the acid–amine binary mixtures. Similarly, the solutes ethyl acetate, acetone and acetonitrile were fully miscible in all acid–amine binary mixtures for all three systems. However, there were a number of solutes which were immiscible in some of the systems.

Diethyl ether has limited solubility in acid–rich compositions in the DMBuA and DMEtA systems. This is surprising, as it is a relatively strong hydrogen bond acceptor ($\beta = 0.47$) and should therefore interact favourably with acetic acid. However, in comparison to the other dipolar aprotic solutes, diethyl ether has the lowest dipole moment of 1.17, which is comparable to diiodomethane, which also had low solubility in these acid–rich compositions. This emphasizes the importance of permanent dipole–dipole interactions between solvent and solute in these acid–amine binary mixtures. This is particularly the case in these acid–rich compositions, which were shown to have extensive ionic nature and would be therefore expected to more favourably solvate dipolar solutes.

Dimethyl sulfoxide is completely miscible in the entire TMEDA and DMEtA binary systems, but is immiscible in the pure DMBuA, the 0.1, 0.2 and 0.3 HOAc compositions and is sparingly soluble in the 0.4 HOAc composition. This lack of miscibility in these compositions can be explained by the lack of either a large dipole moment, hydrogen bond donor capability or polarizable electron density in these compositions. Without these characteristics, solvent–solute interactions in these particular binary mixtures are unfavourable in comparison to solute–solute interactions. For comparison acetonitrile, which has lower dipole moment, hydrogen bond acceptor

capability, London dispersive forces and net solvent–solvent interaction strength than dimethyl sulfoxide, it is fully miscible in these same amine–rich compositions. At higher acid mole fractions, dimethyl sulfoxide is fully miscible, suggesting an increase in both the hydrogen bond donor capability and the dipolarity of the solvent systems.

1,3–Bis(trifluoromethyl)benzene is immiscible in a number of acid–rich compositions of all three systems, despite having a very large dipole moment and large London dispersive forces contributions. It would have been expected that a solute with such a large induced and permanent dipolarity would have been well solvated in the highly ionic media found in the acid–rich compositions as shown in chapter four. This may be because of the great extent of intermolecular hydrogen bonding interactions that take place in these acid–rich compositions, as shown in section 5.3.2.1, while 1,3–bis(trifluoromethyl)benzene does not have any hydrogen bond donor capability at all. That it is soluble in some of the acid–rich compositions suggests that the solute is capable of accepting a hydrogen bond, however there is no literature data to confirm or deny this.

Table 6.14 Miscibility of Diethyl ether, Ethyl acetate, Acetone, Acetonitrile, Dimethyl sulfoxide and 1,3–Bis(trfluoromethyl)benzene in the *N*,*N*–dimethylbutylamine (DMBuA) – acetic acid (HOAc) binary system at 0.1 mole fraction intervals.

Probe Solute	Pure Amine	0.1 HOAc	0.2 HOAc	0.3 HOAc	0.4 HOAc	0.5 HOAc	0.6 HOAc	0.7 HOAc	0.8 HOAc	0.9 HOAc	Pure Acid
Diethyl ether	1	1	1	1	1	1	1	1	0	1	1
Ethyl acetate	1	1	1	1	1	1	1	1	1	1	1
Acetone	1	1	1	1	1	1	1	1	1	1	1
Acetonitrile	1	1	1	1	1	1	1	1	1	1	1
Dimethyl sulfoxide	0	0	0	0	0.5	1	1	1	1	1	1
1,3–Bis(trifluoromethyl)benzene	1	1	1	1	1	1	1	1	0	1	1

Table 6.15 Miscibility of Diethyl ether, Ethyl acetate, Acetone, Acetonitrile, Dimethyl sulfoxide and 1,3–Bis(trfluoromethyl)benzene in the *N*,*N*,*N'*,*N'*–tetramethylethan–1,2–diamine (TMEDA) – acetic acid (HOAc) binary system at 0.1 mole fraction intervals.

Probe Solute	Pure Amine	0.1 HOAc	0.2 HOAc	0.3 HOAc	0.4 HOAc	0.5 HOAc	0.6 HOAc	0.7 HOAc	0.8 HOAc	0.9 HOAc	Pure Acid
Diethyl ether	1	1	1	1	1	1	1	1	1	1	1
Ethyl acetate	1	1	1	1	1	1	1	1	1	1	1
Acetone	1	1	1	1	1	1	1	1	1	1	1
Acetonitrile	1	1	1	1	1	1	1	1	1	1	1
Dimethyl sulfoxide	1	1	1	1	1	1	1	1	1	1	1
1,3–Bis(trifluoromethyl)benzene	1	1	1	1	1	1	0.5	0.5	0.5	1	1

Table 6.16 Miscibility of Diethyl ether, Ethyl acetate, Acetone, Acetonitrile, Dimethyl sulfoxide and 1,3–Bis(trfluoromethyl)benzene in the *N*,*N*–dimethylethanolamine (DMEtA) – acetic acid (HOAc) binary system at 0.1 mole fraction intervals.

Probe Solute	Pure Amine	0.1 HOAc	0.2 HOAc	0.3 HOAc	0.4 HOAc	0.5 HOAc	0.6 HOAc	0.7 HOAc	0.8 HOAc	0.9 HOAc	Pure Acid
Diethyl ether	1	1	1	1	1	0.5	0.5	0	0.5	1	1
Ethyl acetate	1	1	1	1	1	1	1	1	1	1	1
Acetone	1	1	1	1	1	1	1	1	1	1	1
Acetonitrile	1	1	1	1	1	1	1	1	1	1	1
Dimethyl sulfoxide	1	1	1	1	1	1	1	1	1	1	1
1,3–Bis(trifluoromethyl)benzene	1	1	1	1	1	0.5	0.5	0	0	1	1

6.3.1.4 Amphiprotic: ethanol, 1–octanol and water

Due to the combination of a hydrogen bond donor and a hydrogen bond acceptor, acid–amine binary mixtures could be considered to be amphiprotic by nature. As such, it would be expected that these binary mixtures would readily dissolve amphiprotic solutes. This is certainly the case when considering ethanol and 1–octanol: both feature the hydroxyl functional group, which give each solute favourable hydrogen bond donor and acceptor properties (Table 6.4). Both of these amphoteric solutes are fully miscible in all acid–amine binary mixtures, and precursors materials, of all three systems. That ethanol and 1–octanol share the same solubility profile, despite the lipophilic nature of 1–octanol, shows how important the hydrogen bonding interactions are between solvent and solute in acid–amine binary mixtures.

Water is also an amphiprotic solute – being highly capable of donating and accepting hydrogen bonds. However, water is immiscible in pure DMBuA and a number of its amine–rich compositions, sharing the same miscibility profile as dimethyl sulfoxide. Despite having similar hydrogen bonding capabilities as both ethanol and 1–octanol, the solubility of water is not solely dependent on its hydrogen bonding behaviour. Much like dimethyl sulfoxide, water is both highly polarizing (as inferred from π^*) and has a substantial dipolar interaction (most noticeably in terms of the δ_P and dipole moment values). As already discussed, the lack of either a large dipole moment or polarizable electron density from the acid–amine binary mixtures result in unfavourable solvent–solute interactions with water. This again highlights the importance of the non–specific intermolecular interactions in these acid–amine binary mixtures.

Table 6.17 Miscibility of Ethanol, 1–Octanol and Water in the DMBuA–HOAc binary system at 0.1 mole fraction intervals.

Probe Solute	Pure Amine	0.1 HOAc	0.2 HOAc	0.3 HOAc	0.4 HOAc	0.5 HOAc	0.6 HOAc	0.7 HOAc	0.8 HOAc	0.9 HOAc	Pure Acid
Ethanol	1	1	1	1	1	1	1	1	1	1	1
1–Octanol	1	1	1	1	1	1	1	1	1	1	1
Water	0	0	0	0	0.5	1	1	1	1	1	1

Table 6.18 Miscibility of Ethanol, 1–Octanol and Water in the TMEDA–HOAc binary system at 0.1 mole fraction intervals.

Probe Solute	Pure Amine	0.1 HOAc	0.2 HOAc	0.3 HOAc	0.4 HOAc	0.5 HOAc	0.6 HOAc	0.7 HOAc	0.8 HOAc	0.9 HOAc	Pure Acid
Ethanol	1	1	1	1	1	1	1	1	1	1	1
1–Octanol	1	1	1	1	1	1	1	1	1	1	1
Water	1	1	1	1	1	1	1	1	1	1	1

Table 6.19 Miscibility of Ethanol, 1–Octanol and Water in the DMEtA–HOAc binary system at 0.1 mole fraction intervals.

Probe Solute	Pure Amine	0.1 HOAc	0.2 HOAc	0.3 HOAc	0.4 HOAc	0.5 HOAc	0.6 HOAc	0.7 HOAc	0.8 HOAc	0.9 HOAc	Pure Acid
Ethanol	1	1	1	1	1	1	1	1	1	1	1
1–Octanol	1	1	1	1	1	1	1	1	1	1	1
Water	1	1	1	1	1	1	1	1	1	1	1

6.4 Conclusions

By using a qualitative interpretation of the miscibility between a given acid–amine binary system and a series of rationally selected probe solutes, the solvation capability of the three acid–amine binary mixtures has been characterized as a function of composition. Across all solutes, it is clear that the solvation environment changes substantially with both composition and amine functionality. This is easily noticed for solutes which are soluble in the precursor materials, but are insoluble in the binary mixtures. When a solute is immiscible, it can be considered that there were unfavourable solvent–solute interactions in comparison to the solvent–solvent and solute–solute interactions.

With respect to the composition derivative, numerous solutes are immiscible in acid–amine binary mixtures which are soluble in the corresponding precursors. This reduction in solubility appears to correlate well with both the extent of intermolecular hydrogen bonding interactions (as inferred from FIR spectroscopy in section 5.3.2) and the ionic nature of the binary mixture (as discussed in section 5.3.3). This is likely due to the strength of solvent–solvent interactions increasing as a result of mixing, and thus become more preferential to the solvent–solute interactions that take place. A solute can also be immiscible in a precursor component and some acid–amine binary mixtures but becomes soluble as composition changes. Such a composition dependence can be rationalized by an increase in the solvent–solute interactions relative to the solute–solute and solvent–solvent interactions.

The variance in amine functionality, although limited to just three different precursor amine structures, can significantly alter the solvation capabilities of an acid–amine binary system. For example, the DMBuA system, with an alkyl chain functional group, is immiscible with highly polarizable, large dipolar hydrogen bonding solutes (dimethyl sulfoxide and water)

in amine rich compositions, largely due to the lack of strong solvent–solute interactions to solvate these two solutes in amine–rich compositions. The TMEDA system, with a dimethylamino functional group, is capable of dissolving solutes that are immiscible in the DMBuA and DMEtA acid–rich systems. This suggests weaker solvent–solvent interactions in these compositions, due to the increased steric hindrance of the functional group and its low hydrogen bonding capability in comparison to the hydroxyl functional group on DMEtA. Having exhibited the most intermolecular hydrogen bonding interactions and extent of proton transfer at all compositions (as discussed in chapter 5), the DMEtA system is the least capable of solubilizing solutes which do not have strong hydrogen bonding capacity and large dipole moments.

To summarize, the solvation environment of the three acid–amine binary mixtures studied varied significantly, and changed with composition each in their own way. The insight gained into their short–range interactions (as discussed in chapter five) offers an initial explanation as to the observed trends in solvation behaviour. However, this study represents the first stage of screening solvation behaviour of these systems; a more in–depth, quantitative study of solvation capability is required for a more complete appreciation of the solvation behaviour in these systems. What can be shown from this chapter is that there is scope to tuning the solvation in these acid–amine binary mixtures by simply varying the composition.

Concluding Remarks

This thesis presents extensive novel research into the molecular thermodynamics and solvation behaviour in various PIL systems. A wide range of experimental techniques and theory have been employed to key systems which addressed challenges towards the application of PIL systems as potentially sustainable solvents.

Residual water significantly changes the properties in ILs, yet the molecular basis for this phenomenon has been unclear and subject to controversy. This was fuelled by a lack of connection between intermolecular interactions in the IL–water binary mixture and its physical properties. The connection was provided directly from the fundamental theory of statistical thermodynamics which successfully characterized the water–water, water–ion and ion–ion interactions directly from mixing thermodynamics. From this, it is shown that the advent of water clustering in ionic liquids is composition–dependant and that the average ion–ion interactions are not distinctly weakened by the presence of water.[148]

The connection between molecular interactions and physical properties, which was established for AILs which have well–defined anion and cation species, was expanded to elucidate the effect of residual water in PILs, which are more complex due to the proton transfer reaction between species. It was found that the effect of ionic nature (aprotic versus protic) of the ionic liquid–water strength of interaction is strongly composition dependent (for an analogous pair of ILs). Similar to what was shown in chapter two, water does not significantly weaken the average ion–ion interactions PILs. The hydrophilic PIL was found to exhibit more homogeneous solution structure, whereas the hydrophobic PIL exhibits heterogeneous solution structure.[149]

Having clarified the effect of residual water in PILs, attention was focused on understanding how properties of PILs emerge from the molecular structure, which had remained purely speculative by the lack of a molecular basis. The previous assumed empirical relationship of the precursor acid–base chemistry to PIL properties was disproved.[343] By using spectroscopy, the molecular origin of the structure–property relations was revealed, which correlated well with experimental solvation parameters and bulk viscosity of three functionalized PILs.[344] Introducing a hydrogen bond donor functional group increased the ionicity of a PIL, which corresponded to greater cohesive energy density, solvent dipolarity and bulk viscosity.[343,344]

Having established structure–property relationships strictly in PILs, which represent equimolar acid–amine mixtures, it was necessary to study mixtures beyond equimolar composition. This is because mixing behaviour can give deeper insight to molecular interactions, as well as the difficulty in maintaining a precise equimolar composition in practical applications. A connection between mixing thermodynamics and both a) intermolecular hydrogen bonding interaction and b) extent of proton transfer from acid to amine show the dominance of short–range interactions such as hydrogen bonds in these systems. The composition dependence revealed therein paved the way towards a new dimension of tunability for these binary mixtures.

To test this tunability in the context of their role as solvents requires practical solubility assessment. By screening the miscibility of a selection of probe solutes in acid–amine binary mixtures allowed for practical determination of their solvation capability as a function of composition and precursor amine functionality. In many instances, the observed change in solvation capability could be rationalized by the short–range interactions as discussed in

chapter five. That solvation was highly dependent on composition highlighted a potential new strategy to tuning the solvation in PIL systems beyond the equimolar composition.

In summary, three key aspects were identified and investigated from the context of binary liquid mixtures: 1) the effects of residual water as an impurity 2) a molecular basis for structure–property relations in certain PILs and 3) the strong composition dependence on the properties of acid–amine binary mixtures. The results found provided valuable insight towards the solvent design of protic ionic liquids for industrial applications.

Future Work

The described work and its implications open up a wide range of potential future research topics concerning IL systems.

The statistical thermodynamic connection between molecular interactions and physical properties in IL–water binary systems can be generalized to any binary system involving ILs.[148,149] Therefore, this theory can be applied straightaway to clarify many industrially important questions regarding IL–based binary mixtures. For example, IL–gas binary mixtures are particularly interesting in the context of fuel processing, carbon capture and catalysis.[34,88,91,404] Furthermore, the use of IL–cosolvent binary mixtures have been suggested to be more effective solvating media in some applications.[175,405] It is also possible to study more complex systems, such as ternary mixtures involving ILs, using statistical thermodynamics. For example, this could allow for a deeper understanding as to the effect of adding ILs to aqueous processes, such as natural product extraction.[175,406–409]

The connection between short–range interactions and bulk properties of PILs revealed an in–depth understanding of the structure–property relations for these materials. Due to the extensive experimental data required to draw these relations, the work in this thesis was limited

to just three tertiary ammonium acetate PILs.[343,344] By applying this methodology to a wider selection of PILs, featuring various anion and cation structures, structure–property relations on a molecular basis can be established for a wider range of PILs.[52,410] Such a high-precision determination of structure-property relations should be complemented with a high-throughput methodology approach.[410] This would be similar to how the detailed thermochemical results of chapter four are complemented by the straightforward volumetric results of chapter five, both of which were rationalized on a molecular basis from spectroscopy.

The dependence of short–range interactions, bulk properties and solvation capability on the composition in the acid–amine binary mixtures studied highlights an additional dimension of tuneability beyond equimolar mixtures i.e. PILs.[275,280] This could be exploited in the application of acid–amine binary mixtures as solvents, expanding the use of acid-amine binary systems as solvents for various novel applications.[49,52] Furthermore, by performing a quantitative miscibility analysis of acid–amine binary mixtures, a more in–depth assessment of the solvation capability, and its dependence on composition and PIL structure, can be developed. In particular, the determination of phase diagrams for these systems would enable the estimation of mixing quantities such as activity coefficients by using various well-established models.[411,412]

One technique which was not explored in this thesis, yet is likely to provide valuable insight into the molecular thermodynamics and solvation behaviour in protic ionic liquid systems, is small angle neutron scattering. The technique employs the diffraction of neutrons through liquid samples to give structural information of the studied system.[413,414] In combination with computational techniques such as Molecular Dynamics or Reverse Monte-Carlo simulations, deeper insight into the liquid structure through partial radial distribution functions can be obtained.[415–417] Furthermore, the solvation environment within IL systems can

be explored using this strategy, providing valuable insight into the short-range interactions that drive solubilisation in ILs.[418–420] In work carried out in parallel

In conclusion, the work presented herein represents a significant advance over the state of the art regarding knowledge of the molecular level phenomena underpinning many important features of PILs.[100,101,148,149,343,344] A number of future research directions have been identified, through which a more rational design-based approach towards PILs with specific combinations of desirable properties may be realised.

Appendix

A1 Standard Enthalpy of Formation of the Precursor Amines

In order to indirectly calculate the $\Delta_{\mathrm{vap}}H_m^\circ$ of each PIL, it is necessary to know the standard molar enthalpy of formation of the precursor amine for each amine in the gas phase $\Delta_{\mathrm{f}}H_m^\circ$ (B, g). These values can be measured experimentally, however for accurate, repeatable experiments the purity of material required is far greater than what was available for us. In place of this, *ab initio* calculations can be performed to estimate the values of $\Delta_{\mathrm{f}}H_m^\circ$ (B) for each of the precursor amines. The values of ($\Delta_{\mathrm{f}}H_m^\circ$ (B) used in all calculations in Chapter four were performed by Dr. Filipe Agapito of the Faculty of Sciences of the University of Lisbon. His contribution of original computational results towards the discussions in chapter four is gratefully acknowledged. Details of the computational results are re–printed below for context.

A1.1 Computational Details

The structures of DMBuA, TMEDA and DMEtA were optimized using the B3LYP–D3 dispersion corrected[421] hybrid density functional[422,423] together with the cc–pVTZ basis set.[424,425] Density fitting (DF)[426] was performed using the cc–pVTZ/JKFIT basis set.[427] Vibrational frequencies were obtained at the same level of theory, and scaled with 0.9889.[428] The enthalpy of each molecule at 298.15 K was determined with the W1–F12[429] composite procedure. The DF–B3LYP–D3/cc–pVTZ optimized geometries and vibrational frequencies were used in these calculations. The diagonal Born–Oppenheimer corrections[430–432] for each molecule, required by the W1–F12 procedure, were determined using CFOUR.[433] All other calculations were performed using Molpro 2012.1.[434] The individual components of the W1–F12 enthalpies are summarized in Table S4. The gas–phase standard enthalpy of formation for

each of the amines under study was calculated from the respective atomization reaction reaction using the W1–F12 enthalpies, as described in the main text (Table S5).

The calculations rely on the following equations:

$$\Delta_{at}H^{o}_{m} = a\,H^{o}_{m}(\mathrm{C, g}) + b\,H^{o}_{m}(\mathrm{H, g}) + c\,H^{o}_{m}(\mathrm{O, g}) + d\,H^{o}_{m}(\mathrm{N, g}) - H^{o}_{m}(\mathrm{C}_a\mathrm{H}_b\mathrm{O}_c\mathrm{N}_d, \mathrm{g}) \quad (9.1)$$

$$\Delta_{f}H^{o}_{m}(\mathrm{C}_a\mathrm{H}_b\mathrm{O}_c\mathrm{N}_d, \mathrm{g}) = -\Delta_{at}H^{o}_{m} + a\,\Delta_{f}H^{o}_{m}(\mathrm{C, g}) + b\,\Delta_{f}H^{o}_{m}(\mathrm{H, g}) + c\,\Delta_{f}H^{o}_{m}(\mathrm{O, g}) + d\,\Delta_{f}H^{o}_{m}(\mathrm{N, g}) \quad (9.2)$$

where $\Delta_{at}H^{o}_{m}$ refers to the atomization reaction:

$$\mathrm{C}_a\mathrm{H}_b\mathrm{O}_c\mathrm{N}_d(\mathrm{g}) = a\mathrm{C(g)} + b\mathrm{H(g)} + c\mathrm{O(g)} + d\mathrm{N(g)} \quad (9.3)$$

and H^{o}_{m} are the W1–F12 enthalpies of the compounds and their constituent atoms in the gas phase (see Supporting Information). These *ab–initio* calculations allowed the determination of the enthalpies of atomization of DMBuA (8133.9 kJ·mol^{-1}), TMEDA (8742.6 kJ·mol^{-1}) and DMEtA (6194.4 kJ·mol^{-1}), which together with the experimental gas–phase enthalpies of formation of hydrogen (217.998±0.006 kJ·mol^{-1}), carbon (716.680±0.450 kJ·mol^{-1}), oxygen (249.18±0.10·kJ·mol^{-1}) and nitrogen (472.68±0.40 kJ·mol^{-1}),[346] led to the standard molar enthalpies of formation of the amines, shown in Table 4.5. Previously reported data was only found for TMEDA, namely −19.7 kJ·mol^{-1}, estimated by Benson's group contribution method,[435] and −22.6 kJ·mol^{-1} obtained at the G3(MP2) level of theory. These values show a considerable discrepancy relative to the result in Table 1 (−9.2±2.8 kJ·mol^{-1}), which was obtained by the more accurate W1–F12 procedure.

Table A.1 Components of the W1–F12 enthalpies. All data in hartree.

	SCF	val. CCSD	val. T	core–valence	relativistic	spin–orbit	DBOC[a]	*H*(thermal)[b]	*H*°(298.15 K)[c]
C	–37.688596	–0.097659	–0.002630	–0.051452	–0.014935	–0.000135	0.001660	0.002360	–37.851387
H	–0.499967	0.000000	0.000000	0.000000	–0.000006	0.000000	0.000272	0.002360	–0.497341
O	–74.812001	–0.187544	–0.004126	–0.057770	–0.052097	–0.000355	0.002366	0.002360	–75.109167
N	–54.400727	–0.125442	–0.003085	–0.054926	–0.029194	0.000000	0.002005	0.002360	–54.609009
DMBuA	–290.499080	–1.451255	–0.061411	–0.375568	–0.116625	0.000000	0.015431	0.213019	–292.275488
TMEDA	–345.527481	–1.685549	–0.072961	–0.431273	–0.145390	0.000000	0.017663	0.231307	–347.613684
DMEtA	–287.290688	–1.315858	–0.055392	–0.327077	–0.139012	0.000000	0.013462	0.160782	–288.953783

[a] Diagonal Born–Oppenheimer correction. [b] Thermal enthalpy correction at 298.15 K. Includes the zero–point vibrational energy. [c] Enthalpy at T = 298.15 K and p^0 = 1 bar.

Table A.2 Contribution of each component of the W1–F12 procedure to the gas–phase standard enthalpies of formation. All data in kJ mol^{-1}.

	SCF	val. CCSD	val. T	core–valence	relativistic	spin–orbit	DBOC[a]	H(thermal)[b]	$\Delta_{at}H^{\circ}_{m}$[c]	$\Delta_{f}H^{\circ}_{m}$[d]
DMBuA	6477.8	1942.5	111.7	31.3	–6.0	–2.1	1.6	–423.0	8133.9	–91.2 ± 2.7
TMEDA	6813.1	2228.3	133.9	33.4	–7.1	–2.1	1.7	–458.6	8742.6	–9.2 ± 2.8
DMEtA	4788.8	1607.4	98.9	22.5	–5.5	–2.3	1.4	–316.8	6194.4	–207.8 ± 1.8

[a] Diagonal Born–Oppenheimer correction. [b] Thermal enthalpy correction at 298.15 K. Includes the zero–point vibrational energy. [c] Enthalpy of atomization at T = 298.15 K and p^{o} = 1 bar. [d] Enthalpy of formation at T = 298.15 K and p^{o} = 1 bar

References

1 G. Wypych, *Handbook of solvents. Volume 1, Properties*, ChemTec Publishing, Ontario, Canada, 2nd edn., 2010.

2 C. Reichardt and T. Welton, *Solvents and Solvent Effects in Organic Chemistry*, Wiley-VCH Verlag GmbH & Co. KGaA, Weinheim, Germany, 4th edn., 2010.

3 G. Wypych, *Handbook of solvents. Volume 2, Use, health, and environment*, ChemTec Publishing, Ontario, Canada, 2nd edn., 2014.

4 Y. Marcus, *Chem. Soc. Rev.*, 1993, **22**, 409–416.

5 Y. Marcus, *The Properties of Solvents*, Wiley, Chichester, 1st edn., 1998.

6 J. B. Durkee, *Cleaning with solvents : science and technology*, Elsevier Science, 1st edn., 2014.

7 D. F. Williams and W. H. Schmitt, *Chemistry and technology of the cosmetics and toiletries industry*, Blackie Academic and Professional, London, 2nd edn., 1996.

8 M. G. De Navarre and M. L. Schlossman, *The chemistry and manufacture of cosmetics*, Allured Books, 4th edn., 2009.

9 A. G. Fishburn, *An introduction to pharmaceutical formulation*, Pergamon Press, Oxford, 1st edn., 1965.

10 D. Stoye, W. Freitag and Wiley InterScience (Online service), *Paints, coatings, and solvents*, Wiley-VCH, 2nd edn., 1998.

11 J. A. G. Drake, *Chemicals for the automotive industry*, Royal Society of Chemistry, Cambridge, 1st edn., 1991.

12 A. Sethuramiah and R. Kumar, *Modelling of chemical wear : relevance to practice*, Elsevier, Oxford, 1st edn., 2015.

13 A. Illy, R. Viani and F. S. Liverani, *Espresso coffee : the science of quality*, Elsevier Academic, Amsterdam, 2nd edn., 2005.

14 F. Franks, *Water: A Matrix of Life*, Royal Society of Chemistry, Cambridge, 2nd edn., 2000.

15 R. E. Hester and R. M. Harrison, *Sustainable Water*, Royal Society of Chemistry, Cambridge, 1st edn., 2010.

16 Transparency Market Research, Global Solvents Market to Value USD 29.28 Billion by 2018, http://www.transparencymarketresearch.com/pressrelease/solvents-market.htm, (accessed 20 April 2017).

17 M. J. Raymond, C. S. Slater and M. J. Savelski, *Green Chem.*, 2010, **12**, 1826–1834.

18 J. H. Clark, A. Hunt, C. Topi, G. Paggiola and J. Sherwood, *Sustainable Solvents*, Royal Society of Chemistry, Cambridge, 1st edn., 2017.

19 C. J. van. Leeuwen and T. Vermeire, *Risk assessment of chemicals : an introduction*, Springer, Dordrecht, 2nd edn., 2007.

20 C. Bendicho, M. de la. Guardia and S. Garrigues, *Challenges in green analytical chemistry*, Royal Society of Chemistry, Cambridge, 1st edn., 2011.

21 F. Kerton and R. Marriott, *Alternative Solvents for Green Chemistry*, Royal Society of Chemistry, Cambridge, 2nd edn., 2013.

22 T. Welton, *Proc. R. Soc. A*, 2015, **471**, 1–26.

23 REACH - ECHA, https://echa.europa.eu/regulations/reach, (accessed 20 April 2017).

24 J. H. Clark, *Green Chem.*, 1999, **1**, 1–8.

25 R. A. Sheldon, *Green Chem.*, 2005, **7**, 267–278.

26 R. K. Henderson, C. Jiménez-González, D. J. C. Constable, S. R. Alston, G. G. A. Inglis, G. Fisher, J. Sherwood, S. P. Binks and A. D. Curzons, *Green Chem.*, 2011, **13**, 854–862.

27 D. Prat, O. Pardigon, H.-W. Flemming, S. Letestu, V. Ducandas, P. Isnard, E. Guntrum, T. Senac, S. Ruisseau, P. Cruciani and P. Hosek, *Org. Process Res. Dev.*, 2013, **17**, 1517–1525.

28 D. Prat, J. Hayler and A. Wells, *Green Chem.*, 2014, **16**, 4546–4551.

29 C. R. McElroy, A. Constantinou, L. C. Jones, L. Summerton and J. H. Clark, *Green Chem.*, 2015, **17**, 3111–3121.

30 D. Prat, A. Wells, J. Hayler, H. Sneddon, C. R. McElroy, S. Abou-Shehada and P. J. Dunn, *Green Chem.*, 2016, **18**, 288–296.

31 P. G. Jessop and W. Leitner, in *Chemical Synthesis Using Supercritical Fluids*, Wiley-VCH Verlag GmbH, Weinheim, Germany, 2007, pp. 1–36.

32 A. J. Hunt, E. H. K. Sin, R. Marriott and J. H. Clark, *ChemSusChem*, 2010, **3**, 306–322.

33 T. Welton, *Chem. Rev.*, 1999, **99**, 2071–2083.

34 J. P. Hallett and T. Welton, *Chem. Rev.*, 2011, **111**, 3508–3576.

35 R. D. Rogers and K. R. Seddon, *Science*, 2003, **302**, 792–793.

36 C. A. Angell, N. Byrne and J. P. Belieres, *Acc. Chem. Res.*, 2007, **40**, 1228–1236.

37 N. V Plechkova and K. R. Seddon, *Chem Soc Rev*, 2008, **37**, 123–150.

38 K. R. Seddon, A. Stark and M.-J. Torres, *Pure Appl. Chem.*, 2000, **72**, 2275–2287.

39 S. Cuadrado-Prado, M. Domínguez-Pérez, E. Rilo, S. García-Garabal, L. Segade, C. Franjo and O. Cabeza, *Fluid Phase Equilib.*, 2009, **278**, 36–40.

40 M. J. Earle, J. M. S. S. Esperança, M. A. Gilea, J. N. Canongia Lopes, L. P. N. Rebelo, J. W. Magee, K. R. Seddon and J. A. Widegren, *Nature*, 2006, **439**, 831–834.

41 J. P. Leal, J. M. S. S. Esperança, M. E. Minas da Piedade, J. N. Canongia Lopes, L. P. N. Rebelo and K. R. Seddon, *J. Phys. Chem. A*, 2007, **111**, 6176–6182.

42 T. P. Thuy Pham, C. W. Cho and Y. S. Yun, *Water Res.*, 2010, **44**, 352–372.

43 D. Coleman and N. Gathergood, *Chem. Soc. Rev.*, 2010, **39**, 600–637.

44 K. S. Egorova and V. P. Ananikov, *ChemSusChem*, 2014, 7, 336–360.

45 A. Jordan and N. Gathergood, *Chem. Soc. Rev.*, 2015, **44**, 8200–8237.

46 A. P. Abbott, D. Boothby, G. Capper, D. L. Davies and R. Rasheed, *J. Am. Chem. Soc.*, 2004, **126**, 9142–9147.

47 Q. Zhang, K. De Oliveira Vigier, S. Royer and F. Jérôme, *Chem. Soc. Rev.*, 2012, **41**, 7108–7146.

48 E. L. Smith, A. P. Abbott and K. S. Ryder, *Chem. Rev.*, 2014, **114**, 11060–11082.

49 EP1805131, *Eur. Pat. 1 805 131*, 2004.

50 T. L. Greaves and C. J. Drummond, *Chem. Rev.*, 2008, **108**, 206–237.

51 C. Austen Angell, Y. Ansari and Z. Zhao, *Faraday Discuss.*, 2012, **154**, 9–27.

52 T. L. Greaves and C. J. Drummond, *Chem. Rev.*, 2015, 115, 11379–11448.

53 P. Walden, *Bull. Russ. Acad. Sci.*, 1914, 405–422.

54 W. Ramsay, *Philos. Mag. Ser. 5*, 1876, **2**, 269–281.

55 L. Chen, G. E. Mullen, M. Le Roch, C. G. Cassity, N. Gouault, H. Y. Fadamiro, R. E. Barletta, R. A. O'Brien, R. E. Sykora, A. C. Stenson, K. N. West, H. E. Horne, J. M. Hendrich, K. R. Xiang and J. H. Davis, *Angew. Chemie - Int. Ed.*, 2014, **53**, 11762–11765.

56 M. A. B. H. Susan, A. Noda, S. Mitsushima and M. Watanabe, *Chem. Commun.*, 2003, **45**, 938–939.

57 A. Noda, M. A. Bin Hasan Susan, K. Kudo, S. Mitsushima, K. Hayamizu and M. Watanabe, *J. Phys. Chem. B*, 2003, **107**, 4024–4033.

58 W. Xu and C. A. Angell, *Science*, 2003, **302**, 422–425.

59 M. Armand, F. Endres, D. R. MacFarlane, H. Ohno and B. Scrosati, *Nat. Mater.*, 2009, **8**, 621–629.

60 D. R. Macfarlane, N. Tachikawa, M. Forsyth, J. M. Pringle, P. C. Howlett, G. D. Elliott, J. H. Davis, M. Watanabe, P. Simon and C. A. Angell, *Energy Environ. Sci.*, 2014, **7**, 232–250.

61 K. Bica, C. Rijksen, M. Nieuwenhuyzen and R. D. Rogers, *Phys. Chem. Chem. Phys.*, 2010, **12**, 2011–2017.

62 J. Stoimenovski, P. M. Dean, E. I. Izgorodina and D. R. MacFarlane, *Faraday Discuss.*, 2012, **154**, 335–352.

63 S. N. Adamovich, R. G. Mirskov, A. N. Mirskova and M. G. Voronkov, *Russ. Chem. Bull.*, 2012, **61**, 1260–1261.

64 D. N. Moreira, N. Fresno, R. Pérez-Fernández, C. P. Frizzo, P. Goya, C. Marco, M. A. P. Martins and J. Elguero, *Tetrahedron*, 2015, **71**, 676–685.

65 M. Matthias, M. Klemens and V. Uwe, *Chemfiles*, 2005, 5, 4.

66 M. W. Sanders, L. Wright, L. Tate, G. Fairless, L. Crowhurst, N. C. Bruce, A. J.

Walker, G. A. Hembury and S. Shimizu, *J. Phys. Chem. A*, 2009, **113**, 10143–10145.

67 C. Yansheng, Z. Zhida, L. Changping, L. Qingshan, Y. Peifang and U. Welz-Biermann, *Green Chem.*, 2011, **13**, 666–670.

68 N. Goujon, X. Wang, R. Rajkowa and N. Byrne, *Chem. Commun.*, 2012, **48**, 1278–1280.

69 A. W. T. King, J. Asikkala, I. Mutikainen, P. Järvi and I. Kilpeläinen, *Angew. Chemie - Int. Ed.*, 2011, **50**, 6301–6305.

70 A. Idris, R. Vijayaraghavan, A. F. Patti and D. R. Macfarlane, *ACS Sustain. Chem. Eng.*, 2014, **2**, 1888–1894.

71 E. C. Achinivu, R. M. Howard, G. Li, H. Gracz and W. A. Henderson, *Green Chem.*, 2014, **16**, 1114–1119.

72 A. George, A. Brandt, K. Tran, S. M. S. N. S. Zahari, D. Klein-Marcuschamer, N. Sun, N. Sathitsuksanoh, J. Shi, V. Stavila, R. Parthasarathi, S. Singh, B. M. Holmes, T. Welton, B. A. Simmons and J. P. Hallett, *Green Chem.*, 2015, **17**, 1728–1734.

73 C. Chiappe, A. Mezzetta, C. S. Pomelli, B. Masciocchi, A. Gentile and G. Iaquaniello, *Green Chem.*, 2016, **18**, 4982–4989.

74 P. Verdía, A. Brandt, J. P. Hallett, M. J. Ray and T. Welton, *Green Chem.*, 2014, **16**, 1617–1627.

75 L. Chen, M. Sharifzadeh, N. Mac Dowell, T. Welton, N. Shah and J. P. Hallett, *Green Chem.*, 2014, **16**, 3098–3106.

76 T. Rashid, C. F. Kait, I. Regupathi and T. Murugesan, *Ind. Crops Prod.*, 2016, **84**, 284–293.

77 A. J. Walker and N. C. Bruce, *Chem. Commun.*, 2004, **1**, 2570–2571.

78 A. J. Walker and N. C. Bruce, *Tetrahedron*, 2004, **60**, 561–568.

79 R. A. Sheldon, *Chem. - A Eur. J.*, 2016, **22**, 12984–12999.

80 H. Luo, M. Yu and S. Dai, *Zeitschrift fur Naturforsch. - Sect. A J. Phys. Sci.*, 2007, **62**, 281–291.

81 S. Katsuta, Y. Yoshimoto, M. Okai, Y. Takeda and K. Bessho, *Ind. Eng. Chem. Res.*, 2011, **50**, 12735–12740.

82 J. R. Bell, H. Luo and S. Dai, *Sep. Purif. Technol.*, 2014, **130**, 147–150.

83 Y. Watanabe, Y. Araki and S. Katsuta, *Bunseki Kagaku*, 2014, **63**, 563–567.

84 S. Katsuta, M. Okai, Y. Yoshimoto and Y. Kudo, *Anal. Sci.*, 2012, **28**, 1009–1012.

85 J. Qu, J. J. Truhan, S. Dai, H. Luo and P. J. Blau, *Tribol. Lett.*, 2006, **22**, 207–214.

86 Q. Zhao, G. Zhao, M. Zhang, X. Wang and W. Liu, *Tribol. Lett.*, 2012, **48**, 133–144.

87 T. Espinosa, M. Jimenez, J. Sanes, A. E. Jimenez, M. Iglesias and M. D. Bermudez, *Tribol. Lett.*, 2014, **53**, 1–9.

88 K. A. Mumford, S. J. Pas, T. Linseisen, T. M. Statham, N. Johann Nicholas, A. Lee,

K. Kezia, R. Vijayraghavan, D. R. MacFarlane and G. W. Stevens, *Int. J. Greenh. Gas Control*, 2015, **32**, 129–134.

89 R. Vijayraghavan, S. J. Pas, E. I. Izgorodina and D. R. MacFarlane, *Phys. Chem. Chem. Phys.*, 2013, **15**, 19994–19999.

90 L. Bai, Y. Nie, Y. Li, H. Dong and X. Zhang, *Fuel Process. Technol.*, 2013, **108**, 94–100.

91 Z. Li, J. Xu, D. Li and C. Li, *RSC Adv.*, 2015, **5**, 15892–15897.

92 P. T. Anastas and J. C. Warner, *Green chemistry : theory and practice*, Oxford University Press, Oxford, 1st edn., 2000.

93 B. Peric, E. Martí, J. Sierra, R. Cruañas, M. Iglesias and M. A. Garau, *Environ. Toxicol. Chem.*, 2011, **30**, 2802–2809.

94 Y. J. Ding, Y. Nie and Y. Yu, *Chem. Res. Chinese Univ.*, 2011, **27**, 651–654.

95 B. Peric, J. Sierra, E. Martí, R. Cruañas, M. A. Garau, J. Arning, U. Bottin-Weber and S. Stolte, *J. Hazard. Mater.*, 2013, **261**, 99–105.

96 B. Peric, J. Sierra, E. Martí, R. Cruañas and M. A. Garau, *Ecotoxicol. Environ. Saf.*, 2015, **115**, 257–262.

97 M. V. S. Oliveira, B. T. Vidal, C. M. Melo, R. de C. M. de Miranda, C. M. F. Soares, J. A. P. Coutinho, S. P. M. Ventura, S. Mattedi and Á. S. Lima, *Chemosphere*, 2016, **147**, 460–466.

98 A. Tzani, M. Elmaloglou, C. Kyriazis, D. Aravopoulou, I. Kleidas, A. Papadopoulos, E. Ioannou, A. Kyritsis, E. Voutsas and A. Detsi, *J. Mol. Liq.*, 2016, **224**, 366–376.

99 B. Peric, J. Sierra, E. Martí, R. Cruañas and M. A. Garau, *Chemosphere*, 2014, **108**, 418–425.

100 J. E. S. J. Reid, H. Prydderch, M. Spulak, S. Shimizu, A. J. Walker and N. Gathergood, *Sustain. Chem. Pharmacol.*, 2017, Accepted.

101 J. E. S. J. Reid, N. Sullivan, L. Swift, G. A. Hembury, S. Shimizu and A. J. Walker, *Sustain. Chem. Process.*, 2015, **3**, 17.

102 B. N. Ames, J. McCann and E. Yamasaki, *Mutat. Res. Mutagen. Relat. Subj.*, 1975, **31**, 347–363.

103 J. McCann, E. Choi, E. Yamasaki and B. N. Ames, *Proc. Natl. Acad. Sci. U. S. A.*, 1975, **72**, 5135–5139.

104 D. Maron, J. Katzenellenbogen and B. N. Ames, *Mutat. Res. Toxicol.*, 1981, **88**, 343–350.

105 K. Mortelmans and E. Zeiger, *Mutat. Res.*, 2000, **455**, 29–60.

106 E. de Jong and G. Jungmeier, in *Industrial Biorefineries & White Biotechnology*, Elsevier, 1st edn., 2015, pp. 3–33.

107 S. W. Breeden, J. H. Clark, T. J. Farmer, D. J. Macquarrie, J. S. Meimoun, Y. Nonne and J. E. S. J. Reid, *Green Chem.*, 2013, **15**, 72–75.

108 A. J. J. Straathof, *Chem. Rev.*, 2014, **114**, 1871–1908.

109 C. S. K. Lin, L. A. Pfaltzgraff, L. Herrero-Davila, E. B. Mubofu, S. Abderrahim, J. H. Clark, A. A. Koutinas, N. Kopsahelis, K. Stamatelatou, F. Dickson, S. Thankappan, Z. Mohamed, R. Brocklesby and R. Luque, *Energy Environ. Sci.*, 2013, **6**, 426–464.

110 Avelino Corma, Sara Iborra and A. Velty, *Chem. Rev.*, 2007, **107**, 2411–2502.

111 L. R. Lynd, J. H. Cushman, R. J. Nichols and C. E. Wyman, *Science*, 1991, **251**, 1318–1323.

112 G. W. Huber, J. N. Chheda, C. J. Barrett and J. A. Dumesic, *Science*, 2005, **308**, 1446–1450.

113 George W. Huber, A. Sara Iborra and A. Corma, *Chem. Rev.*, 2006, **106**, 4044–4098.

114 D. M. Alonso, J. Q. Bond and J. A. Dumesic, *Green Chem.*, 2010, **12**, 1493–1513.

115 C. O. Tuck, E. Pérez, I. T. Horváth, R. A. Sheldon and M. Poliakoff, *Science*, 2012, **337**, 695–699.

116 US990191 A, 1911.

117 F. W. Lichtenthaler, *Acc. Chem. Res.*, 2002, **35**, 728–737.

118 A. Biswas, B. K. Sharma, J. L. Willett, S. Z. Erhan and H. N. Cheng, *Energy Environ. Sci.*, 2008, **1**, 639–644.

119 G. T. Tsao, N. J. Cao, J. Du and C. S. Gong, in *Recent Progress in Bioconversion of Lignocellulosics*, Springer Berlin Heidelberg, 1999, pp. 243–280.

120 X.-S. Zhang, G.-X. Yang, H. Jiang, W.-J. Liu and H.-S. Ding, *Sci. Rep.*, 2013, **3**, 1120–1126.

121 O. Hromatka and H. Ebner, *Ind. Eng. Chem.*, 1959, **51**, 1279–1280.

122 S. Okino, M. Inui and H. Yukawa, *Appl. Microbiol. Biotechnol.*, 2005, **68**, 475–480.

123 Kenta Fukumoto, A. Masahiro Yoshizawa and H. Ohno, *J. Am. Chem. Soc.*, 2005, **127**, 2398–2399.

124 H. Ohno and K. Fukumoto, *Acc. Chem. Res.*, 2007, **40**, 1122–1129.

125 S. Tian, S. Ren, Y. Hou, W. Wu and W. Peng, *J. Chem. Eng. Data*, 2013, **58**, 1885–1892.

126 J. Wang, T. L. Greaves, D. F. Kennedy, A. Weerawardena, G. Song and C. J. Drummond, *Aust. J. Chem.*, 2011, **64**, 180–189.

127 X. D. Hou, Q. P. Liu, T. J. Smith, N. Li and M.-H. Zong, *PLoS One*, 2013, **8**, e59145.

128 D. J. Tao, Z. Cheng, F. F. Chen, Z. M. Li, N. Hu and X. S. Chen, *J. Chem. Eng. Data*, 2013, **58**, 1542–1548.

129 W. Gouveia, T. F. Jorge, S. Martins, M. Meireles, M. Carolino, C. Cruz, T. V. Almeida and M. E. M. Araújo, *Chemosphere*, 2014, **104**, 51–56.

130 A. Jordan, A. Haiß, M. Spulak, Y. Karpichev, K. Kümmerer and N. Gathergood,

Green Chem., 2016, **18**, 4374–4392.

131 Y. Deng, I. Beadham, M. Ghavre, M. F. Costa Gomes, N. Gathergood, P. Husson, B. Legeret, B. Quilty, M. Sancelme and P. Besse-Hoggan, *Green Chem.*, 2015, **17**, 1479–1491.

132 H. Prydderch, A. Heise and N. Gathergood, in *Ionic Liquids in the Biorefinery Concept: Challenges and Perspectives*, Royal Society of Chemistry, Cambridge, 2015, pp. 168–201.

133 A. Haiß, A. Jordan, J. Westphal, E. Logunova, N. Gathergood and K. Kümmerer, *Green Chem.*, 2016, **18**, 4361–4373.

134 H. Prydderch, A. Haiβ, M. Spulak, B. Quilty, K. Kümmerer, A. Heise and N. Gathergood, *RSC Adv.*, 2017, **7**, 2115–2126.

135 Y. Kohno and H. Ohno, *Chem. Commun.*, 2012, **48**, 7119–7130.

136 Y. Cao, Y. Chen, X. Sun, Z. Zhang and T. Mu, *Phys. Chem. Chem. Phys.*, 2012, **14**, 12252–12262.

137 J. A. Widegren, A. Laesecke and J. W. Magee, *Chem. Commun.*, 2005, 1610–1612.

138 J. Jacquemin, P. Husson, A. A. H. Padua and V. Majer, *Green Chem.*, 2006, **8**, 172–180.

139 C. M. S. S. Neves, M. L. S. Batista, A. F. M. Cláudio, L. M. N. B. F. Santos, I. M. Marrucho, M. G. Freire and J. A. P. Coutinho, *J. Chem. Eng. Data*, 2010, **55**, 5065–5073.

140 K. Machanová, A. Boisset, Z. Sedláková, M. Anouti, M. Bendová and J. Jacquemin, *J. Chem. Eng. Data*, 2012, **57**, 2227–2235.

141 M. Khodadadi-Moghaddam, A. Habibi-Yangjeh and M. R. Gholami, *Monatshefte fur Chemie*, 2009, **140**, 329–334.

142 S. Trivedi, N. I. Malek, K. Behera and S. Pandey, *J. Phys. Chem. B*, 2010, **114**, 8118–8125.

143 N. D. Khupse and A. Kumar, *J. Phys. Chem. B*, 2011, **115**, 711–718.

144 Y. Chen, Y. Cao, X. Lu, C. Zhao, C. Yan and T. Mu, *New J. Chem.*, 2013, **37**, 1959–1967.

145 Richard P. Swatloski, Scott K. Spear, A. John D. Holbrey and R. D. Rogers, *J. Am. Chem. Soc.*, 2002, **124**, 4974–4975.

146 C. F. Poole and S. K. Poole, *J. Chromatogr. A*, 2010, **1217**, 2268–2286.

147 J. H. Clark and S. J. Tavener, *Org. Process Res. Dev.*, 2007, **11**, 149–155.

148 J. E. S. J. Reid, A. J. Walker and S. Shimizu, *Phys. Chem. Chem. Phys.*, 2015, **17**, 14710–14718.

149 J. E. S. J. Reid, R. J. Gammons, J. M. Slattery, A. J. Walker and S. Shimizu, *J. Phys. Chem. B*, 2017, **121**, 599–609.

150 L. Cammarata, S. G. Kazarian, P. A. Salter and T. Welton, *Phys. Chem. Chem. Phys.*, 2001, **3**, 5192–5200.

151 Y. Danten, M. I. Cabaço and M. Besnard, *J. Phys. Chem. A*, 2009, **113**, 2873–2889.

152 Y. Danten, M. I. Cabaço and M. Besnard, *J. Mol. Liq.*, 2010, **153**, 57–66.

153 G. M. Wilson, *J. Am. Chem. Soc.*, 1964, **86**, 127–130.

154 X. Zhu, Y. Wang and H. Li, *Am. Inst. Chem. Eng. J.*, 2009, **55**, 198–205.

155 M. López-Pastor, M. J. Ayora-Cañada, M. Valcárcel and B. Lendl, *J. Phys. Chem. B*, 2006, **110**, 10896–10902.

156 A. Dominguez-Vidal, N. Kaun, M. J. Ayora-Cañada and B. Lendl, *J. Phys. Chem. B*, 2007, **111**, 4446–4452.

157 A. Maiti, A. Kumar and R. D. Rogers, *Phys. Chem. Chem. Phys.*, 2012, **14**, 5139–5146.

158 U. Schröder, J. D. Wadhawan, R. G. Compton, F. Marken, P. A. Z. Suarez, C. S. Consorti, R. F. de Souza and J. Dupont, *New J. Chem.*, 2000, **24**, 1009–1015.

159 A. Mele, C. D. Tran and S. H. De Paoli Lacerda, *Angew. Chemie - Int. Ed.*, 2003, **42**, 4364–4366.

160 M. Brehm, H. Weber, A. S. Pensado, A. Stark and B. Kirchner, *Zeitschrift für Phys. Chemie*, 2013, **227**, 177–204.

161 W. Shi, K. Damodaran, H. B. Nulwala and D. R. Luebke, *Phys. Chem. Chem. Phys.*, 2012, **14**, 15897–15908.

162 P. Stange, K. Fumino and R. Ludwig, *Angew. Chemie - Int. Ed.*, 2013, **52**, 2990–2994.

163 T. L. Greaves, D. F. Kennedy, A. Weerawardena, N. M. K. Tse, N. Kirby and C. J. Drummond, *J. Phys. Chem. B*, 2011, **115**, 2055–2066.

164 G. L. Burrell, N. F. Dunlop and F. Separovic, *Soft Matter*, 2010, **6**, 2080–2086.

165 J. Chen, L. Chen, Y. Lu and Y. Xu, *J. Mol. Liq.*, 2014, **197**, 374–380.

166 R. Zarrougui, M. Dhahbi and D. Lemordant, *J. Solution Chem.*, 2015, **44**, 686–702.

167 N. Yaghini, L. Nordstierna and A. Martinelli, *Phys. Chem. Chem. Phys.*, 2014, **16**, 9266–9275.

168 N. Yaghini, J. Pitawala, A. Matic and A. Martinelli, *J. Phys. Chem. B*, 2015, **119**, 1611–1622.

169 S. Zahn, K. Wendler, L. Delle Site and B. Kirchner, *Phys. Chem. Chem. Phys.*, 2011, **13**, 15083–15093.

170 D. H. Dagade, K. R. B. Madkar, S. P. Shinde and S. S. Barge, *J. Phys. Chem. B*, 2013, **117**, 1031–1043.

171 J. Skowronek, M. Geppert-Rybczyńska, J. Jacquemin, P. Goodrich, J. A. Vicente, M. Chorążewski, S. Jężak, M. Zorębski, E. Zorębski, M. Żarska, W. Kaca, P. Berdyczko and M. Dzida, *J. Solution Chem.*, 2015, **44**, 824–837.

172 I. Bahadur, T. M. Letcher, S. Singh, G. G. Redhi, P. Venkatesu and D. Ramjugernath, *J. Chem. Thermodyn.*, 2015, **82**, 34–46.

173 J. Łuczak, J. Hupka, J. Thöming and C. Jungnickel, *Colloids Surfaces A*

Physicochem. Eng. Asp., 2008, 329, 125–133.

174 J. Bowers, C. P. Butts, P. J. Martin, M. C. Vergara-Gutierrez and R. K. Heenan, *Langmuir*, 2004, **20**, 2191–2198.

175 A. F. M. Cláudio, M. C. Neves, K. Shimizu, J. N. Canongia Lopes, M. G. Freire and J. A. P. Coutinho, *Green Chem.*, 2015, **17**, 3948–3963.

176 H. Rodríguez, J. F. Brennecke, Héctor Rodríguez and J. F. Brennecke*, *J. Chem. Eng. Data*, 2006, **51**, 2145–2155.

177 M. Anouti, M. Caillon-Caravanier, Y. Dridi, J. Jacquemin, C. Hardacre and D. Lemordant, *J. Chem. Thermodyn.*, 2009, **41**, 799–808.

178 S. Wang, J. Jacquemin, P. Husson, C. Hardacre and M. F. Costa Gomes, *J. Chem. Thermodyn.*, 2009, **41**, 1206–1214.

179 D. Singh, V. Singh and R. L. Gardas, *J. Solution Chem.*, 2015, **44**, 634–651.

180 M. Anouti, A. Vigeant, J. Jacquemin, C. Brigouleix and D. Lemordant, *J. Chem. Thermodyn.*, 2010, **42**, 834–845.

181 R. Anantharaj and T. Banerjee, *J. Ind. Eng. Chem.*, 2012, **18**, 331–343.

182 B. Docampo-Álvarez, V. Gómez-González, T. Méndez-Morales, J. Carrete, J. R. Rodríguez, Ó. Cabeza, L. J. Gallego and L. M. Varela, *J. Chem. Phys.*, 2014, **140**, 214502.

183 R. Hayes, S. Imberti, G. G. Warr and R. Atkin, *Angew. Chemie - Int. Ed.*, 2012, **51**, 7468–7471.

184 K. Fumino, V. Fossog, P. Stange, K. Wittler, W. Polet, R. Hempelmann and R. Ludwig, *ChemPhysChem*, 2014, **15**, 2604–2609.

185 M. Huang and H. Weingärtner, *ChemPhysChem*, 2008, **9**, 2172–2173.

186 M. Ekimova, D. Fröhlich, S. Stalke, T. Lenzer and K. Oum, *ChemPhysChem*, 2012, **13**, 1854–1859.

187 H. F. D. Almeida, H. Passos, J. A. Lopes-da-silva, A. M. Fernandes, M. G. Freire and J. A. P. Coutinho, *J. Chem. Eng. Data*, 2012, **57**, 3005–3013.

188 A. Bhattacharjee, J. A. P. Coutinho, M. G. Freire and P. J. Carvalho, *J. Solution Chem.*, 2015, **44**, 703–717.

189 K. Bica, M. Deetlefs, C. Schröder and K. R. Seddon, *Phys. Chem. Chem. Phys.*, 2013, **15**, 2703–2711.

190 C. E. S. Bernardes, K. Shimizu, J. N. C. Lopes, P. Marquetand, E. Heid, O. Steinhauser and C. Schröder, *Phys. Chem. Chem. Phys.*, 2016, **18**, 1665–1670.

191 P. K. Chhotaray, S. Jella and R. L. Gardas, *J. Chem. Thermodyn.*, 2014, **74**, 255–262.

192 G. Sharma, R. L. Gardas, A. Coronas and G. Venkatarathnam, *Fluid Phase Equilib.*, 2016, **415**, 1–7.

193 J.-P. Belieres and C. A. Angell, *J. Phys. Chem. B*, 2007, **111**, 4926–4937.

194 M. Yoshizawa, W. Xu and C. A. Angell, *J. Am. Chem. Soc.*, 2003, **125**, 15411–

15419.

195 M. S. Miran, H. Kinoshita, T. Yasuda, M. A. B. H. Susan and M. Watanabe, *Phys. Chem. Chem. Phys.*, 2012, **14**, 5178–5186.

196 T. L. Greaves, A. Weerawardena, C. Fong, I. Krodkiewska and C. J. Drummond, *J. Phys. Chem. B*, 2006, **110**, 22479–22487.

197 K. Ueno, Z. Zhao, M. Watanabe and C. A. Angell, *J. Phys. Chem. B*, 2012, **116**, 63–70.

198 S. Nazari, S. Cameron, M. B. Johnson and K. Ghandi, *J. Mater. Chem. A*, 2013, **1**, 11570–11579.

199 A. M. Moschovi, V. Dracopoulos and V. Nikolakis, *J. Phys. Chem. B*, 2014, **118**, 8673–8683.

200 T. L. Greaves, D. F. Kennedy, S. T. Mudie and C. J. Drummond, *J. Phys. Chem. B*, 2010, **114**, 10022–10031.

201 R. W. Berg, J. N. Canongia Lopes, R. Ferreira, L. P. N. Rebelo, K. R. Seddon and A. A. Tomaszowska, *J. Phys. Chem. A*, 2010, **114**, 10834–41.

202 R. W. Berg, A. Riisager and R. Fehrmann, *J. Phys. Chem. A*, 2008, **112**, 8585–8592.

203 J. Vitorino, J. P. Leal, M. E. Minas da Piedade, J. N. Canongia Lopes, J. M. S. S. Esperança and L. P. N. Rebelo, *J. Phys. Chem. B*, 2010, **114**, 8905–8909.

204 J. Vitorino, C. E. S. Bernardes, M. E. Minas da Piedade, E. S. Bernardes and M. E. Minas, *Phys. Chem. Chem. Phys.*, 2012, **14**, 4440–4446.

205 J. Vitorino, F. Agapito, M. F. M. Piedade, C. E. S. Bernardes, H. P. Diogo, J. P. Leal and M. E. Minas da Piedade, *J. Chem. Thermodyn.*, 2014, **77**, 179–189.

206 V. N. Emel'yanenko, S. P. Verevkin and A. Heintz, *J. Am. Chem. Soc.*, 2007, **129**, 3930–3937.

207 H. Zhu, X.; Wang, Y.;Li, *Phys. Chem. Chem. Phys.*, 2011, **13**, 17445–17448.

208 V. N. Emel'yanenko, G. Boeck, S. P. Verevkin and R. Ludwig, *Chem. - A Eur. J.*, 2014, **20**, 11640–11645.

209 A. Ostonen, J. Bervas, P. Uusi-Kyyny, V. Alopaeus, D. H. Zaitsau, V. N. Emel'Yanenko, C. Schick, A. W. T. King, J. Helminen, I. Kilpeläinen, A. A. Khachatrian, M. A. Varfolomeev and S. P. Verevkin, *Ind. Eng. Chem. Res.*, 2016, **55**, 10445–10454.

210 D. H. Zaitsau, V. N. Emel'yanenko, P. Stange, C. Schick, S. P. Verevkin and R. Ludwig, *Angew. Chemie - Int. Ed.*, 2016, 11682–11686.

211 K. Dong, S. Zhang and J. Wang, *Chem. Commun.*, 2016, **52**, 6744–6764.

212 N. Byrne and C. A. Angell, *Chem. Commun.*, 2009, **13**, 1046–1048.

213 F. Falcioni, H. R. Housden, Z. Ling, S. Shimizu, A. J. Walker and N. C. Bruce, *Chem. Commun.*, 2010, **46**, 749–751.

214 P. Attri and P. Venkatesu, *Int. J. Biol. Macromol.*, 2012, **51**, 119–128.

215 P. Attri and P. Venkatesu, *Process Biochem.*, 2013, **48**, 462–470.

216 L. K. J. Hauru, M. Hummel, A. W. T. King, I. Kilpeläinen and H. Sixta, *Biomacromolecules*, 2012, **13**, 2896–2905.

217 A. Parviainen, A. W. T. King, I. Mutikainen, M. Hummel, C. Selg, L. K. J. Hauru, H. Sixta and I. Kilpeläinen, *ChemSusChem*, 2013, **6**, 2161–2169.

218 K. Fumino, A. Wulf and R. Ludwig, *Angew. Chem. Int. Ed. Engl.*, 2009, **48**, 3184–3186.

219 K. Fumino, A. Wulf and R. Ludwig, *Phys. Chem. Chem. Phys.*, 2009, **11**, 8790–8794.

220 K. Fumino, E. Reichert, K. Wittler, R. Hempelmann and R. Ludwig, *Angew. Chemie - Int. Ed.*, 2012, **51**, 6236–6240.

221 K. Fumino, V. Fossog, K. Wittler, R. Hempelmann and R. Ludwig, *Angew. Chemie - Int. Ed.*, 2013, **52**, 2368–2372.

222 K. Fumino, S. Reimann and R. Ludwig, *Phys. Chem. Chem. Phys.*, 2014, **16**, 21903–21929.

223 K. Fumino, T. Peppel, M. Geppert-Rybczynka, D. H. Zaitsau, J. K. Lehmann, S. P. Verevkin, M. Kokerling and R. Ludwig, *Phys. Chem. Chem. Phys.*, 2011, **13**, 14064–14075.

224 M. S. Miran, H. Kinoshita, T. Yasuda, M. A. Susan and M. Watanabe, *Chem. Commun.*, 2011, **47**, 12676–12678.

225 A. Mondal and S. Balasubramanian, *J. Phys. Chem. A*, 2015, **119**, 1994–2002.

226 J. Hunger, T. Sonnleitner, L. Liu, R. Buchner, M. Bonn and H. J. Bakker, *J. Phys. Chem. Lett.*, 2012, **3**, 3034–3038.

227 M. Krüger, E. Bründermann, S. Funkner, H. Weingärtner and M. Havenith, *J. Chem. Phys.*, 2010, **132**, 101101.

228 M. Krüger, M. M. Huang, E. Bründermann, H. Weingärtner and M. Havenith, *IEEE Trans. Terahertz Sci. Technol.*, 2011, **1**, 313–319.

229 D. A. Turton, T. Sonnleitner, A. Ortner, M. Walther, G. Hefter, K. R. Seddon, S. Stana, N. V. Plechkova, R. Buchner and K. Wynne, *Faraday Discuss.*, 2012, **154**, 145–153.

230 T. Sonnleitner, D. A. Turton, G. Hefter, A. Ortner, S. Waselikowski, M. Walther, K. Wynne and R. Buchner, *J. Phys. Chem. B*, 2015, **115**, 8826–8841.

231 D. R. MacFarlane and K. R. Seddon, *Aust. J. Chem.*, 2007, **60**, 3–5.

232 J. Stoimenovski, E. I. Izgorodina and D. R. Macfarlane, *Phys. Chem. Chem. Phys.*, 2010, **12**, 10341–10347.

233 R. Lindemann and G. Zundel, *J. Chem. Soc. Faraday Trans. 2 Mol. Chem. Phys.*, 1972, **68**, 979–990.

234 R. Lindemann and G. Zundel, *J. Chem. Soc., Faraday Trans. 2*, 1977, **73**, 788–803.

235 R. Lindemann and G. Zundel, *Biopolymers*, 1978, **17**, 1285–1304.

236 G. Zundel, A. Nagyrevil and A. Nagyrevi, *J. Phys. Chem.*, 1978, **82**, 685–689.

237 G. S. Denisov, G. V Gusakova and A. L. Smolyansky, *J. Mol. Struct.*, 1973, **15**, 377–382.

238 M. Wierzejewska-Hnat, Z. Mielke and H. Ratajczak, *J. Chem. Soc. Faraday Trans. 2*, 1980, **76**, 834–843.

239 P. Barczynski, Z. Degaszafran and M. Szafran, *J. Chem. Soc. Trans. 2*, 1985, **6**, 765–771.

240 G. Zundel, *J. Mol. Struct.*, 1988, **177**, 43–68.

241 R. Krämer and G. Zundel, *J. Chem. Soc., Faraday Trans.*, 1990, **86**, 301–305.

242 M. Szafran, *J. Mol. Struct.*, 1996, **381**, 39–64.

243 D. F. Detar and R. W. Novak, *J. Am. Chem. Soc.*, 1970, **92**, 1361–1365.

244 S. K. Davidowski, F. Thompson, W. Huang, M. Hasani, S. A. Amin, C. A. Angell and J. L. Yarger, *J. Phys. Chem. B*, 2016, **120**, 4279–4285.

245 G. L. Burrell, I. M. Burgar, N. F. Dunlop, F. Separovic and N. F. Dunlop, *Phys. Chem. Chem. Phys.*, 2010, **12**, 1571–1577.

246 M. S. C. Flett, *J. Chem. Soc.*, 1951, 962–967.

247 Y. Cui, J. Yin, C. Li, S. Li, A. Wang, G. Yang, Y. Jia, Y. Cui, S. Li, J. Yin, A. Wang, G. Yang and Y. Jia, *Phys. Chem. Chem. Phys.*, 2016, **18**, 19731–19737.

248 M. Shen, Y. Zhang, K. Chen, S. Che, J. Yao and H. Li, *J. Phys. Chem. B*, 2017, **121**, 1372–1376.

249 N. V Drichko, G. Y. Kerenskaia and V. M. Schreiber, *J. Mol. Struct.*, 1999, **477**, 127–141.

250 H. Nakamoto, A. Noda, K. Hayamizu, S. Hayashi, H. O. Hamaguchi and M. Watanabe, *J. Phys. Chem. C*, 2007, **111**, 1541–1548.

251 J. A. Bautista-Martinez, L. Tang, J.-P. Belieres, R. Zeller, C. A. Angell and C. Friesen, *J. Phys. Chem. C*, 2009, **113**, 12586–12593.

252 X. Sun, B. Cao, X. Zhou, S. Liu, X. Zhu and H. Fu, *J. Mol. Liq.*, 2016, **221**, 254–261.

253 T. D. N. Reddy and B. S. Mallik, *Phys. Chem. Chem. Phys.*, 2017, **19**, 10358–10370.

254 A. B. Patil and B. M. Bhanage, *Phys. Chem. Chem. Phys.*, 2016, **18**, 26020–26025.

255 M. H. Abraham, *Chem. Soc. Rev.*, 1993, **22**, 73–83.

256 P. G. Jessop, D. Jessop, D. Fu and L. Phan, *Green Chem.*, 2012, **14**, 1245–1259.

257 C. Reichardt, *Angew. Chemie Int. Ed. English*, 1965, **4**, 29–40.

258 C. Reichardt, *Chem. Rev.*, 1994, **94**, 2319–2358.

259 C. Reichardt, *Green Chem.*, 2005, **7**, 339–351.

260 M. J. Kamlet, J.-L. M. Abboud, M. H. Abraham and R. W. Taft, *J. Org. Chem.*, 1983, **48**, 2877–2887.

261 S. K. Shukla, N. D. Khupse and A. Kumar, *Phys. Chem. Chem. Phys.*, 2012, **14**, 2754–2761.

262 C. Adam, M. V. Bravo and P. M. E. Mancini, *Tetrahedron Lett.*, 2014, **55**, 148–150.

263 H. Salari, A. Reza, M. R. Elahifard, A. R. Harifi-Mood, M. R. Elahifard and M. R. Gholami, *J. Solution Chem.*, 2010, **39**, 1509–1519.

264 H. Salari, M. Khodadadi-Moghaddam, A. R. Harifi-mood and M. R. Gholami, *J. Phys. Chem. B*, 2010, **114**, 9586–9593.

265 H. Salari, S. Ahmadvand, A. R. Harifi-Mood, M. Padervand and M. R. Gholami, *J. Solution Chem.*, 2013, **42**, 1757–1769.

266 R. Cabot and C. A. Hunter, *Chem. Soc. Rev.*, 2012, **41**, 3485–3492.

267 J. H. Hildebrand and R. L. Scott, *Regular Solutions*, Prentice-Hall, Inc., Englewood Cliffs, New Jersey, 1st edn., 1962.

268 A. W. Davidson, H. H. Sisler and R. Stoenner, *J. Am. Chem. Soc.*, 1944, **66**, 779–782.

269 H. S. van Klooster and W. A. Douglas, *J. Phys. Chem.*, 1945, **49**, 67–70.

270 B. Becker and A. W. Davidson, *J. Am. Chem. Soc.*, 1963, **85**, 157–159.

271 N. S. Nhlapo, W. W. Focke and E. Vuorinen, *Thermochim. Acta*, 2012, **546**, 113–119.

272 P. E. Hansen, T. Lund, J. Krake, J. Spanget-Larsen and S. Hvidt, *J. Phys. Chem. B*, 2016, **120**, 11279–11286.

273 Y. Lv, Y. Guo, X. Luo and H. Li, *Sci. China Chem.*, 2012, **55**, 1688–1694.

274 F. Kohler, E. Liebermann, G. Miksch and C. Kainz, *J. Phys. Chem.*, 1972, **76**, 2764–2768.

275 F. Kohler, R. Gopal, G. Gotze, H. Atrops, M. A. Demiriz, E. Liebermann, E. Wilhelm, F. Ratkovics and B. Palagyl, *J. Phys. Chem.*, 1981, **85**, 2524–2529.

276 H. Yamamoto, K. Sakamoto, Y. Bando, S. Matsumoto and J. Shibata, *J. Chem. Eng. Data*, 1997, **42**, 238–242.

277 K. Orzechowski, M. Pajdowska, J. Przybylski, J. Gli'nski and H. A. Ko\lodziej, *Phys. Chem. Chem. Phys.*, 2000, **2**, 4676–4681.

278 K. Orzechowski, M. Pajdowska, M. Czarnecki and U. Kaatze, *J. Mol. Liq.*, 2007, **133**, 11–16.

279 H. Eyring, *J. Chem. Phys.*, 1936, **4**, 283–291.

280 F. Kohler, H. Atrops, H. Kalali, E. Liebermann, E. Wilhelm, F. Ratkovics and T. Salamon, *J. Phys. Chem.*, 1981, **85**, 2520–2524.

281 K. Orzechowski, M. Pajdowska, K. Fuchs and U. Kaatze, *J. Chem. Phys.*, 2003, **119**, 8558–8566.

282 S. Karlsson, S. Backlund and R. Friman, *Colloid Polym. Sci.*, 2000, **278**, 8–14.

283 P. D. A. Pudney, K. J. Mutch and S. Zhu, *Phys. Chem. Chem. Phys.*, 2009, **11**,

5010–5018.

284 J. Päivärinta, S. Karlsson, M. Hotokka and A. Poso, *Chem. Phys. Lett.*, 2000, **327**, 420–424.

285 J. Päivärinta, S. Karlsson, A. Poso and M. Hotokka, *Chem. Phys.*, 2001, **263**, 127–138.

286 M. Hasani, J. L. Yarger and C. A. Angell, *Chem. - A Eur. J.*, 2016, **22**, 13312–13319.

287 J. G. Kirkwood, F. P. Buff and P. F. Buff, *J. Chem. Phys.*, 1951, **19**, 774–777.

288 D. G. Hall, *Trans. Faraday Soc.*, 1971, **67**, 2516–2524.

289 A. Ben-Naim, *J. Chem. Phys.*, 1977, **67**, 4884–4890.

290 S. Shimizu and Hue Sun Chan, *J. Chem. Phys.*, 2001, **115**, 3424–3431.

291 R. Chitra and P. E. Smith, *J. Phys. Chem. B*, 2002, **106**, 1491–1500.

292 S. Shimizu and C. L. Boon, *J. Chem. Phys.*, 2004, **121**, 9147–9155.

293 S. Shimizu, *Proc. Natl. Acad. Sci. U. S. A.*, 2004, **101**, 1195–1199.

294 J. J. Booth, S. Abbott and S. Shimizu, *J. Phys. Chem. B*, 2012, **116**, 14915–14921.

295 S. Shimizu, J. J. Booth and S. Abbott, *Phys. Chem. Chem. Phys.*, 2013, **15**, 20625–20632.

296 S. Shimizu and N. Matubayasi, *J. Phys. Chem. B*, 2014, **118**, 3922–3930.

297 S. Shimizu, *Food Funct.*, 2015, **6**, 3228–3235.

298 S. Shimizu and S. Abbott, *J. Phys. Chem. B*, 2016, **120**, 3713–3723.

299 S. Abbott, J. J. Booth and S. Shimizu, *Green Chem.*, 2017, **19**, 68–75.

300 V. Lesch, A. Heuer, C. Holm and J. Smiatek, *Phys. Chem. Chem. Phys.*, 2015, **17**, 8480–8490.

301 V. Lesch, A. Heuer, C. Holm and J. Smiatek, *ChemPhysChem*, 2016, **17**, 387–394.

302 T. Kobayashi, J. E. S. J. Reid, S. Shimizu, M. Fyta and J. Smiatek, *Phys. Chem. Chem. Phys.*, 2017, **19**, 18924–18937.

303 L. Almásy, M. Turmine and A. Perera, *J. Phys. Chem. B*, 2008, **112**, 2382–2387.

304 S. Shimizu and N. Matubayasi, *J. Phys. Chem. B*, 2014, **118**, 10515–10524.

305 E. A. Ploetz and P. E. Smith, *J. Chem. Phys.*, 2011, **135**, 44506.

306 S. Shimizu, W. M. McLaren and N. Matubayasi, *J. Chem. Phys.*, 2006, **124**, 234905.

307 H. Katayanagi, K. Nishikawa, H. Shimozaki, K. Miki, P. Westh and Y. Koga, *J. Phys. Chem. B*, 2004, **108**, 19451–19457.

308 H. Kato, K. Nishikawa, H. Murai, T. Morita and Y. Koga, *J. Phys. Chem. B*, 2008, **112**, 13344–13348.

309 E. Rilo, J. Pico, S. García-Garabal, L. M. Varela and O. Cabeza, *Fluid Phase Equilib.*, 2009, **285**, 83–89.

310 E. Vercher, a V. Orchille, P. J. Miguel and A. Martinez-Andreu, *J. Chem. Eng. Data*, 2007, **52**, 1468–1482.

311 I. Krossing, J. M. Slattery, C. Daguenet, P. J. Dyson, A. Oleinikova and H. Weingärtner, *J. Am. Chem. Soc.*, 2006, **128**, 13427–13434.

312 C. Wakai, A. Oleinikova, M. Ott and H. Weingärtner, *J. Phys. Chem. B*, 2005, **109**, 17028–17030.

313 T. Singh and A. Kumar, *J. Phys. Chem. B*, 2008, **112**, 12968–12972.

314 H. Weingärtner, *J. Mol. Liq.*, 2014, **192**, 185–190.

315 C. Schröder, T. Rudas, G. Neumayr, S. Benkner and O. Steinhauser, *J. Chem. Phys.*, 2007, **127**, 234503.

316 C. Schröder, M. Sega, M. Schmollngruber, E. Gailberger, D. Braun and O. Steinhauser, *J. Chem. Phys.*, 2014, **140**, 204505.

317 N. Yaghini, M. N. Garaga and A. Martinelli, *Fuel Cells*, 2016, **16**, 46–54.

318 R. Stenner, N. Matubayasi and S. Shimizu, *Food Hydrocoll.*, 2016, **54**, 284–292.

319 J. Smiatek, *J. Phys. Chem. B*, 2014, **118**, 771–782.

320 I. Prigogine, R. Defay and D. H. Everett, *Chemical Thermodynamics (Treatise of Thermodynamics)*, Longmans, Green and Co., London, 2nd edn., 1954.

321 H. L. Friedman and P. S. Ramanathan, *J. Phys. Chem.*, 1970, **74**, 3756–3765.

322 R. J. L. Andon, J. D. Cox and E. F. G. Herington, *Trans. Faraday Soc.*, 1957, **53**, 410–426.

323 L. Almásy and G. Jancsó, *J. Mol. Liq.*, 2004, **113**, 61–66.

324 A. B. Bhatia and D. E. Thornton, *Phys. Rev. B*, 1970, **2**, 3004–3012.

325 K. Nishikawa, *Chem. Phys. Lett.*, 1986, **132**, 50–54.

326 L. Wright, M. W. Sanders, L. Tate, G. Fairless, L. Crowhurst, N. C. Bruce, A. J. Walker, G. A. Hembury and S. Shimizu, *Phys. Chem. Chem. Phys.*, 2010, **12**, 9063–9066.

327 R. J. Gammons, University of York, 2015.

328 I. Khan, K. A. Kurnia, T. E. Sintra, J. A. Saraiva, S. P. Pinho and J. A. P. Coutinho, *Fluid Phase Equilib.*, 2014, **361**, 16–22.

329 J. A. L. Willcox, H. Kim and H. J. Kim, *Phys. Chem. Chem. Phys.*, 2016, **18**, 14850–14858.

330 A. M. Moschovi and V. Dracopoulos, *J. Mol. Liq.*, 2015, **210**, 189–199.

331 T. M. Chang, L. X. Dang, R. Devanathan and M. Dupuis, *J. Phys. Chem. A*, 2010, **114**, 12764–12774.

332 N. Haron, N. A. Sairi and V. S. Lee, *Mol. Simul.*, 2016, **42**, 655–666.

333 M. Haberler, C. Schröder and O. Steinhauser, *J. Chem. Theory Comput.*, 2012, **8**, 3911–3928.

334 S. Shimizu, *Chem. Phys. Lett.*, 2013, **582**, 129–133.

335 A. Perera and R. Mazighi, *J. Chem. Phys.*, 2015, **143**, 154502.

336 K. Nishikawa, Y. Kodera and T. Iijima, *J. Phys. Chem.*, 1987, **91**, 3694–3699.

337 L. Almásy, L. Cser and G. Jancsó, *J. Mol. Liq.*, 2002, **101**, 89–98.

338 K. Nishikawa, Y. Kasahara and T. Ichioka, *J. Phys. Chem. B*, 2002, **106**, 693–700.

339 P. Nockemann, K. Binnemans, B. Thijs, T. N. Parac-vogt, K. Merz, A. Mudring, P. C. Menon, R. N. Rajesh, G. Cordoyiannis, J. Thoen, J. Leys and C. Glorieux, *J. Phys. Chem. B*, 2009, **113**, 1429–1437.

340 A. J. L. Costa, M. R. C. Soromenho, K. Shimizu, I. M. Marrucho, J. M. S. S. Esperança, J. N. C. Lopes and L. P. N. Rebelo, *J. Phys. Chem. B*, 2012, **116**, 9186–9195.

341 C. G. Hanke and R. M. Lynden-Bell, *J. Phys. Chem. B*, 2003, **107**, 10873–10878.

342 T. Köddermann, C. Wertz, A. Heintz and R. Ludwig, *Angew. Chemie - Int. Ed.*, 2006, **45**, 3697–3702.

343 J. E. S. J. Reid, F. Agapito, C. E. S. Bernardes, F. Martins, A. J. Walker, S. Shimizu, M. E. M. da Piedade and M. E. Minas da Piedade, *Phys. Chem. Chem. Phys.*, 2017, **19**, 19928–19936.

344 J. E. S. J. Reid, C. E. S. Bernardes, F. Agapito, F. Martins, S. Shimizu, M. E. Minas da Piedade and A. J. Walker, *Phys. Chem. Chem. Phys.*, 2017, **19**, 28133–28138.

345 H. E. Gottlieb, V. Kotlyar and A. Nudelman, *J. Org. Chem.*, 1997, **62**, 7512–7515.

346 J. D. Cox, D. D. Wagman and V. A. Medvedev, *Key Values for Thermodynamics*, Hemisphere, New York, 1st edn., 1989.

347 T. Kiyobayashi and M. E. Minas da Piedade, *J. Chem. Thermodyn.*, 2001, **33**, 11–21.

348 B. N. Taylor and C. E. Kuyatt, *Guidelines for Evaluating and Expressing the Uncertainty of NIST Measurement Results (NIST Technical Note 1297)*, National Institute of Standards and Technology, Gaithersburg, 1994.

349 J. A. Martinho Simões, M. E. Minas da Piedade, J. A. M. Simoes, M. E. Minas da Piedade, J. A. Martinho Simões, M. E. Minas da Piedade, J. A. M. Simoes and M. E. Minas da Piedade, *Molecular Energetics*, Oxford University Press, New York, 2008.

350 M. Tanaka, G. Girard, R. Davis, A. Peuto and N. Bignell, *Metrologia*, 2001, **38**, 301–309.

351 M. A. Kessler and O. S. Wolfbeis, *Chem. Phys. Lipids*, 1989, **50**, 51–56.

352 L. Crowhurst, P. R. Mawdsley, J. M. Perez-arlandis, P. A. Salter and T. Welton, *Phys. Chem. Chem. Phys.*, 2003, **5**, 2790–2794.

353 R. L. Wagman, D. D.; Evans, W. H.; Parker, V. B.; Schumm, R. H.; Halow, I.; Bailey, S. M.; Churney, K. L.; Nuttall, *J. Phys. Chem. Ref. Data*, 1982, **11**, Suppl. n. 2.

354 B. Ruscic, *Active Thermochemical Tables (ATcT) values based on ver. 1.118 of the*

Thermochemical Network, available at ATcT.anl.gov, 2015.

355 K. Fumino, V. Fossog, P. Stange, D. Paschek, R. Hempelmann and R. Ludwig, *Angew. Chemie - Int. Ed.*, 2015, **54**, 2792–2795.

356 H. U. Ung, A. R. Moehlig, S. Khodagholian, G. Berden, J. Oomens and T. H. Morton, *J. Phys. Chem. A*, 2013, **117**, 1360–1369.

357 S. W. Benson, *J. Am. Chem. Soc.*, 1996, **118**, 10645–10649.

358 F. Gharagheizi, P. Ilani-Kashkouli, W. E. Acree, A. H. Mohammadi and D. Ramjugernath, *Fluid Phase Equilib.*, 2013, **360**, 279–292.

359 S. P. Verevkin, D. H. Zaitsau, V. N. Emel'Yanenko, A. V. Yermalayeu, C. Schick, H. Liu, E. J. Maginn, S. Bulut, I. Krossing and R. Kalb, *J. Phys. Chem. B*, 2013, **117**, 6473–6486.

360 A. Razzouk, A. Hajjaji, I. Mokbel, P. Mougin and J. Jose, *Fluid Phase Equilib.*, 2009, **282**, 11–13.

361 S. Kapteina, K. Slowik, S. P. Verevkin and A. Heintz, *J. Chem. Eng. Data*, 2005, **50**, 398–402.

362 B. Nuthakki, T. L. Greaves, I. Krodkiewska, A. Weerawardena, M. I. Burgar, R. J. Mulder and C. J. Drummond, *Aust. J. Chem.*, 2007, **60**, 21–28.

363 M. M. Kreevoy and S.-W. Oh, *J. Am. Chem. Soc.*, 1973, **95**, 4805–4810.

364 D. R. Lide, in *CRC Handbook of Chemistry and Physics, 89th Edition*, 2009, pp. 8–42.

365 R. L. Gustafson and A. E. Martell, *J. Am. Chem. Soc.*, 1959, **81**, 525–529.

366 R. J. Littel, M. Bos and G. J. Knoop, *J. Chem. Eng. Data*, 1990, **35**, 276–277.

367 S. Bratoz, D. Hadzi and N. Sheppard, *Spectrochmica Acta*, 1956, **8**, 249–261.

368 B. N. Mohr, Peter J., Newell, David B., Taylor, *Rev. Mod. Phys.*, 2016, **88**, 35009.

369 E. B. Tada, L. P. Novaki and O. a. El Seoud, *J. Phys. Org. Chem.*, 2000, **13**, 679–687.

370 M. Reis, L. Moreira, N. Nunes, R. Leitão and F. Martins, *J. Therm. Anal. Calorim.*, 2012, **108**, 761–767.

371 Y. Koga, *Solution thermodynamics and its application to aqueous solutions : a differential approach*, Elsevier, Amsterdan, 2nd edn., 2017.

372 A. Mariani, M. Campetella, C. Fasolato, M. Daniele, F. Capitani, L. Bencivenni, P. Postorino, S. Lupi, R. Caminiti and L. Gontrani, *J. Mol. Liq.*, 2017, **226**, 2–8.

373 T. M. Aminabhavi and B. Gopalakrishna, *J. Chem. Eng. Data*, 1995, **40**, 856–861.

374 P. S. Nikam, L. N. Shirsat, M. Hasan, P. Chemistry, M. S. G. College and M. Camp, *Engineering*, 1998, **9568**, 732–737.

375 P. Brocos, A. Pineiro, R. Bravo and A. Amigo, *Phys. Chem. Chem. Phys.*, 2003, **5**, 550–557.

376 K. M. Johansson, E. I. Izgorodina, M. Forsyth, D. R. MacFarlane and K. R. Seddon, *Phys. Chem. Chem. Phys.*, 2008, **10**, 2972–2978.

377 M. Meot-Ner, *Chem. Rev.*, 2005, 105, 213–284.

378 W. J. Hurley, I. D. Kuntz Jr. and G. E. Leroi, *J. Am. Chem. Soc.*, 1966, **88**, 3199–3202.

379 R. F. Lake and H. W. Thompson, *Proc. R. Soc. London A*, 1966, 291, 469–477.

380 R. J. Jakobsen, Y. Mikawa and J. W. Brasch, *Spectrochim. Acta Part A Mol. Spectrosc.*, 1967, **23**, 2199–2209.

381 A. Witkowski, *J. Chem. Phys.*, 1970, **52**, 4403–4406.

382 R. Langner and G. Zundel, *J. Phys. Chem. A*, 1998, **102**, 6635–6642.

383 A. Matei, N. Drichko, B. Gompf and M. Dressel, *Chem. Phys.*, 2005, **316**, 61–71.

384 K. Fumino, P. Stange, V. Fossog, R. Hempelmann and R. Ludwig, *Angew. Chemie - Int. Ed.*, 2013, **52**, 12439–12442.

385 R. Ludwig, *Phys. Chem. Chem. Phys.*, 2015, **17**, 13790–13793.

386 G. Bringas, P. Navarro-Santos, R. López-Rendón, J. López-Lemus and F. Bresme, *J. Phys. Chem. B*, 2015, **119**, 5035–5046.

387 H. Bertagnolli, *Chem. Phys. Lett.*, 1982, **93**, 287–292.

388 S. Imberti and D. T. Bowron, *J. Phys. Condens. Matter*, 2010, **22**, 404212.

389 T. Takamuku, Y. Kyoshoin, H. Noguchi, S. Kusano and T. Yamaguchi, *J. Phys. Chem. B*, 2007, **111**, 9270–9280.

390 I. Nahringbauer, *Acta Cryst*, 1967, **23**, 956–965.

391 I. Nahringbauer, *Acta Chem. Scand.*, 1968, **22**, 1141–1158.

392 I. Nahringbauer, *Acta Chem. Scand.*, 1969, **23**, 1653–1666.

393 C. M. Hansen, *Hansen solubility parameters : a user's handbook*, CRC Press, London, 2nd edn., 2007.

394 S. Abbott, HSP Basics | Practical Solubility Science | Prof Steven Abbott, https://www.stevenabbott.co.uk/practical-solubility/hsp-basics.php, (accessed 6 June 2017).

395 A. L. McClellan, *Tables of Experimental Dipole Moments.*, W. H. Freeman & Co., San Francisco, 1st edn., 1963.

396 M. J. Kamlet, J. L. Abboud and R. W. Taft, *J. Am. Chem. Soc.*, 1977, **99**, 6027–6038.

397 R. Stenutz, Kamlet-Taft solvent parameters, http://www.stenutz.eu/chem/solv26.php, (accessed 6 June 2017).

398 M. J. Kamlet and R. W. Taft, *J. Am. Chem. Soc.*, 1976, **98**, 377–383.

399 C. Laurence, P. Nicolet, M. Lucon, T. Dalati and C. Reichardt, *J. Chem. Soc. Perkin Trans. 2*, 1989, 873–876.

400 J. P. Wagner and P. R. Schreiner, *Angew. Chemie Int. Ed.*, 2015, **54**, 12274–12296.

401 L. Spialter and J. A. Pappalardo, *The Acyclic Aliphatic Tertiary Amines*, The

Macmillan Company, New York, First Edit., 1965.

402 A. Perera, F. Sokolic and L. Zoranic, *Phys. Rev. E*, 2007, **75**, 60502.

403 L. Zoranić, F. Sokolic and A. Perera, *J. Chem. Phys.*, 2007, **127**, 24502.

404 K. R. J. Lovelock, *Phys. Chem. Chem. Phys.*, 2012, **14**, 5071–5089.

405 V. Zeindlhofer, D. Khlan, K. Bica and C. Schröder, *RSC Adv.*, 2017, **7**, 3495–3504.

406 M. G. Bogdanov, I. Svinyarov, R. Keremedchieva and A. Sidjimov, *Sep. Purif. Technol.*, 2012, **97**, 221–227.

407 M. G. Bogdanov and I. Svinyarov, *Sep. Purif. Technol.*, 2013, **103**, 279–288.

408 M. G. Bogdanov, R. Keremedchieva and I. Svinyarov, *Sep. Purif. Technol.*, 2015, **155**, 13–19.

409 I. Svinyarov, R. Keremedchieva and M. G. Bogdanov, *Sep. Sci. Technol.*, 2016, **51**, 2691–2699.

410 T. L. Greaves, K. Ha, B. W. Muir, S. C. Howard, A. Weerawardena, N. Kirby and C. J. Drummond, *Phys. Chem. Chem. Phys.*, 2015, **17**, 2357–2365.

411 J. M. Prausnitz, R. N. Lichtenthaler and E. G. de Azevedo, *Molecular thermodynamics of fluid-phase equilibria.*, Prentice Hall PTR, Upper Saddle River, 3rd edn., 1999.

412 B. E. Poling, J. M. Prausnitz and J. P. (John P. O'Connell, *The properties of gases and liquids*, McGraw-Hill, London, 5th edn., 2001.

413 R. Hayes, G. G. Warr and R. Atkin, *Chem. Rev.*, 2015, **115**, 6357–6426.

414 T. Murphy, R. Atkin and G. G. Warr, *Curr. Opin. Colloid Interface Sci.*, 2015, **20**, 282–292.

415 A. Mariani, O. Russina, R. Caminiti and A. Triolo, *J. Mol. Liq.*, 2015, **212**, 947–956.

416 O. Russina, A. Mariani, R. Caminiti and A. Triolo, *J. Solution Chem.*, 2015, **44**, 669–685.

417 J. A. McCune, A. H. Turner, F. Coleman, C. M. White, S. K. Callear, T. G. A. Youngs, M. Swadźba-Kwaśny and J. D. Holbrey, *Phys. Chem. Chem. Phys.*, 2015, **17**, 6767–6777.

418 T. G. A. Youngs, J. D. Holbrey, M. Deetlefs, M. Nieuwenhuyzen, M. F. Costa Gomes and C. Hardacre, *ChemPhysChem*, 2006, **7**, 2279–2281.

419 C. Hardacre, J. D. Holbrey, M. Nieuwenhuyzen and T. G. A. Youngs, *Acc. Chem. Res.*, 2007, **40**, 1146–1155.

420 T. G. A. Youngs, J. D. Holbrey, C. L. Mullan, S. E. Norman, M. C. Lagunas, C. D'Agostino, M. D. Mantle, L. F. Gladden, D. T. Bowron and C. Hardacre, *Chem. Sci.*, 2011, **2**, 1594–1605.

421 S. Grimme, J. Antony, S. Ehrlich and H. Krieg, *J. Chem. Phys.*, 2010, **132**, 154104.

422 T. H. Dunning, *J. Chem. Phys.*, 1989, **90**, 1007–1023.

423 P. J. Stephens, F. J. Devlin, C. F. Chabalowski and M. J. Frisch, *J. Phys. Chem.*,

1994, **98**, 11623–11627.

424 T. Van Mourik, A. K. Wilson and T. H. Dunning, *Mol. Phys.*, 1999, **96**, 529–547.

425 D. E. Woon and T. H. Dunning, *J. Chem. Phys.*, 1995, **103**, 4572–4585.

426 R. Polly, H.-J. Werner, F. R. Manby and P. J. Knowles, *Mol. Phys.*, 2004, **102**, 2311–2321.

427 F. Weigend, *Phys. Chem. Chem. Phys.*, 2002, **4**, 4285–4291.

428 M. K. Kesharwani, B. Brauer and J. M. L. Martin, *J. Phys, Chem. A*, 2015, **119**, 1701–1714.

429 A. Karton and J. M. L. Martin, *J. Chem. Phys.*, 2012, **136**, 124114.

430 A. Tajti, P. G. Szalay and J. Gauss, *J. Chem. Phys.*, 2007, **127**, 14102.

431 W. Kutzelnigg, *Mol. Phys.*, 1997, **90**, 909–916.

432 N. C. Handy, Y. Yamaguchi and H. F. Schaefer III, *J. Chem. Phys.*, 1986, **84**, 4481–4484.

433 *CFOUR, a quantum chemical program package written by J.F. Stanton, J. Gauss, M.E. Harding, P.G. Szalay with contributions from A.A. Auer, R.J. Bartlett, U. Benedikt, C. Berger, D.E. Bernholdt, Y.J. Bomble, L. Cheng, O. Christiansen, M. Heckert, O. Heun, C,* .

434 H.-J. Werner, P. J. Knowles, G. Knizia, F. R. Manby, M. Schütz, P. Celani, T. Korona, R. Lindh, A. Mitrushenkov, G. Rauhut, K. R. Shamasundar, T. B. Adler, R. D. Amos, A. Bernhardsson, A. Berning, D. L. Cooper, M. J. O. Deegan, A. J. Dobbyn, F. Eckert, E. Goll, C. Hampel, A. Hesselmann, G. Hetzer, T. Hrenar, G. Jansen, C. Köppl, Y. Liu, A. W. Lloyd, R. A. Mata, A. J. May, S. J. McNicholas, W. Meyer, M. E. Mura, A. Nicklass, D. P. O'Neill, P. Palmieri, D. Peng, K. Pflüger, R. Pitzer, M. Reiher, T. Shiozaki, H. Stoll, A. J. Stone, R. Tarroni, T. Thorsteinsson and M. Wang, *MOLPRO, version 2012.1, a package of ab initio programs*, Cardiff, UK, 2012.

435 S. G. Lias, J. E. Bartmess, J. F. Liebman, J. L. Holmes, R. D. Levin and W. G. Mallard, *J. Phys. Chem. Ref. Data, Suppl. 1*, 1988, 17, 1–861.